# Improving OLED Technology for Displays

by

Jennifer J. Yu

Submitted to the Department of Electrical Engineering and Computer Science
in partial fulfillment of the requirements for the degree of

Doctor of Philosophy in Computer Science and Engineering

at the

MASSACHUSETTS INSTITUTE OF TECHNOLOGY

September 2008



Author ..... .....
Department of Electrical Engineering and Computer Science
August 28th, 2008

Certified by ..... .....
Vladimir Bulovic
Associate Professor
Thesis Supervisor

Accepted by ..... .....
Terry P. Orlando
Chair, Department Committee on Graduate Students

# Improving OLED Technology for Displays

by

Jennifer J. Yu

Submitted to the Department of Electrical Engineering and Computer Science
on August 28th, 2008, in partial fulfillment of the
requirements for the degree of
Doctor of Philosophy in Computer Science and Engineering

## Abstract

Organic light emitting devices (OLEDs) are brightly emissive, efficient, have fast switching speeds, and are paper-thin in format, propelling their use as an emerging flat panel display technology. However, two primary challenges prevent OLEDs from dominating the large-area display market: the extension of OLED display lifetime and development of simple, scalable fabrication techniques compatible with small molecule organic thin films. The principle contributions we report are (1) introduction and analysis of a novel optical feedback technique for extending the lifetime of OLED displays (2) the experimental demonstration and theoretical analysis of contact stamping for patterning multi-color OLED displays.

Thesis Supervisor: Vladimir Bulovic
Title: Associate Professor

# Acknowledgments

I would like to thank:

My advisor, Vladimir Bulovic, for his ideas and enthusiasm.

My collaborators on the various projects I've worked on – Charles Sodini and Yaakov Tischler on edge-emitted optical feedback. Gerry Chen and Hao Huang on inkjet patterning and stamping of QD-LEDs.

The entire laboratory of organic optics and electronics (LOOE) group, for being a great bunch of people.

Yaakov Tischler, Gerry Chen, and Luke Theogarajan for their advice, scientific discussion, and making science fun and exciting.

John Ho and Alexi Arango for being my cohorts in the whole grad school experience and keeping the lab running.

LeeAnn Kim for being an awesome person.

My mom, dad, and brother for everything else.

Funding for this work was provided by the Materials Research Science & Engineering Centers (MRSEC), Defense Advanced Research Projects Agency and Hewlett-Packard (DARPA-HP), and Focus Center for Circuit & System Solutions (C2S2), one of five research centers funded under the Focus Center Research Program, a Semiconductor Research Corporation Program and the (PECASE).

# Contents

# List of Figures

# List of Tables

# Chapter 1

# Introduction

## 1.1 Thesis overview

In this chapter, organic light emitting device (OLED) technology is reviewed to motivate its use in displays. This includes a discussion of OLED structure and operation, the requirements for display technology, and performance comparison between liquid crystal displays (LCD) and OLED displays. This section ends by introducing the two major challenges facing OLEDs for use in displays, which are covered in two parts in the thesis. The first part of the thesis covers OLED display lifetime. Chapter 2 discusses OLED degradation and other issues that affect display stability. Chapter 3 discusses optical feedback as a proposed solution to solve these degradation and stability issues. The second part of the thesis covers OLED display fabrication. Chapter 4 reviews fabrication techniques for patterning OLEDs in displays. Chapter 5 and 6 discuss contact stamping as a proposed solution for patterning organic layers and metal cathodes in OLED displays. Chapter 7 introduces a new approach towards patterning the emissive layer of a display with quantum dots. The final sections of the thesis comment on the potential of OLED displays and the future research opportunities and applications that are made possible with the results of this work.

## 1.2 OLEDs

### 1.2.1 Structure

In 1963, the early device structure of an OLED consisted of a single crystal of anthracene sandwiched between two silver paste electrodes [32]. Although a bright blue light was emitted, the need for high purity crystals and high operational voltages made these devices impractical for commercial applications. In 1982, this OLED structure was thinned down by an order of magnitude by vapor-depositing the anthracene as a thin film, allowing generation of high fields at low voltages and an improvement in device efficiency [33]. In 1987, a key breakthrough in device performance was made by separating the function of charge transport and emission in the device [34]. This device consisted of an anode, hole transport layer (HTL), electron transport layer (ETL) and cathode. An OLED representative of this device structure is shown in Figure 1-1c with indium tin oxide (ITO) anode, N,N'-Bis(3-methylphenyl)- N,N'- bis(phenyl)-benzidine (TPD) HTL, Tris(8-hydroxy-quinolinato)aluminium (Alq3) ETL, and Mg:Ag/Ag cathode. It is typical for OLED structures to now use separate layers in the device structure for charge injection, charge transport, and emission.

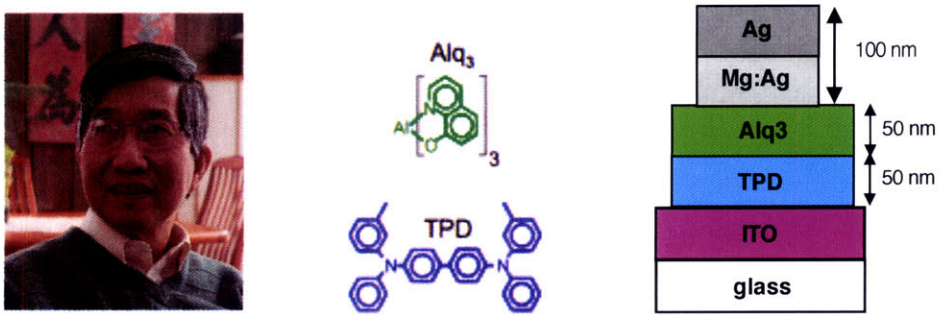


Figure 1-1: First efficient, low-voltage OLED technology: (a) Ching Tang, inventor at Eastman Kodak, (b) chemical structure of organic material TPD and Alq3 and (c) device structure.

### 1.2.2 Fabrication

OLED fabrication can involve dry or wet techniques. Dry techniques are applicable to small molecule organic material and usually involve thermal evaporation. Wet techniques such as spin-casting or ink jet printing, are usually associated with polymeric organics, which cannot be deposited with dry techniques. In this thesis, the focus is on dry fabrication techniques which are currently used in commercial OLED production, having the advantage of higher efficiencies and lifetimes that are more suitable for display technology.

The first layer in the OLED structure is the ITO anode. The ITO is sputter deposited onto the substrate and can be easily patterned using lithographic techniques, since it is a robust inorganic material deposited before the organic layers during OLED fabrication. The organic layers and subsequent metal cathode are deposited using thermal evaporation, as shown in Figure 1-2. The source material is placed in a metal boat, made from high-melting temperature metals such as W, Ta, and Mo, or a ceramic crucible. High current is passed through the metal boat or a heating coil surrounding the ceramic crucible to heat the source material until it melts or sublimes. This process occurs in a vacuum chamber with pressures under $10^{-6}$ torr so that the evaporated material is free to travel in the chamber without colliding into particles, until it hits a surface and condenses. The substrate is usually placed at the top of the chamber on a rotating stage for more uniform deposition of material, and a crystal thickness monitor is used to measure the thickness of the deposited film.

### 1.2.3 Operation

An OLED emits light when a forward bias is applied across the electrodes, as shown in Figure 1-3a. When bias is applied, electrons and holes are injected into the OLED device as shown in the energy band diagram in Figure 1-3b. Electrons are injected from the cathode into the lowest unoccupied molecular orbital (LUMO) for the Alq3. These electrons hop from molecule to molecule until they reach the Alq3-TPD interface. Holes are injected from the ITO anode into the highest occupied molecular

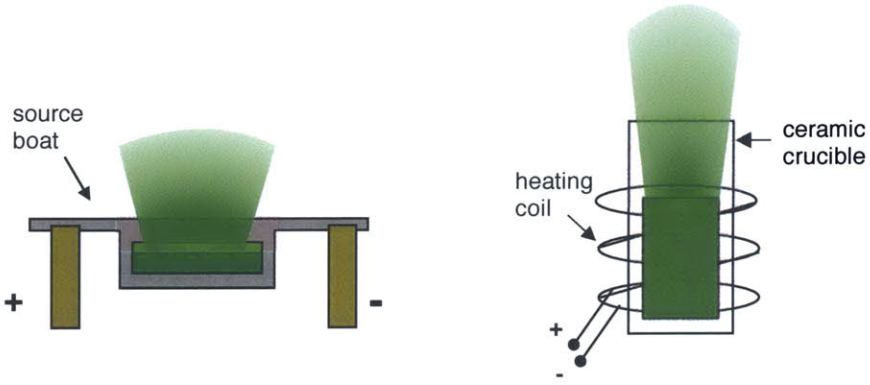


Figure 1-2: Thermal evaporation of material by joule heating from applying bias to source boat or heating coil.

orbital (HOMO) of the TPD and also travel by hopping from molecule to molecule until they reach the TPD-Alq3 interface. Holes and electrons accumulate at this interface due to energy band mismatch, as shown in Figure 1-3c, and reduced carrier mobility in the opposite charge transport material. Some of the holes or electrons are able to escape onto Alq3 or TPD molecules, forming a tightly bound electron hole pair known as an exciton. The exciton can then diffuse through the organic material, energy transfer to another molecule, or stay on the molecule and relax, losing the energy as heat or light. Radiative relaxation of the exciton results in light emission of the device with color characteristic of the optical bandgap of the molecule on which the exciton relaxed.

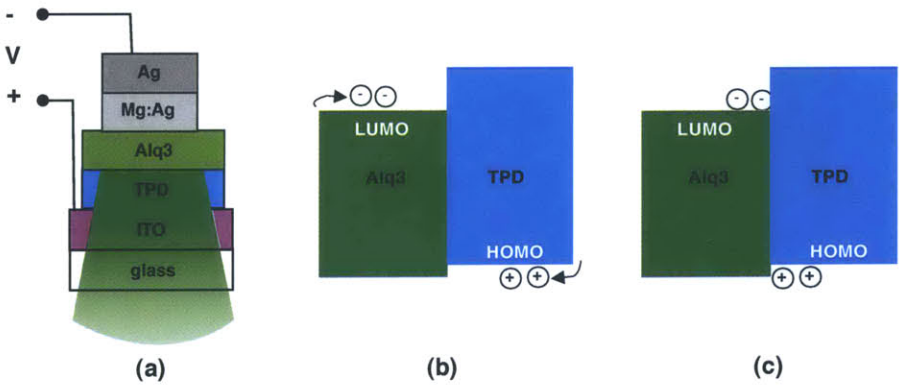


Figure 1-3: (a) OLED device structure under applied bias and energy band diagram showing (b) charge injection from electrodes (c) charge accumulation at interface.

Tuning the color of light emission is achieved by changing the organic molecule the exciton chooses to radiatively relax from. This can be done by controlling the exciton formation region in a device and by selecting appropriate fluorescent or phosphorescent dopants in the appropriate host material. For example, a TPD/Alq3 bilayer device emits green light because all excitons generated at the interface energy transfer to Alq3 before radiatively relaxing. For blue light emission, a hole blocking layer (HBL) of 3-(4-Biphenylyl)-4-phenyl-5-tert-butylphenyl-1,2,4-triazole (TAZ) can be inserted between the Alq3 and TPD layers, which results in exciton generation at the TPD/TAZ interface as shown in Figure 1-4a. The TAZ separates exciton formation from the Alq3 layer, preventing energy transfer so that radiative relaxation of excitons occur on TPD molecules, whose optical bandgap corresponds to emission of blue light. A simple way to create red emission in a TPD-Alq3 device is to dope the Alq3 near the interface with 4-(Dicyanomethylene)-2-methyl-6-julolidyl-9-enyl-4H-pyran (DCM2) fluorescent dopant as shown in Figure 1-4b. Excitons formed in TPD energy transfer to Alq3, which energy transfer to DCM2, emitting red light upon radiative relaxation. The chemical structure of TAZ and DCM2 are shown in Appendix B.

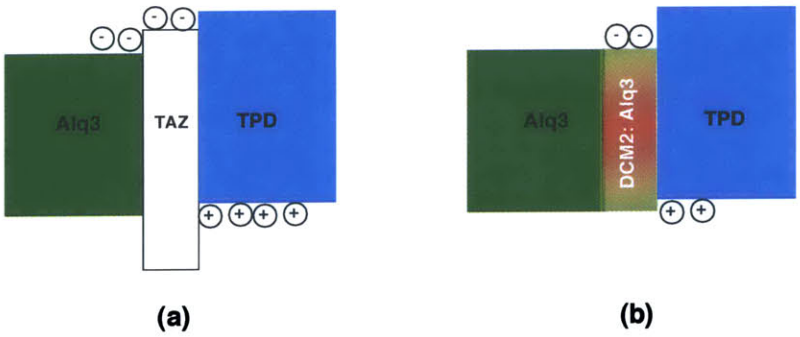


Figure 1-4: Energy band diagram of (a) blue emitting device where exciton formation occurs TAZ/TPD interface (b) red emitting device where exciton formation occurs at the DCM2:Alq3/TPD interface.

### 1.2.4 Device characteristics

A typical OLED has the following approximate current, voltage and luminance (I,V, and L) relationships during operation:

$$I \ \alpha \ V^m \tag{1.1}$$

$$L \ \alpha \ I \tag{1.2}$$

Current is related to voltage by a high exponent, typically m $\geq$ 6. Luminance and current are linearly related. Note that a small change in voltage results in a large change in current and luminance. For this reason, OLEDs are current driven devices.

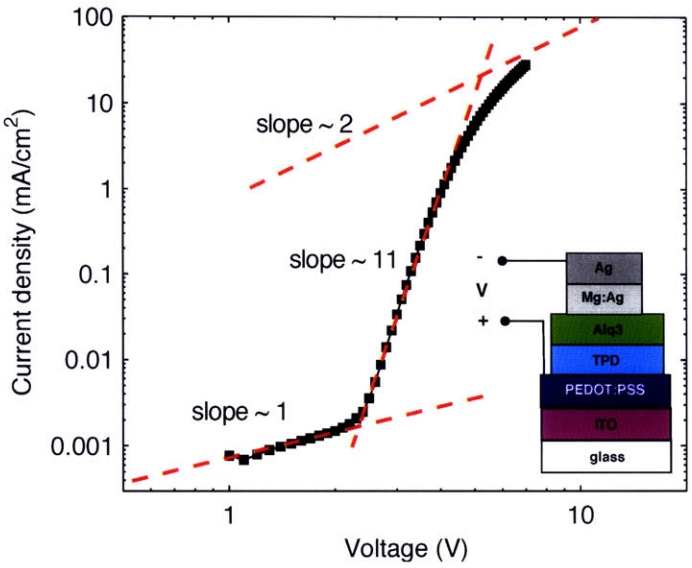


Figure 1-5: Current density vs. voltage characteristics for typical OLED structure shown in bottom right. The full chemical name and structure of PEDOT:PSS is shown in Appendix B.

Typical I-V characteristics of an OLED device is shown in Figure 1-5. Note that the I-V characteristics deviate from the approximate expression in Equation 1.1. At low voltages, the OLED operates in the ohmic regime in which conduction relies on thermally generated free charge. In this mode the current depends directly on the applied voltage, and is represented by Equation 1.3 where $J$ is current density, $q$ is

the electronic charge, $\mu_n$ is the electron mobility, $n_o$ is the thermally generated free charge density, $V$ is the applied voltage, and $d$ is the ETL thickness.

$$J = q\mu_n n_o V/d \tag{1.3}$$

This regime is observable in Figure 1-5 at low voltages, having a slope of 1 on the log-log plot. At moderate voltages, the OLED operates in a trap-charge-limited conduction regime. In this regime, the applied voltage begins to inject carriers into the OLED and these carriers fill trap sites that exist in the band gap of the organic layer. This reduces the available density of traps and increases the effective mobility of the carriers, resulting in rapid increase in current with respect to voltage described in Equation 1.1. This operating regime is evidenced in Figure 1-5 as the high slope region, m = 11, on the log-log plot. Finally, at high voltages the carriers eventually fill up all the trap states in the organic and the OLED operates in a space-charge-limited conduction regime. In this regime, the injected charge eventually builds up an internal field opposite to the injecting electrodes which limits further injection of charge into the device. This I-V relationship is described in Equation 1.4 where $\epsilon$ is the permittivity of the organic.

$$J = (9/8)\mu_n \epsilon V^2/d^3 \tag{1.4}$$

This regime is observable in Figure 1-5 at high voltages, which tends toward a slope of 2 on the log-log plot.

Figure 1-6 shows the linear relationship between luminance and current density for a typical OLED structure [35]. At higher current densities, the L-I characteristics deviate as well, which has been explained by field-assisted exciton dissociation, exciton-exciton and exciton-charge carrier annihilation, although these mechanisms do not entirely explain the large EQE roll-off at very high current densities [36].

External quantum efficiency, the ratio of photons out for electrons into a device, is a useful metric for comparing OLED efficiencies, given that OLEDs are easiest to describe as current-driven devices. The external quantum efficiency is roughly

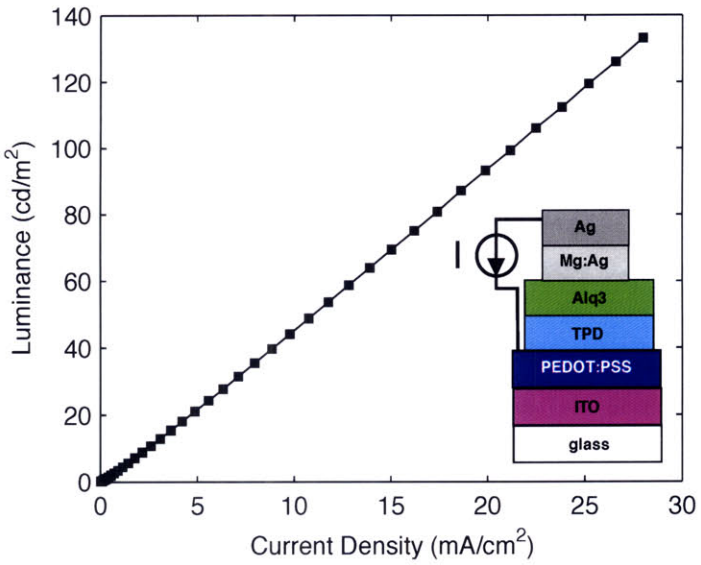


Figure 1-6: Luminance vs current density characteristics for typical OLED structure.

dependent on the product of the fraction of emissive species $\beta$ , the photoluminescence efficiency $\phi_{pl}$, and the light out coupling fraction $\chi$. For a typical Alq3 device, $\beta \approx 0.22$ [37] , $\phi_{pl} \approx 0.32$ [38], and $\chi \approx 0.17$ [39], yielding an external quantum efficiency of about 1.7%. Other factors, such as how well the number of holes and electrons are matched, also effect quantum efficiency, giving measured values of quantum efficiency less than 1%, as shown in Figure 1-7. By using efficient phosphorescent dopants, $\beta$ and $\phi_{pl}$ can be increased to 1, increasing the external quantum efficiencies of OLEDs to about 20%.

Power efficiency is a useful metric to compare OLEDs to different technologies. The current status of OLED efficiency is shown in Table 1.1, which range from 10 to 90 Lumens/Watt ($lm/W$) for different colored devices. For comparison, a compact fluorescent light bulb can operate at 70 $lm/W$ while an incandescent light bulb can run at 17 $lm/W$ [40].

OLED lifetime is conventionally measured in terms of device half-life, the time it takes an OLED to decay to half its initial brightness when ran at constant current, as shown in Figure 1-8. Table 1.2 lists the status of OLED half life, which has been extended to over 100,000 hours for red and green, but blues remain at around 30,000

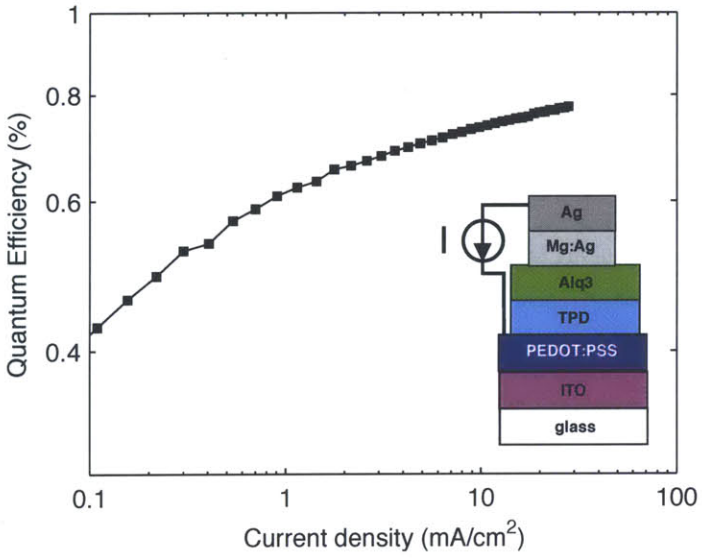


Figure 1-7: Quantum efficiency vs current density characteristics for typical OLED structure.

hours at video brightness (100 $cd/m^2$). For comparison, a fluorescent light source lasts approximately 10,000 hours and an inorganic LED lasts 50,000 hours.

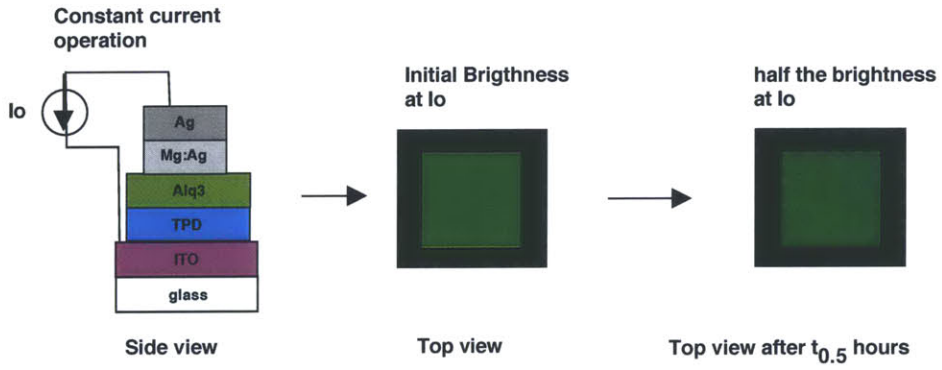


Figure 1-8: A illustration of OLED half-life, time it takes an OLED to reach half its initial brightness when operated at constant current.

Table 1.1: Efficiency data for stable OLEDs that have more than a 10,000 hour lifetime for devices measured at 500 $cd/m^2$ for red, 1000 $cd/m^2$ for green, and 1000 $cd/m^2$ for blue assuming 7V operation (actual voltage 6-8V). Demonstrated efficiences are from hero devices measured at 300 $cd/m^2$ and 2.9V for red, 600 $cd/m^2$ and 2.9V for green, and 100 $cd/m^2$ and 3.4V for blue. [16]

| Color | Stable Device $(lm/W)$ | Demonstrated Device $(lm/W)$ |
|---|---|---|
| Red | 6.7 | 20 |
| Green | 28 | 90 |
| Blue | 2.6 | 9.2 |

Table 1.2: Lifetime data for phosphorescent OLED devices. Normalized column indicates projected lifetime at 100 $cd/m^2$. The blue is sky blue in appearance, and dark blues are still under development. [30]

| Color | Initial Luminance $(cd/m^2)$ | Lifetime $(h)$ | Normalized $(h)$ |
|---|---|---|---|
| Red | 500 | $100{,}000^+$ | $500{,}000^+$ |
| Green | 1,000 | 25,000 | 250,000 |
| Blue | 200 | 15,000 | 30,000 |

## 1.3 Displays

### 1.3.1 Cathode ray tube

The cathode ray tube (CRT) initially dominated the display market starting from the 1930s. Figure 1-9b shows a schematic of the key components of this technology. Electrons are boiled off of a cathode and focused into a ray of streaming electrons by a positive anode. This ray is aimed at a phosphor coated screen which emits light when electrons hit the phosphor.

### 1.3.2 Liquid crystal display

With the rise of portable electronics, it became apparent that the CRT was too heavy, large, and energy inefficient to be used in the portable consumer products. The liquid crystal display (LCD) was first developed in 1968, and the first commercial LCDs

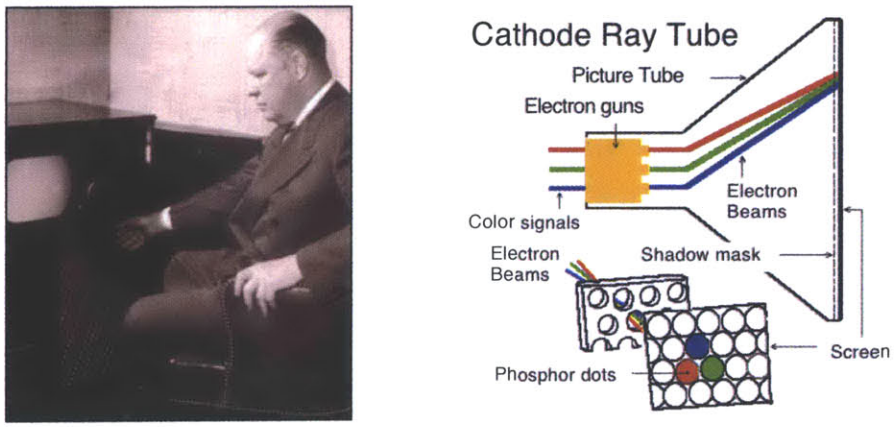


Figure 1-9: Allen Du Mont, inventor of CRT display and (b) basic CRT technology. [1]

appeared in a Sharp pocket calculator in 1973. In 1988, the LCD was commercially available as a 14-inch display, and LCDs became the dominant display technology around the year 2000 [3].

LCDs operate by using a white backlight source which is modulated in brightness with liquid crystals and then sent through a color filter before the signal reaches the viewer as shown in Figure 1-10b. The basic structure is responsible for many initial challenges that faced LCDs: low efficiencies, low contrast ratios, slow switching speeds, and limited viewing angles.

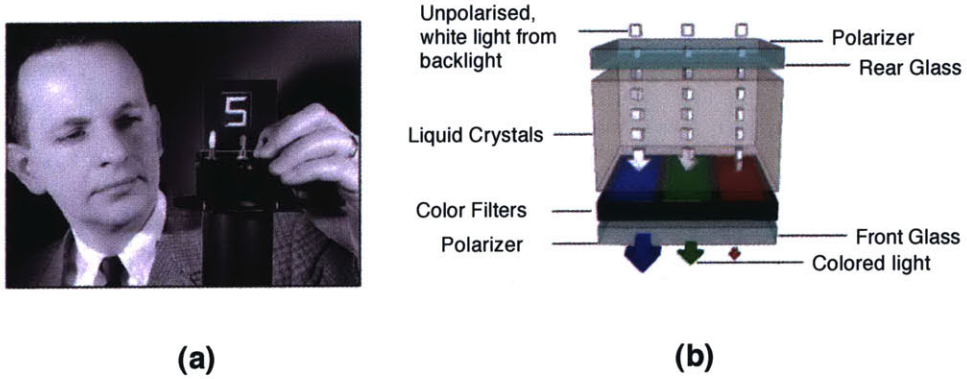


Figure 1-10: Basic LCD technology: (a) George Heilmeier, inventor of the LCD at RCA and (b) basic LCD structure includes backlight, polarizers, liquid crystal, and color filters. [2]

Low efficiencies are the result of using a backlight source which is sent through polarizers and color filters. To create the on-state of the pixel, the backlight is sent through a rear polarizer which filters out about half of the light and then through liquid crystal material which is naturally twisted to align to the front polarizer, allowing the passage of light as shown in Figure 1-11a. Finally, the polarized, white light is sent through a color filter, cutting out about a third of the light before reaching the viewer. At best, LCDs give you a sixth of the original efficiency of the backlight source. In addition, LCDs do not save energy when a dark pixel is displayed. To create a dark pixel, a voltage is applied across the liquid crystal so that it does not affect the polarization of the light so that the light cannot pass through the front polarizer, as shown in Figure 1-11b. In this case, even though a pixel is in its off-state, a voltage needs to be applied to align the liquid crystal and the backlight is still operating in its brightest mode. Low contrast ratio stems from the backlight always being on, which allows for some light leakage through the front polarizer making a dark pixel less black [3]. Slow switching speeds are a result of the physical response of the liquid crystal material to a voltage, which barely makes the required display minimum of 16 ms. Finally, LCD displays have poor viewing angles because of the relatively thick pixel structure which make the light output of the display highly directional.

Most of these initial challenges with LCDs have been resolved. Recently, use of inorganic LED backlight panels have been developed to improve the efficiency and contrast ratio of LCDs [41] [42]. Contrast ratios have been improved by optimization of LCD fabrication and structure [43]. Switching speeds are improved by overdriving the liquid crystals [44] [45], but have higher power consumption due to the increase in applied voltage. Viewing angles are less of a problem due to improved liquid crystal cell structure [46] [47] [48].

### 1.3.3 OLED displays

The first commercial OLED display was a small-molecule passive-matrix monochrome car stereo display from Pioneer in 1999. This was soon followed with a full color active-matrix display in 2003, at 2.2 inches, 512 x 218 pixels in a Kodak digital camera [49].

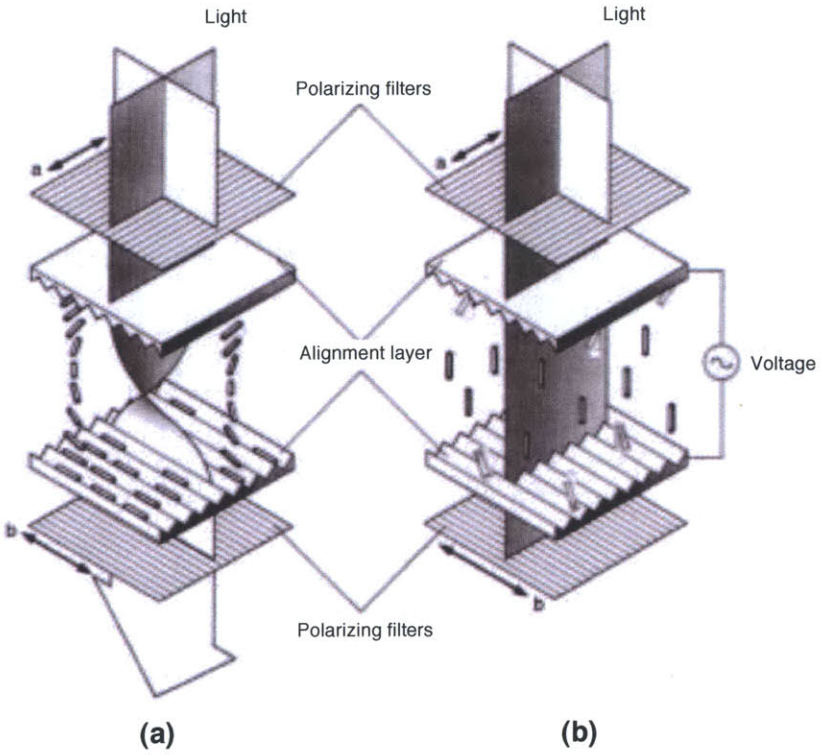


Figure 1-11: Liquid crystal at work: (a) on and (b) off modes of an LCD pixel. [3]

In 2007, the first commercial OLED TV was available in Japan. All 1,300 units of this display sold out one day after they were introduced, which prompted Sony to release the display in the US the following year [50] [51].

In comparison to LCDs, active matrix OLED displays promise better efficiencies, contrast ratios, and response times due to their simple structure. In OLED displays, a pixel can be turned on and off and directly modulated in brightness by an electrical signal. In addition, OLEDs can be color-tuned by changing the chemical structure of the organic molecule and can be engineered to have good color saturation. The switching speed of an OLED is determined by electroluminescence response of an OLED, which is on the order of $10\mu s$, well exceeding the minimum 16 ms needed for displays. The contrast ratio for OLED displays is limited only by the maximum brightness of an OLED pixel since the off-state of a pixel produces no light output. Finally, the large viewing angle of these displays comes inherently with the technology because the light emission from a luminescent film is omnidirectional. The main

advantages of OLEDs over LCDs are summarized in Table 1.3.

Table 1.3: Main advantages of OLED displays over LCDs

| | OLED | LCD |
|---|---|---|
| Efficiency [52] | 10 $lm/W$ | 2 $lm/W$ |
| Contrast Ratio [53] [54] | 1,000,000:1 | 500,000:1 |
| Response Time [55] [56] | 10 $\mu s$ | 10 $ms$ |

## 1.4 Challenges of OLED technology in displays

### 1.4.1 Lifetimes

The typical lifetime of a commercial display is 50,000 hours while the lifetime of an OLED display is quoted at 30,000 hours [54]. Even 30,000 hours is an over-estimate, for pixels are used different amounts in a display and OLED external quantum efficiency degrades according to usage [57]. For this reason, an OLED display will become non-uniform before OLED half-life is reached. Figure 1-12 illustrates an extreme case to demonstrate that OLED half-life does not translate to display lifetime. In this figure, some pixels of a display have been aged to half their initial brightness while other pixels have not been degraded. It is clear that non-uniform aging of individual pixels will have a large effect on the usable lifetime of a display.

### 1.4.2 Patterning

Current OLED fabrication techniques are limited in resolution and difficult to scale to larger areas. The largest commercial OLED display has an 11-inch diagonal. Typical LCD display diagonals that begin at 13-inch laptop displays, 20-inch computer displays, and increase up to 108-inch TV displays. Figure 1-13 shows the comparison of first commercial 11-inch OLED TV to a typical 50-inch commercial TV display [4].

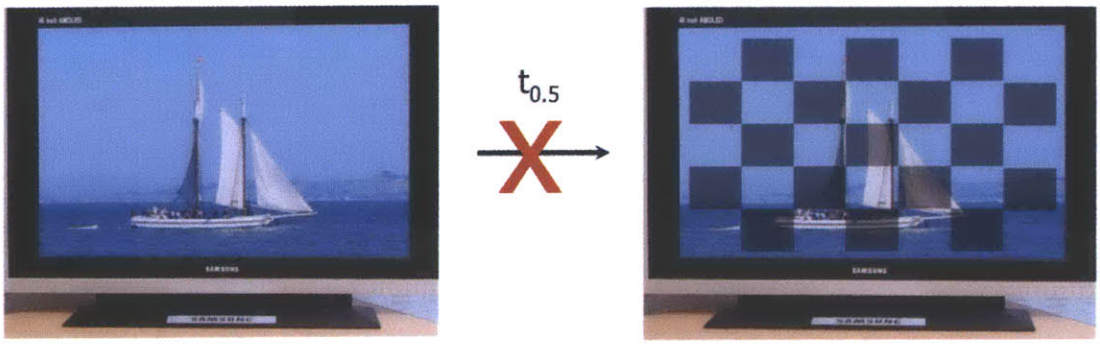


Figure 1-12: Display lifetime is not equal to OLED half-life: A 50% decrease in initial brightness is easily detected in neighboring pixels. The figure on the left illustrates a working OLED display. If this display is aged to half-life in a checkerboard fashion, some of the pixels will display the image as half as bright. The figure on the right illustrates this case in which the aged pixels are able to display the image as brightly as the original display while the aged pixels display the image as half as bright.

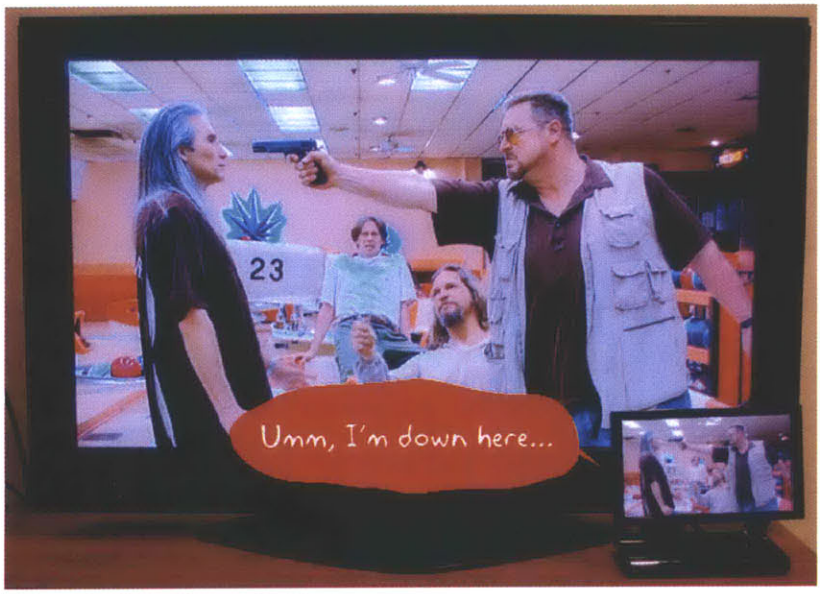


Figure 1-13: Size comparison of the first commercial 11-inch OLED TV to a 50-inch commercial plasma display. [4]

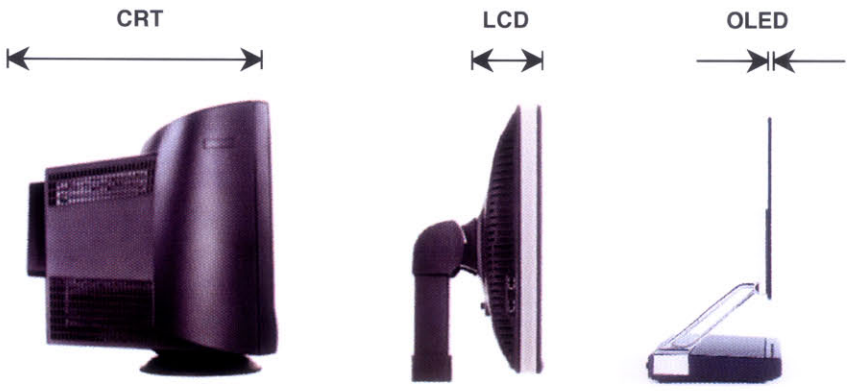


Figure 1-14: Thickness evolution from CRT, LCD, to OLED Display

### 1.4.3 Outlook

It took LCDs $30^{+}$ years from the introduction of its first commercial display to replace CRTs as the dominant display technology. The advantage of LCD over CRT is higher efficiency and ability to be lightweight and thin [58]. Today, OLEDs have the same advantages over LCDs that LCDs once had over CRTs. Figure 1-14 shows the evolution in display thickness from CRT, LCD, to an OLED display. In addition, OLED displays have the advantage of being an emissive technology with good color saturation. Recent reports claim that Sony aims to produce a 20-inch commercial OLED display in 2009 while Sharp does not have any OLED production plans in the near future, adopting the view that LCD technology will remain dominant for at least the next ten years [59]. Although industry views differ on opinions of OLED technology in displays, it is clear that the question is not *whether* but rather *when* OLEDs will become the next dominant display technology.

# Chapter 2

# OLED Stability

## 2.1 Introduction

The primary problem with using OLEDs in displays is the change of their external quantum efficiency with operation, which limits the usable lifetime and quality of a display. This section begins by explaining degradation mechanisms, the main problem with OLED stability. Also covered in this section are other stability issues from temperature, variation in organic film thickness, and threshold voltage shift of thin film transistors with operation, which also affect OLED stability in displays.

## 2.2 Degradation

Degradation occurs when materials undergo a chemical reaction to produce products that inhibit luminescence. This occurs in OLEDs with exposure to oxygen and moisture which results in cathode reaction and delamination or organic reaction and production of non-emissive organic species [17] [60]. During operation, degradation is exacerbated with the production of heat and charged organic molecules that favor chemical reactions leading to more stable, non-emissive products [61] [12]. Improvement in OLED lifetime generally comes with increasing efficiency of the device, which results in lower operating currents, less heating, and less charging of molecules during operation.

### 2.2.1 Extrinsic degradation

Extrinsic degradation occurs as a loss of emissive area of the device. In early days of the OLED technology, this was the primary degradation mechanism with a time constant as short as minutes. Extrinsic degradation starts at a single point on the device, called a nucleation site, and grows in size with OLED operation. Eventually, these dark, non-emissive spots take over the emissive area of the device, and the OLED stops emitting light. Figure 2-1 shows this process occurring for magnesium electrodes operated in 100% humidity.

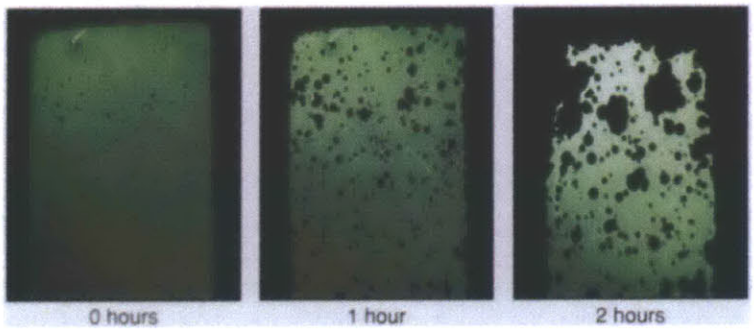


Figure 2-1: Extrinsic degradation in OLEDs with Mg electrodes operated under 100% humidity [5]

Nucleation sites on the OLED structure are introduced during substrate processing, ITO deposition, and organic or cathode deposition [7] [62] [63]. These defect sites allow oxygen and moisture to penetrate into the structure and accelerate the degradation process. Figure 2-2 shows a rough depiction of a nucleation site and an example of their introduction from either the cathode or from the anode or substrate. Nucleation sites can be observable before device operation. For example, grain clusters from cathode deposition are usually less than 1 $\mu$m in size and can be easily identified before a dark spot appears with operation [64]. However, nucleation sites can also be unobservable before the device is operated, but allow for high current passage so that they appear after the device is operated [65].

The loss of luminance in extrinsic degradation comes primarily from losing electrical contact with the cathode. From a nucleation site, enhanced exposure to oxygen

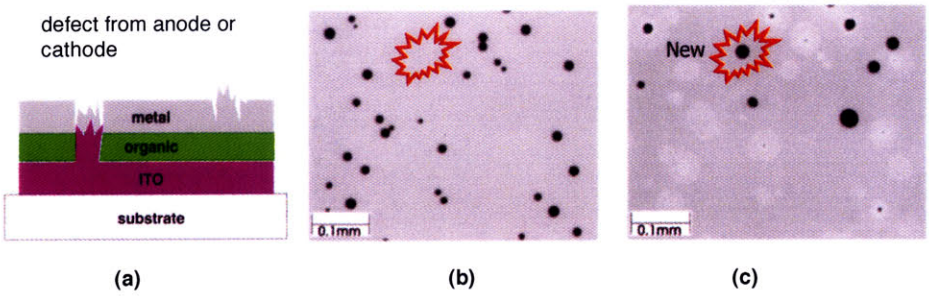


Figure 2-2: (a) Nucleation sites are introduced from anode or cathode deposition. (b) OLED is aged and shows resulting dark spots. (c) After cathode is removed and redeposited, the OLED is aged again and reveals new dark spots, demonstrating introduction of nucleation sites through cathode deposition. Some old dark spots reappear with a fresh cathode, demonstrating nucleation site from the organicl anode or substrate. [6]

or moisture and heating from high current passage result in chemical reactions that produce gas, causing the cathode to delaminate from the OLED. A magnesium cathode reacts strongly with water, as demonstrated in Figure 2-1. Operating condition of 100% humidity induces growth of dark spots in hours while little or no growth is observed under dry oxygen or nitrogen conditions [5]. For an aluminum cathode, reaction with oxygen produces hydrogen or oxygen gas which cause cathode bubbles to form on their release. Figure 2-3 demonstrates aluminum cathode delamination from an OLED and the proposed chemical reaction. In addition, cathode reaction with moisture or oxygen can also produce metal oxides or metal hydroxide species that are non-conductive [7] [66]. Localized heating from nucleation sites can also accelerate inter-diffusion of materials, crystallization of organic material leading to cathode delamination, and formation of non-emissive products that quench luminescence [67] [9] [8]. Figure 2-4 shows chemical reactions of Alq3 with water and oxygen to produce non-emissive species as well as an example of crystalline growth of Alq3 from an originally amorphous film.

Extrinsic degradation has been controlled by decreasing nucleation sites, creating more stable organic materials, and limiting exposure to oxygen and moisture. Insertion of a buffer layer on top of ITO can increase adhesion between organic and inorganic layers and smooth surface defects to reduce nucleation sites for dark spot

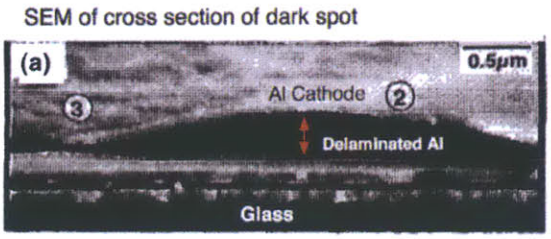


Figure 2-3: (a) SEM of delaminated aluminum cathode and (b) chemical reaction to produce non-conductive electrode. [7]

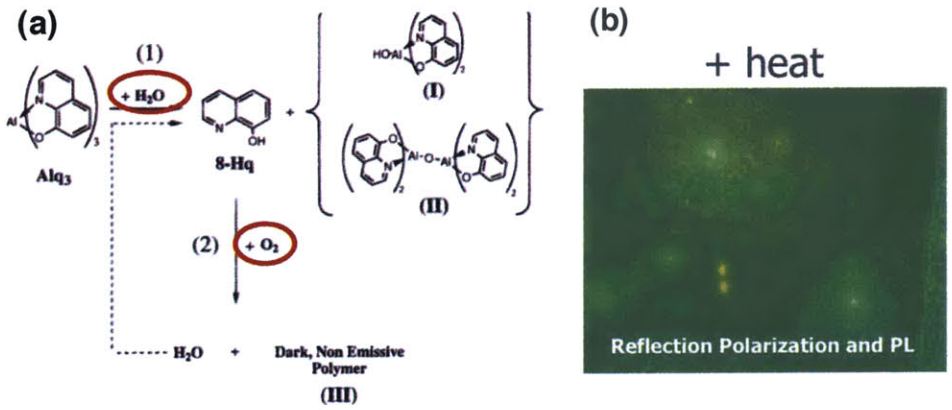


Figure 2-4: (a) Organic crystallization mechanisms [8] and (b) optical microscope photoluminescence (PL) image of crystallized organic. [9]

defects [68] [69]. New hole transporting materials have been developed with high thermal glass transition temperature to resist crystallization and show greater longevity under elevated temperature driving conditions [70] [71] [72] [73]. Finally, hermetically sealed encapsulation or multilayer coatings prevent oxygen and moisture from reaching sensitive cathode or organic materials in the OLED stack [17] [74]. These preventative measures, as shown in Figure 2-5, have shown orders of magnitude increase in OLED lifetime. Although there are still packaging issues for extrinsic degradation, particularly with flexible displays, the mechanism for extrinsic degradation is thought to be a well-controlled and understood process.

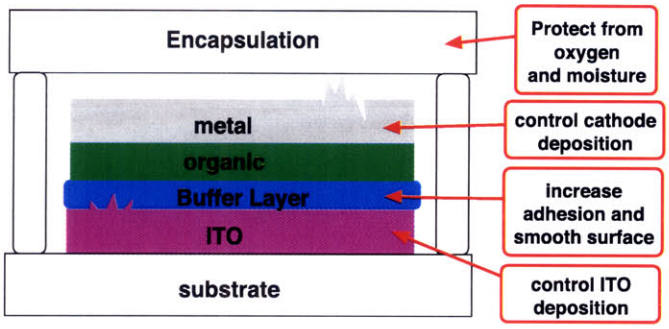


Figure 2-5: Encapsulation and careful control of deposition parameters for combating extrinsic degradation in OLEDs.

### 2.2.2 Intrinsic degradation

Unlike extrinsic degradation, the problems with intrinsic degradation are more elusive, largely material dependent and harder to solve. Intrinsic degradation manifests itself as a gradual decrease in quantum efficiency during device operation. The expression for external quantum efficiency can be expressed in terms of the major factors leading to production of light in an OLED, shown in Equation 2.1.

$$\eta_\phi(external) = \gamma * \beta * \phi_{pl} * \chi \tag{2.1}$$

Here $\gamma$ is the charge balance fraction, $\beta$ is the fraction of emissive excitons, $\phi_{pl}$ is the PL efficiency, and $\chi$ is the light out coupling fraction. The decrease in quantum efficiency during operation can be associated with reduction of any of these parameters. Improving the initial quantum efficiency of the device generally reduces the rate of intrinsic degradation. Because intrinsic degradation is largely material dependent, the majority of intrinsic degradation studies involve Alq3, a common emitter and electron transport layer.

Intrinsic degradation is a direct result of operating an OLED, or injecting charge into the device. To understand the mechanism of intrinsic decay it is important to understand how charge is distributed in the OLED device. One way to probe charge distribution is through capacitance-voltage (CV) measurements, as shown in Figure 2-6. For typical bilayer structures, two well-defined capacitances can be measured:

one associated with the total organic layer thickness and the other with the Alq3 layer thickness. When a large negative bias is applied to the OLED, the capacitance of the device is related to the total thickness of the organic layer as shown in Figure 2-7a. This is the state in which neither the hole nor electron transport layer conducts charge, and the charge buildup is at the electrodes of the device, sandwiching the total organic thickness. As the negative bias is decreased and turns positive, the capacitance eventually increases to one related to the Alq3 layer thickness, as shown in Figure 2-7b. In this case, the anode is able to inject holes into the device but the cathode is unable to inject electrons into the device. Therefore, the charge distribution in the device consists of a positive charge buildup at the interface and negative charge buildup at the cathode which sandwiches the Alq3 layer. At higher biases, this tendency still exists because of the large difference in carrier mobility ($\mu_{h,NPB} >> \mu_{e,Alq3} >> \mu_{h,Alq3}$), implying a charge imbalance that favors a buildup of positive charge at the heterojunction interface.

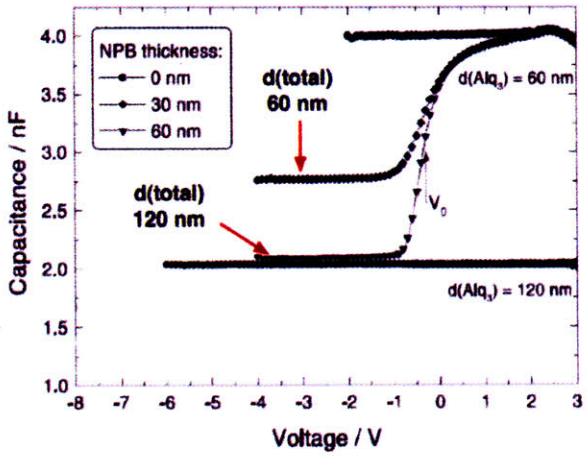


Figure 2-6: Capacitance-voltage measurements show a capacitance dependent on total organic layer thickness for large negative bias and a capacitance dependent on the Alq3 layer thickness at higher biases. [10]

Several studies show that improving $\gamma$, the charge balance fraction in the quantum efficiency expression, which also reduces the positive charge buildup at the interface for bilayer devices, decreases the rate of OLED degradation. This can be achieved by

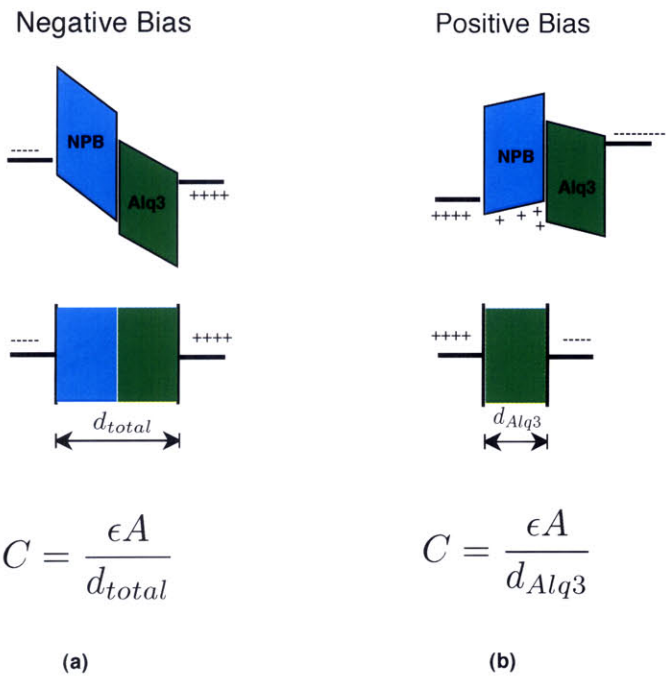


Figure 2-7: Energy band diagram of a bilayer device, capacitor view, and capacitance expression under (a) reverse and (b) forward bias.

reducing the hole mobility of the HTL, increasing hole injection barrier, or decreasing electron injection barrier in an OLED [75] [76] [77]. In addition, mixed-emitter layer devices have been developed to remove the interface of the bilayer device. A mixed-emitter device is fabricated by simultaneously depositing the hole and electron transport layer as the emitting layer of the device. This structure allows charge carriers to sit on their preferred molecule when they reach the emitting layer of the OLED and extending the lifetime of these devices[78] [79].

While studies demonstrate that improving $\gamma$ in an OLED or can reduce the degradation rate, this factor is not largely responsible for the decrease of quantum efficiency during device operation. Figure 2-8a shows that for Alq3 emitting device, the decrease in quantum efficiency during operation is primarily caused by a decrease in $\phi_{pl}$. A time resolved measurement on Alq3 fluorescence is shown in Figure 2-8b, demonstrating a reduction in the fluorescent lifetime of an aged device [80] [11]. Further investigation reveals that hole transport through Alq3 is primarily responsible for the decrease in $\phi_{pl}$. By sandwiching a thin AlQ3 layer between electron transporting or

hole transporting material, a primarily electron or hole transporting device can be created. Running these devices at the same current results in noticable $\phi_{pl}$ degradation in the primarily hole transporting device over the time period as shown in Figure 2-9 [12].

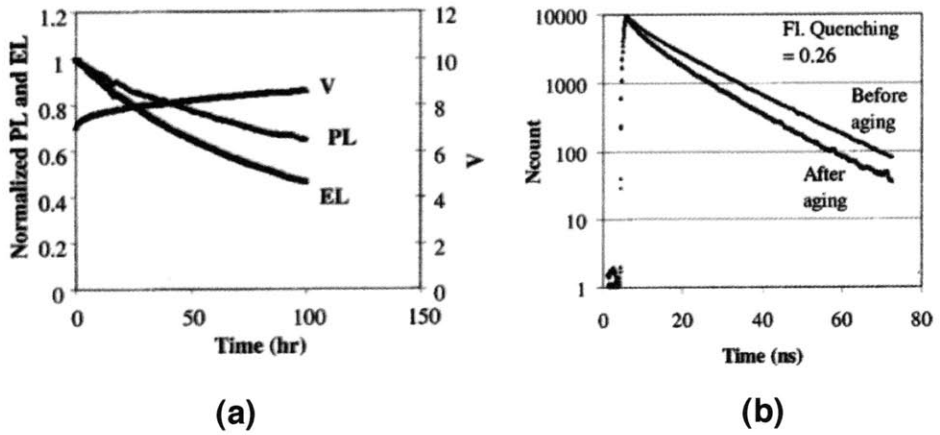


Figure 2-8: (a) Simultaneous EL and PL decrease for Alq3 emitter during device operation at constant current driving conditions and (b) decrease in PL lifetime for Alq3. [11]

The proposed mechanism to explain the decrease in $\phi_{pl}$ is formation of an unstable cationic species that react more readily to form fluorescence quenchers. This theory is supported by a study that neutral Alq3 requires 24.2 $Kcal\ mol^{-1}$ to react with water while cationic Alq3 only requires 9.5 $Kcal\ mol^{-1}$ [81]. This reduced reaction energy for cationic Alq3 suggests why intrinsic degradation is enhanced by positively charging Alq3 molecules. Although one might argue that a good packaging scheme can reduce the existence of water in the OLED, residual water exists in the structure from fabrication and has been shown to have a large effect on the lifetime of OLEDs. The amount of residual water in the device can be controlled by changing the pressure at which the device is grown. Under ultra-high vacuum conditions, less water is introduced into the device at $10^{-8}$ $torr$ than $10^{-7}$ $torr$. The initial current-luminance characteristics were the same for these devices, yet the half-life of the devices grown under higher vacuum had an increase of half-life by an order of magnitude when operated under the same conditions [82].

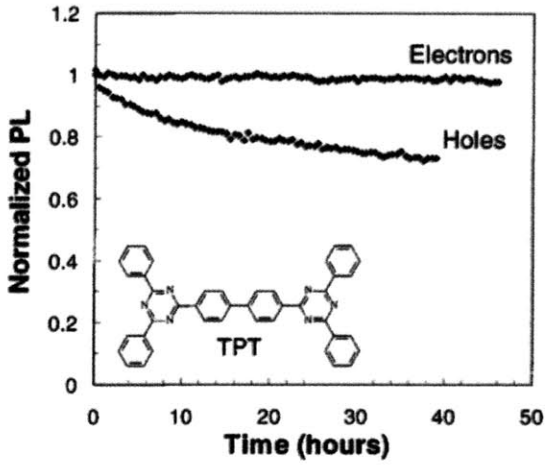


Figure 2-9: Alq3 insertion in hole (NPB) and electron transporting (TPT) material demonstrate that PL degradation is evident in the primarily hole transporting device. [12]

Other factors which can explain a gradual decrease in quantum efficiency with operation is mobile ion migration, as illustrated in Figure 2-10. Mobile ions exist in OLEDs as impurities from fabrication or metals from electrodes. During device operation, the applied electric field causes the ions to migrate across the organic, reducing the effective field across the device. To maintain the same current, assuming bulk-limited transport, increasing voltage has to be applied. Other mechanisms such as trap filling have also been proposed to explain the voltage increase, since the filling of traps would also require and increase in voltage to support the same current. However, experiments show that the increase in voltage is accelerated when the OLEDs are aged at higher temperatures. A trap-filling mechanism would show slower voltage increase because thermal energy is available to free the trapped carriers. Mobile ions, however, would have increased mobilities at elevated temperature, accelerating ion migration [83]. Figure 2-11 demonstrates temperature dependent voltage increase. Additional evidence to support mobile ion migration comes from voltage recovery, the decrease in voltage that is observed after an operating OLED is left unbiased for a period of time. Voltage recovery is accelerated with applied negative bias, and occurs over hundreds of hours, which cannot be explained by trapping mechanisms

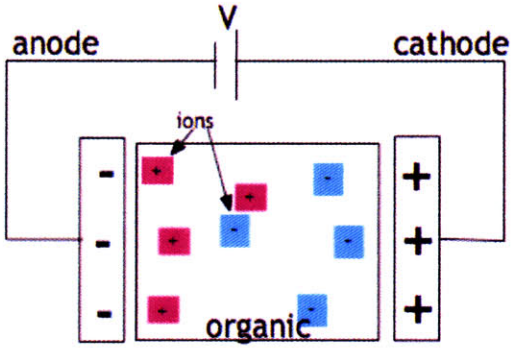


Figure 2-10: Mobile ion migration due to applied field during operation.

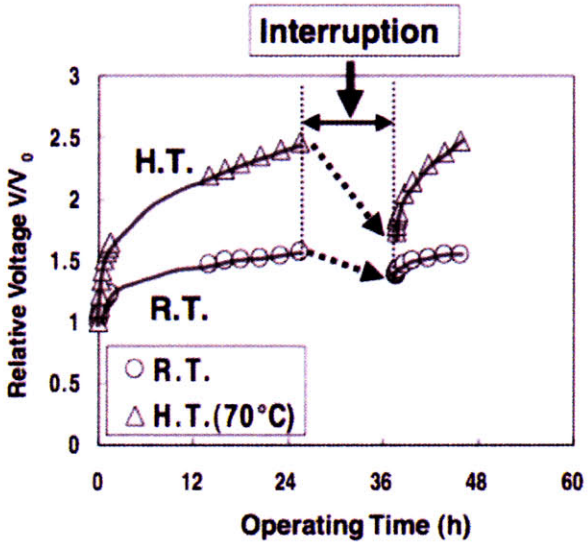


Figure 2-11: Voltage shift and recovery is accelerated at elevated temperatures.

that operate on shorter time scales [84]. Evidence of mobile ions have been found in aged devices by using secondary ion mass spectroscopy (SIMS). One study aged an OLED to half-life and then compared the composition of the aged OLED to an unaged OLED, showing the existence of indium closer to the cathode for an aged device than the unaged device. The SIMS setup and results of this study is shown in Figure 2-12. In addition, doping Alq3 with indium results in a drop in EL efficiency, especially when the doping occurs at the the interface of Alq3 and NPB [85]. Mobile ion migration can be mitigated by adding a buffer layer to reduce diffusion of indium ions [86] [87], and using a pulsed or alternate current to reduce diffusion of mobile ions [88] [89] [90] [91].

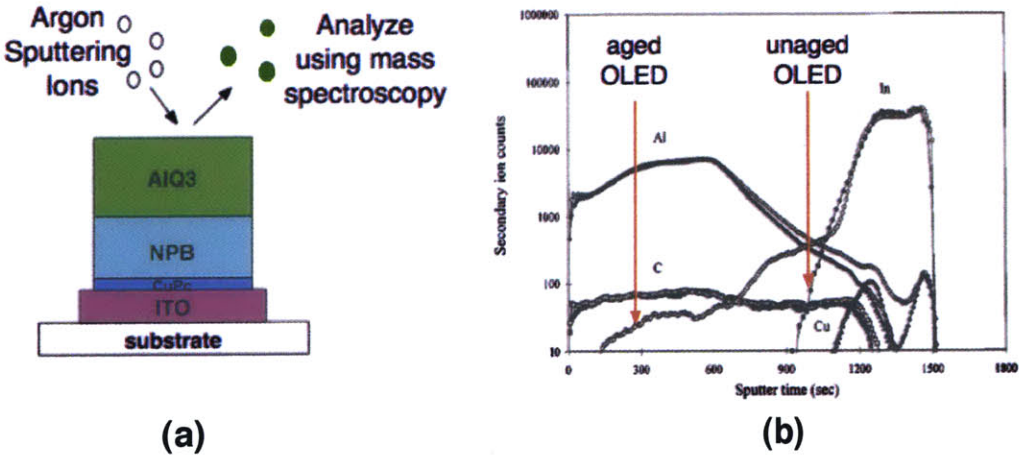


Figure 2-12: (a) Secondary mass ion spectroscopy is a destructive analysis technique (b) Results that show the presence of indium in an aged device before an unaged device, indicating presence of indium closer to the cathode.

The remaining components of the quantum efficiency expression which have not yet been discussed are the fraction of emissive excitons, $\beta$, and the light outcoupling fraction, $\chi$. Improving $\beta$ can be done by introducing a phosphorescent emitter. Using a phosphorescent emitter improves both $\beta$ and $\phi_{pl}$. Increasing the $\beta$ means reducing possible non-emissive pathways that are available with fluorescent emitters, which reduces generation of heat during operation. The heat reduction decreases the energy available for reactions that can lead to non-emissive products. In addition, increasing

$\phi_{pl}$ means that a device can run at lower currents, also reducing the amount of charge introduced in the device, and therefore the likelihood of unfavorably charged species as well as heat evolution. Indeed, phosphorescent devices are known to have the longest lifetimes [92].

Finally, improving the out coupling fraction, $\chi$, could decrease the amount of degradation by running the device at lower currents for the same brightness. However, it is difficult to increase this factor. Some techniques include trying to out-couple the light with a lens which has also been shown to compromise the image quality [93].

## 2.3 Other sources of instability

Even if OLED degradation issues are mitigated through materials and device structure advancements, yielding suitable lifetimes, OLED displays can exhibit additional sources of instability: temperature-dependent current-voltage characteristics, non-linear relationship between efficiency and current, non-uniform thickness of organic layer, and threshold voltage shift of pixel drivers. These additional sources of instability compromise the quality of the display and can possibly reduce the effective lifetime of the display.

### 2.3.1 Temperature dependent characteristics

OLEDs have highly non-linear current voltage characteristics which is explained by trap charge limited (TCL) conduction. Organic materials have low intrinsic carrier concentration, and carrier concentration in the device depends on charge injection from electrodes. Many trap states exist in the OLED because of the amorphous organic material and interfaces in the device structure. These trap states initially outnumber the injected carriers for low voltages, so that the injected carriers first fill the trap states and little current passes through the OLED. As the voltage increases, the injected carriers eventually fill up the trap states, leading to an abrupt rise in current once this happens. As a result, the OLED has highly nonlinear current voltage characteristics and a temperature dependence in the exponent of the voltage

[13] [94]. Figure 2-13 show current voltage dependence on temperature for fluorescent and phosphorescent OLEDs. As OLED displays are built on glass substrates, the poor thermal conductance of glass can result in uneven convection cooling of the display plane contributing to temperature gradients across the display surface, which increases with larger display area [95].

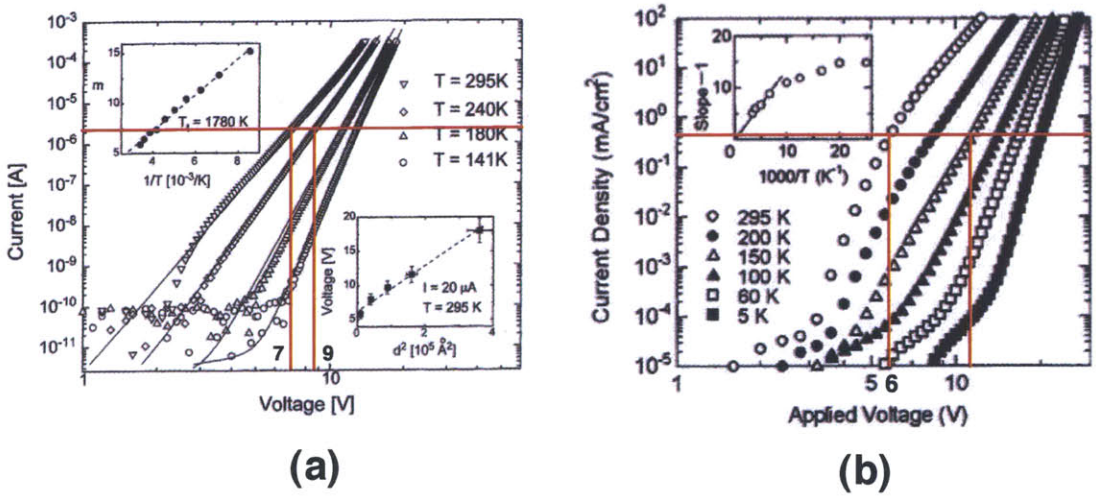


Figure 2-13: Horizontal line represents current which produces 100 cd/m$^2$ brightness. Current vs voltage temperature dependent characteristics of (a) fluorescent [13] and (b) phosphorescent OLED. [14]

Fluorescent OLEDs have temperature dependent quantum efficiencies which increase with decreasing temperature. This is due primarily to an increase of photoluminescence efficiency, $\phi_{pl}$ of the emissive species because of reduced non-radiative pathways at lower temperatures. Phosphorescent OLEDs are known to have stable $\phi_{pl}$ relationship with temperature, but still have a temperature dependency from change in carrier mobilities of the organic layers or change in location of recombination region which affect the charge balance fraction or light outcoupling fraction [14]. Figure 2-14 shows quantum efficiency dependency on temperature for typical flourescent and phosphorescent OLEDs.

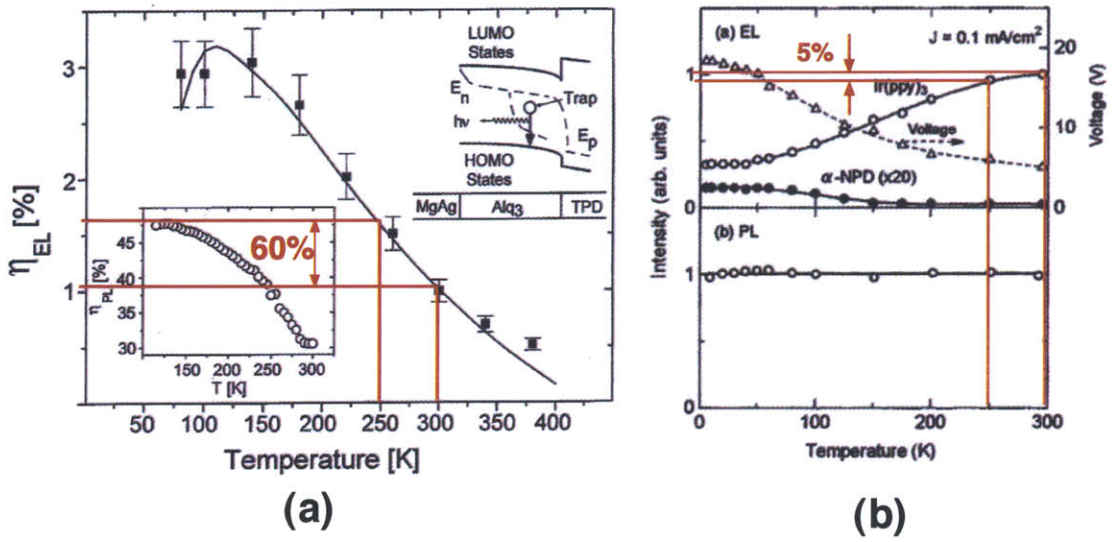


Figure 2-14: (a) A 60% change in quantum efficiency for fluorescent OLED with 50 K change in temperature. [13] (b) A 5% change in quantum efficiency for phosphorescent OLED with 50 K change in temperature. [14]

### 2.3.2 Current dependent quantum efficiency

OLED efficiency also changes non-linearly with increasing drive current due to exciton-exciton and exciton-polaron annihilation, complicating the linear scaling of pixel brightness with current. These effects are most pronounced in phosphorescent OLEDs with long-lived excitons [15]. Figure 2-15 shows this dependence for phosphorescent devices.

### 2.3.3 Organic thickness dependency

Thickness uniformity of OLED charge transport and luminescent layers of OLEDs is more difficult to maintain across large area substrates, and can also affect the brightness uniformity of a display [96]. Figure 2-16 shows how a blanket deposition of organic over a large area substrate can vary with distance from the source.

The deposition thickness $d$ can be expressed as

$$d = \frac{M_e \cos\phi}{4\pi\rho r^2} \tag{2.2}$$

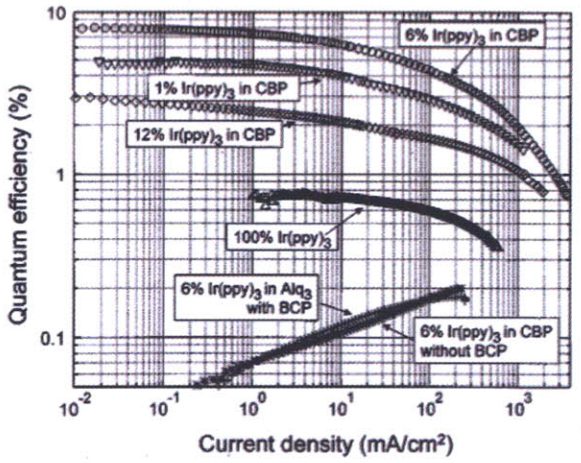


Figure 2-15: Decrease in quantum efficiency with increasing current density for some phosphorescent OLEDs. [15]

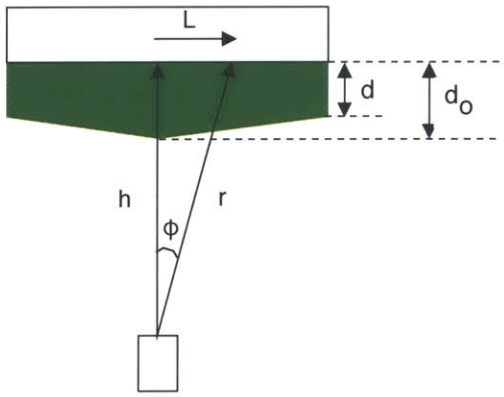


Figure 2-16: Deposition geometry for a substrate. [16]

and the ratio of the deposition thickness at any position $d$ to that at the center $d_o$ is approximately

$$\frac{d}{d_o} = \frac{1}{[1+(L/h)^2]^2} \tag{2.3}$$

. Figure 2-17 shows the dependency of voltage and quantum efficiency due to variation of the organic layer thickness. To keep the quantum efficiency variation low, Alq3 thickness should not vary more than 5%. Assuming a thickness of 40 nm, the variation should not be more than 2 nm. This places a restriction in the L/h ratio to 0.16. For a 100 inch display, the throw distance from the source to the substrate has to be increased to about 800 inches. Being a difficult requirement to meet, the uniformity

of the organic thickness will likely be compromised, although there are fabrication solutions which can mitigate this problem with added complexity and cost.

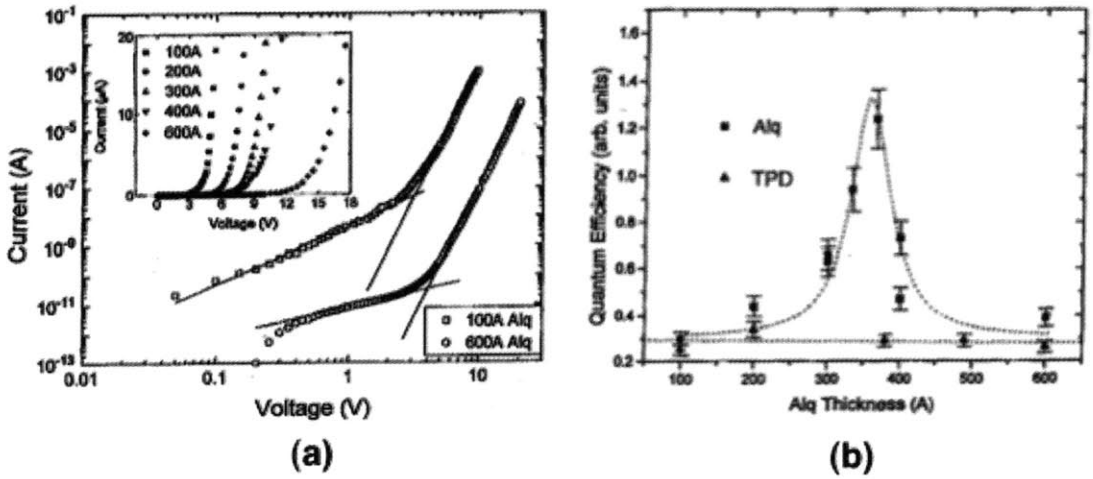


Figure 2-17: Dependency on organic thickness for (a) voltage (b) quantum efficiency [17]

### 2.3.4 Threshold voltage

The thin film transistors (TFT)s that drive OLED pixels also have stability problems, which affect the stability of the display. Poly-silicon TFTs have been considered a good candidate for the pixel drivers because of their ability to support high current. However, the excimer laser annealing process that is used to make the TFTs is hard to control over large areas, and threshold voltage of TFTs can vary from transistor to transistor across a substrate. Amorphous-silicon (a-Si) TFTs have a less of a problem with transistor to transistor variation in threshold voltage across a substrate. However, a-Si TFTs do have a threshold voltage shift with operation. This ultimately affects the brightness of the OLED pixel and has a detrimental affect on OLED display stability. More complex driving circuits with a-Si have been made to address the problem of threshold voltage shift so that it is less of a problem in displays [97].

## 2.4 Outlook

OLED lifetimes are limited by blue devices, with approximately 30,000 hours in half-life. While it may be possible to extend the blue OLED half-life through improvements in device structures or better materials, there are other stability issues due to variation in organic film thickness, threshold voltage of TFTs, and ambient temperature. Table 2.1 summarizes some of the key stability issues for typical OLEDs. Optical feedback, discussed in the next chapter, is likely the only method of simultaneously correcting for all sources of brightness non-uniformities in OLED displays.

| (a) | Change in pixel brightness xx% | | | |
|---|---|---|---|---|
| | 0.1% | 1% | 5% | 10% |
| at constant current as a function of time | 30 h | 320 h | 1700 h | 3900 h |
| at constant voltage with temperature change | 0.026°C | 0.26°C | 1.3°C | 2.8°C |

| (b) | Change in voltage | | | |
|---|---|---|---|---|
| | 1 V | 2 V | 3 V | |
| ETL thickness xx nm | 15 nm | 30 nm | 45 nm | |
| at constant current with temperature change | 24°C | 46°C | 66°C | |

Table 2.1: (a) Change in pixel brightness with time for phosphorescent OLEDs under constant current aging with initial brightness 100 cd/m$^2$, assuming a half-life of 50,000 hours. [18] Also shown is change in pixel brightness for fluorescent OLEDs at constant voltage aging for change in temperature change above ambient. These OLEDs have I-V characteristics of the form ($I\alpha V^{m+1}$) with $m = T_t/T$, $T_t = 1780 \pm 50$ K, and T = temperature. [13] (b) Change in voltage from variation in thickness of the ETL for a typical Alq3-TPD OLED. [31] Also shown is change in voltage from constant current driven fluorescent OLEDs with temperature change above ambient. These OLEDs have the same I-V characteristics of the form ($I\alpha V^{m+1}$) with $m = T_t/T$, $T_t = 1780 \pm 50$ K, and T = temperature. [13]

# Chapter 3

# Optical feedback solution

## 3.1 Introduction

OLED lifetime is typically characterized by half-life ($t_{0.5}$) at constant drive current, the time it takes to age an OLED to 50% of its initial brightness. Although half-life is a useful metric in comparing different OLED structures, higher luminescence output precision is needed for an OLED display. An active matrix display in which OLEDs are emissive pixels has a much lower tolerance for degradation due to the high sensitivity of a human eye to detect a contrast between neighboring pixels. Optical feedback can correct for pixel non-uniformities in either active matrix or passive matrix displays. In addition to compensating for OLED non-uniformities due to pixel aging, optical feedback also corrects for other pixel imperfections, such as variations in pixel-to-pixel driver electronics of active matrix backplanes, and variable resistance of bus lines in passive matrix displays.

## 3.2 Display lifetime

Stability of pixel brightness in information displays is necessitated by the high sensitivity of human vision to brightness variation [34] [98], with an average human eye capable of distinguishing a 2% difference in relative intensity of neighboring pixels [99]. The conventionally stated metric of OLED half-life, $t_{0.5}$ is therefore unsuitable

for evaluating viability of particular OLED technology in information displays that contain large numbers of neighboring pixels that degrade different amounts according to usage. Consequently, OLED display lifetime is defined as a conservative estimate of $t_{0.98}$, the time it takes an OLED pixel to degrade to 98% of its initial brightness, when operated under constant current conditions.

The stretched exponential decay has recently been used for accurately fitting the shape of particular OLED degradation curves [100] and is shown as follows

$$L = L_o \exp[-(\frac{t}{\tau})^{\beta}] \tag{3.1}$$

where $L$ is the luminance, $L_o$ is the initial luminance, $\tau$ is dependent on the driving conditions, and $\beta$ is dependent on a particular device structure. The relationship between $t_{0.98}$ and $t_{0.5}$ can then be written as

$$t_{0.98} = t_{0.5}(\frac{ln(0.98)}{ln(0.5)})^{1/\beta} \tag{3.2}$$

for the single exponential decay and for the stretched exponential decay. In this analysis, $\beta = 1$ is used in equation 3.2 to compute the lower limit for the required OLED half-life. Figure 3-1 plots the relationship between $t_{0.98}$, $t_{0.97}$, $t_{0.95}$, and $t_{0.5}$, assuming that the OLED luminescence efficiency degrades as an inverse exponential of the operating time.

Therefore, displays with 2% brightness accuracy over 10,000 hours of operation require OLEDs with $t_{0.5} > 343{,}000$ hours (which we calculated by setting $t_{0.98} = 10{,}000$ in the above expression). Displays with more relaxed brightness accuracy condition, allowing for 3% or 5% brightness non-uniformity, require OLEDs with $t_{0.5} > 227{,}000$ hours and $t_{0.5} > 135{,}000$ hours, respectively. Recently published data on phosphorescent OLEDs shows that $t_{0.5}$ has been extended to over 100,000 hours for yellow-green and deep-red devices operated at video brightness [30], [101]. However, the shorter blue half-life does not meet even the more relaxed half-life requirements. Also, note that setting $\beta < 1$ necessitates OLEDs with longer $t_{0.5}$. For example, with the green phosphorescent devices analyzed in this study [18], average $\beta$ for

accelerated aging conditions is 0.76 which requires $t_{0.5}$ >1,000,000 hours to maintain 2% brightness accuracy over 10,000 hours.

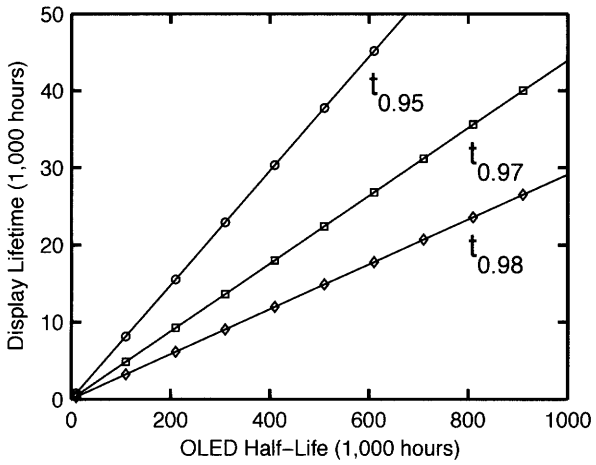


Figure 3-1: OLED display lifetime, defined as uniformity within 2% ($t_{0.98}$), 3% ($t_{0.97}$) or 5% ($t_{0.95}$) of initial luminance, for a given OLED half-life, $t_{0.5}$ with $\beta = 1$.

If OLEDs are to be used as pixel elements in information displays with 10,000 hours of stable operating lifetime, $t_{0.5}$ has to be extended beyond 300,000 hours. To date, only a handful of red OLED structures [30] show such long $t_{0.5}$, implying a significant challenge to the viability of OLEDs in long-lived, high color quality information displays.

## 3.3 Optical feedback solutions

### 3.3.1 Constant current

Philips research lab have developed a constant current optical feedback solution for extending OLED display lifetime [102] [103]. Figure 3-2 shows the basic circuit and display lifetime extension of this optical feedback technique. In this solution the OLED is operated at high brightness for some fraction of the picture frame cycle, which is slowly extended as the OLED pixel ages. OLED pixels are driven at a high constant current with a photo-transistor circuit monitoring and integrating the light

output which is then compared to the desired output luminance. When the target output luminance is reached, the OLED is turned off. The useful display operating lifetime is reached when an OLED pixel needs to stay turned on for times longer than the entire frame cycle. Therefore, the initial OLED driving conditions and display refresh rate ultimately limit the achievable display lifetime. This optical feedback solution also requires OLED pixel operation at high constant currents, an operating regime that reduces the quantum efficiency and power efficiency of OLED pixels. Lower power efficiency and higher current operation also raises the fraction of power that contributes towards heating of the display, with higher temperatures resulting in accelerated device degradation [104].

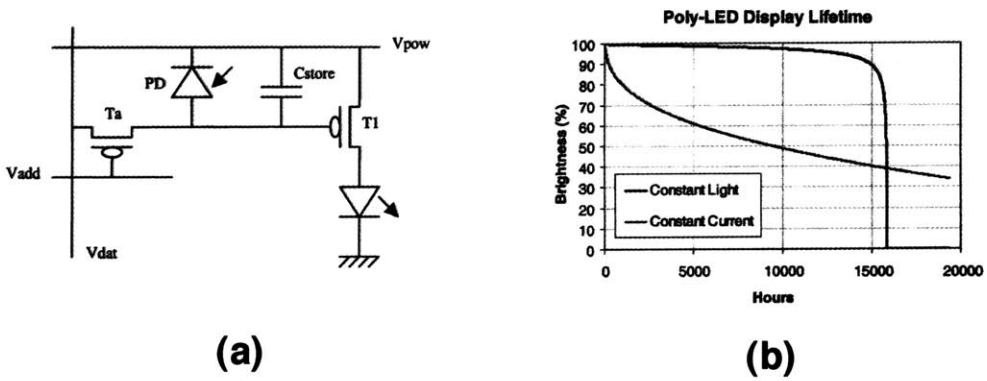


Figure 3-2: Philips Research Lab constant current optical feedback solution: (a) Feedback circuit and (b) display lifetime extension.

### 3.3.2 Adjustable current

The solution proposed in this thesis is a current-correcting optical feedback technique in which the drive current is adjusted to achieve the desired luminescence output [105] [106]. Figure 3-3 shows the basic feedback circuit and display lifetime extension of this optical feedback technique. As the pixels age with use, the drive current that is required to produce video brightness increases. The useful display lifetime is therefore determined by the ability of an aged OLED pixel to produce video brightness given appropriate drive current and voltage. An additional limit is set by the maximum

voltage and current that can be supplied by the drive electronics. In comparison to the optical feedback scheme described in the previous paragraph, our optical compensation method does not overdrive OLED pixels, as the pixels are turned-on during the entire picture-frame cycle. The useful operating lifetime of an OLED display that utilizes our feedback scheme can be projected by analyzing OLED efficiency degradation curves at variable drive currents.

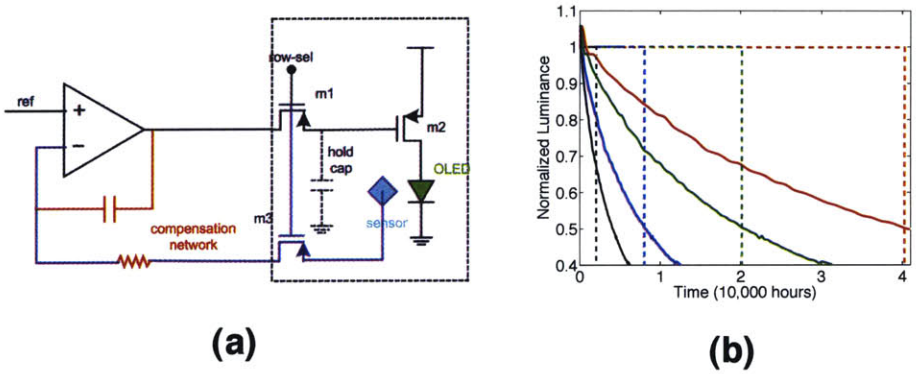


Figure 3-3: MIT current-correcting optical feedback solution: (a) Feedback circuit and (b) display lifetime extension.

A set of data on performance degradation in high quality OLEDs, published by Kwong et al. [18] of Universal Display Corporation and reproduced in Figure 3-4, shows aging data points of three identical phosphorescent OLED pixels at three different initial brightnesses. This data set projects a $t_{0.5}$ of 50,000 hours when operated at video brightness of 100 $cd/m^2$. For this device structure, the efficiency degradation is coulombic and depends on aggregate charge flow in the device [101]. This dependence can be seen by replotting the Kwong et al. data obtained at different initial brightnesses against charge and is shown in the inset of Figure 3-4a. The OLEDs aged at different drive currents to produce the initial brightness of 1000, 500, or 200 $cd/m^2$ converge to a single degradation curve when normalized efficiency is plotted against total charge that has passed through the devices. Therefore, the efficiency degradation of a device can be approximated by the amount of charge that has passed through the device.

In Figure 3-4 the device with initial brightness of 1000 $cd/m^2$ device is used to

predict the aging curves for devices with initial brightness of 100 , 200, or 500 $cd/m^2$. The plots of predicted aging for 200 $cd/m^2$ or 500 $cd/m^2$ initial brightness match well with the data obtained from measuring the aging of actual devices at these initial brightnesses. This technique can also be applied to simulate the required current for the current-correcting optical feedback. Starting with an initial brightness and drive current, the efficiency degradation is known and can be monitored until the brightness decreases to 98% of its initial value. The current is proportional to the brightness, so required increase in current is simply 1/0.98 of the initial current, roughly $1.02I_o$ where $I_o$ is the initial current. This process is repeated, following the efficiency degradation for the increased drive current.

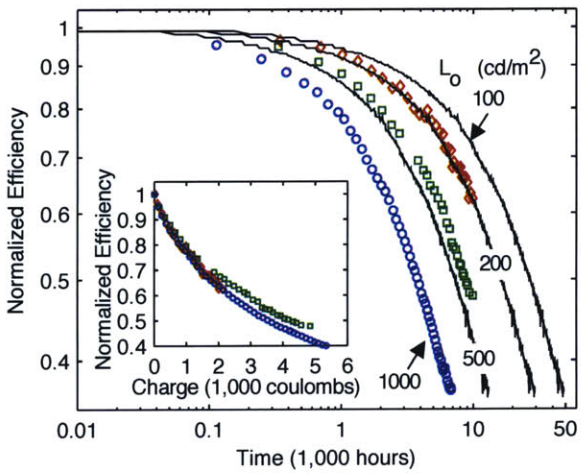


Figure 3-4: Luminance degradation of three identical phosphorescent OLEDs operated at different initial brightness (data points [18]) is compared to projections of luminance degradation (solid lines) determined by scaling the luminance output of the device that is operated at Lo = 1000 $cd/m^2$. The inset verifies that luminance degradation is related to total charge that passed through the devices.

Figure 3-5 shows the current and voltage required for constant brightness operation of an OLED, extrapolating from device of initial brightness of 1000 $cd/m^2$. For example, to maintain 100 $cd/m^2$ in such constant-brightness mode of operation, the OLED drive current will increase to twice the initial value after 20,000 hours of OLED operation. The increase in current will be accompanied by a rise in voltage across the device, which is plotted in the inset of Figure 3-5 for different constant-

brightness conditions and amounts to a 10% rise for 20,000 hours of operation at 100 $cd/m^2$. To operate the same device in constant 100 $cd/m^2$ brightness mode for 30,000 hours, the drive current would increase to three-times the initial current with 15% rise in voltage. These rise in voltages are estimated by using the initial current-voltage characteristics of the device. However, the current-voltage characteristics also change with time. Consequently, there is an estimated maximum of 25% error in the stated projected voltage rise.

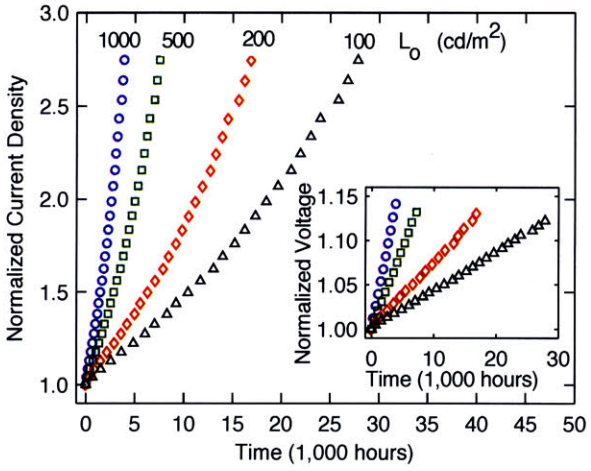


Figure 3-5: Normalized drive current needed to maintain constant brightness using optical feedback. Inset shows corresponding normalized drive voltage.

In contrast, OLEDs operated in the constant current mode at video brightness with no optical-feedback compensation would lose 2% of their brightness accuracy after 300 hours of operation, and 5% of their brightness accuracy after 900 hours. From this example, it is evident that large gains in utility of OLED displays can be gained by implementing optical feedback.

## 3.4 Edge Emitted Light

The proposed optical feedback solution can be realized by growing a transparent organic LED [107] [108] pixel on top of silicon photodetectors, as has previously been suggested[106]. However, the optical signal from each pixel can also be obtained by

measuring the light emitted from the edge of the glass substrate on which OLEDs are grown [109] [110] [111]. Figure 3-6 shows both of these configurations.

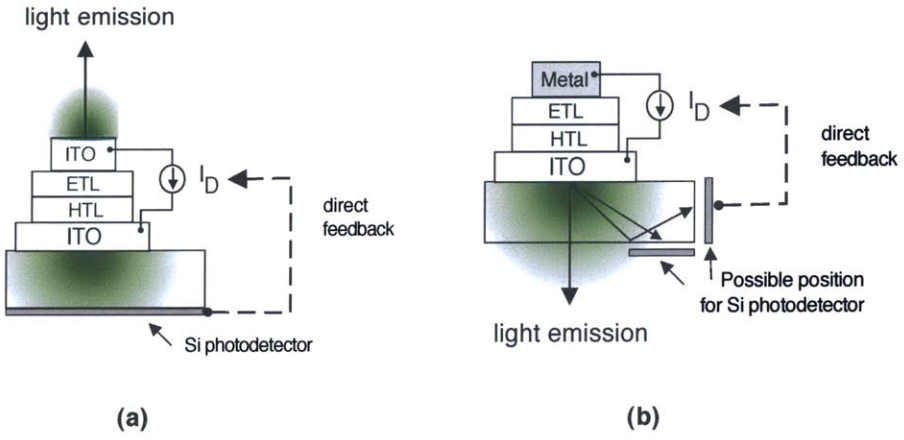


Figure 3-6: (a) Proposed structure for MIT optical feedback with transparent OLED structure or (b) with regular OLED structure utilizing edge emitted light.

The edge emitted light in a display can be explained by Snell's Law, as shown in Figure 3-7 which describes the pathway of light through different mediums. Equation 3.3 applies Snell's Law for the glass and air interface of an OLED display to solve for the case in which light gets trapped in the display. The index of refraction of glass, $n_{glass}$, is 1.5 while $n_{air} = 1$, and light is trapped when $\theta_{air}$ becomes greater than 90°. Thus, total internal reflection occurs with any light emitted at an angle greater than $\theta_{critical}$ to the normal surface. However, this internal light can be captured by placing a photodetector on the edge of the glass with an index matching material.

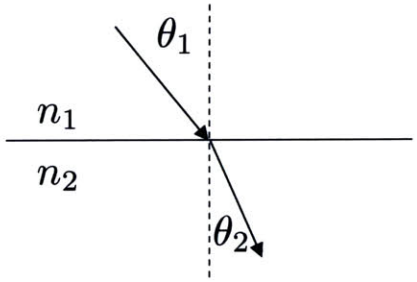


$$n_1 sin\theta_1 = n_2 sin\theta_2$$

Figure 3-7: Depiction and Equation for Snell's Law

$$n_{air} * \sin(\theta_{air}) = n_{glass} * \sin(\theta_{glass}) \quad (3.3)$$

$$\theta_{critical} = \arcsin(1/1.5) \quad (3.4)$$

$$\theta_{critical} \approx 42^{\circ} \quad (3.5)$$

Analysis and measurement of the optical modes of an OLED [112] show that OLED pixel light intensity emitted from the edge of a substrate is comparable to the light intensity emitted through the front plane. Consequently, photodetectors mounted on the edges of the display can measure the light that is normally trapped in the glass substrate and provide intensity measurements to the optical feedback system. The ratio of the edge-emitted to the forward-emitted light is maintained as the device ages since the optical geometry of the OLED pixel is maintained throughout OLED use. The stability of the silicon photodetector exceeds OLED stability due to the atmospheric inertness of the covalently bonded single crystal silicon as compared to van der Waals bonded organic thin film structures comprising OLEDs. Additionally, the current density that passes through the photodetector is significantly smaller than the current density through the OLEDs by at least an order of magnitude, contributing to significantly slower charge-initiated degradation in the photodetector.

Use of edge-mounted detectors is accompanied by more complex calibration of the pixels. The intensity of the detected signal is inversely proportional to the distance away from the pixel. Figure 3-8a shows this dependency comes from a geometric relationship as the ratio of the detector length over the collection circumference of the pixel radiation. This is confirmed by optically exciting a spot on a glass substrate coated with a luminescent organic thin film and measuring the photocurrent from an edge detector, as shown in Figure 3-8b. This dependency can be used to calculate the fraction of edge-emitted light collected from each pixel on a display by a fixed detector size along one of the edges of the display in Figure 3-9. A change the intensity of the optical signal scales the detected output by the same factor.

Implementing the edge-emitted solution depends largely on the sensitivity of the

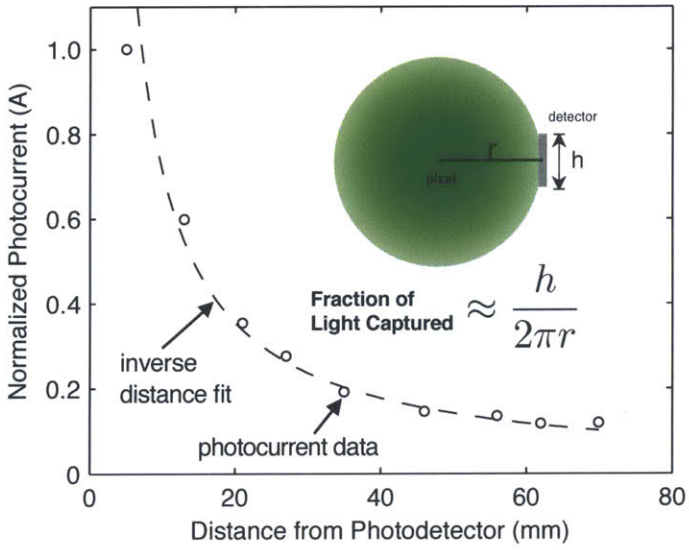


Figure 3-8: Edge emitted light captured from an OLED structure of glass/ITO/50 $nm$ Alq3/50 $nm$ Mg:Ag/ 100 $nm$ Ag excited by a 408 $nm$ laser is inversely proportional to distance from the detector. Cartoon image depicts the underlying geometrical dependence which explains this relationship.

photo detector. For example, an edge-detector with sensitivity of 0.3 $A/W$ spanning a 1920x1080 pixel OLED display on a 1 mm thick glass substrate with 100x100 $\mu m^2$ pixel size would capture 0.45 $nA$ photocurrent in the worst case scenario. This assumes that the pixel is emitting from a center-minimum geometry at 100 $cd/m^2$ and 555 $nm$ peak emission. The eye is less sensitive to red and blue light, therefore requiring more photon emission at those wavelengths to achieve video brightness. Assuming a dark current density of 1 $pA/mm^2$ implies 0.19 $nA$ of dark current signal, which is less than the detected signal in the worst case scenario. For lower resolution displays the photodetetector signal increases while the dark current signal is reduced, facilitating easier implementation of the proposed feedback scheme. Increasing display size changes pixel size by the square of the scaling factor while the detector area changes linearly by the scaling factor. Therefore, detected signal increases by the scale factor squared while the dark current increases only by the scale factor. Increasing display size can help mitigate the challenges of sensor sensitivity and feedback.

A single edge-mounted detector is capable of measuring output of only a single

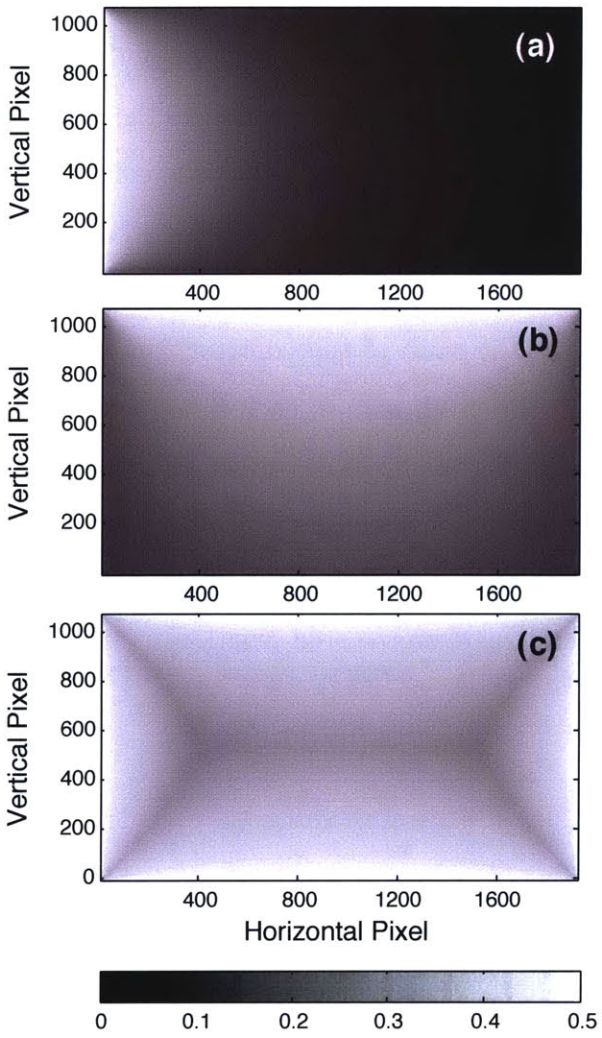


Figure 3-9: The fraction of edge emitted light captured from a single pixel on a 1920x1080 display with photodetector spanning the left (a) or top (b) edge of the display, and the maximum fraction of edge emitted light captured from a single pixel to a single photodetector that spans any edge of the display (c).

pixel at a time, so that calibration of a one-million-pixel display requires turning-on-then-off all of the pixels in sequence. Typical response of an OLED pixel is limited by their RC-time constant, which is on the order of a few $\mu s$ [55]. By allotting 10 $\mu s$ for each pixel, the display calibration would therefore require 10 $s$. To increase the speed of calibration, multiple photodetectors can be mounted around the display perimeter, allowing multiple pixels to be turned on and measured simultaneously, thereby reducing the calibration time in proportion to the number of mounted photodetectors [109]. For example, start with two photodetectors on the top and bottom edge of the display. The amount of light that reaches each detector from each pixel is a known quantity, dependent on pixel location relative to the detector and the geometry of the display. As long as the ratio of the contribution of one pixel to the other is unique for each detector, the brightness of each individual pixel can be determined. This process can be expanded to multiple detectors, enabling simultaneous calibration of the same number of pixels as detectors. Alternatively, the calibration can be accomplished any time the display is instructed to turn off, as for example when the lap-top screen is placed in the closed/stored position.

## 3.5 Summary

The lifetime for an OLED display requires a different metric than the typically measured OLED half-life. If constant-current driven OLEDs are to be used in a display with 2% brightness accuracy over 10,000 hours of operation, then the OLED half-life has to be extended beyond 300,000 hours. Additionally, other sources of operational instability such temperature-dependent current-voltage characteristics, non-linear drive-current dependent device efficiencies, variation in thicknesses and threshold voltage can compromise the uniformity of an OLED display. Optical feedback is likely the only solution to stabilize the light output of an OLED display. By using a drive-current-correcting optical-feedback scheme, more than a ten-fold display lifetime improvement is expected while aging individual OLED pixels to the point of two- or three-fold decrease in their luminescence efficiency. Using published data on

phosphorescent OLEDs, the operating lifetime of an OLED display can be extended close to the OLED half-life using a current-correcting optical feedback with less than a three-fold increase in drive current.

# Chapter 4

# OLED fabrication for displays

Organic materials are characterized by having weak intermolecular van der Waals bonds, which are not robust enough to adopt conventional microelectronic fabrication techniques developed for inorganic materials. Typical fabrication for small molecule OLEDs in displays uses shadow masking because it is simple, non-destructive, and applicable to small-molecule organic and electrode materials. However, this technique is not easily scaled to larger areas. There are two ways to avoid patterning the organic material of OLED displays, which could help enable their production to larger areas. The first method is to use color filters, in which a white OLED is aligned to red, green, blue color filters to produce the patterned sub-pixels. The second method is to use color conversion, in which a blue OLED is aligned to an array of fluorescent green and red sub-pixels. Both of these techniques have the disadvantages of reducing OLED efficiency and losing color-saturation [113]. Therefore, many alternative techniques have been developed for patterning OLEDs which are discussed in this section.

## 4.1 Shadow masking

OLEDs are typically patterned via shadow masking, inserting a thin stencil membrane between the source material and the substrate. Figure 4-1 shows a basic shadow masking technique for producing patterned red, green, and blue sub pixels. While shadow masking is a simple and non-destructive patterning technique, it is limited

in scalability and resolution. The thickness of the stencil and control of the stencil proximity to the substrate set the pattern quality, where for the highest resolution thin shadow masks are needed, but these are susceptible to warping and distortion under their own weight, limiting the ability to scale shadow mask processing to large array areas.

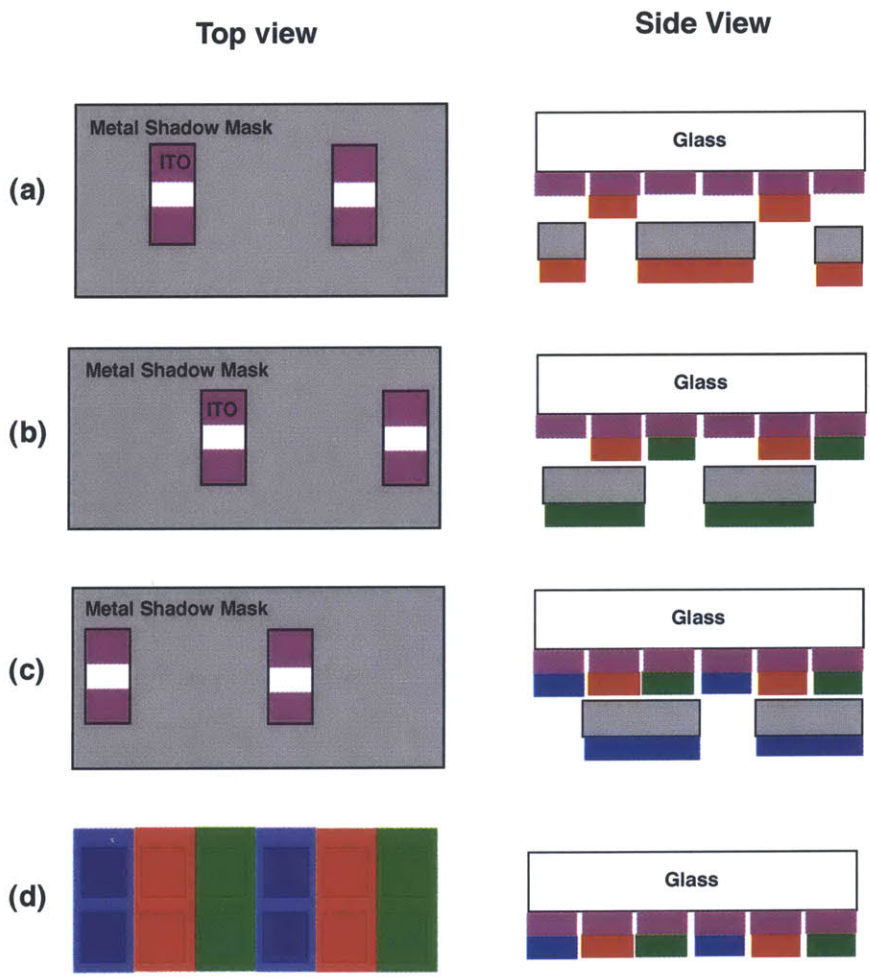


Figure 4-1: Basic metal shadow masking technique to pattern (a) red, (b) green, and (c) blue subpixels for displays. The finished product is shown in (d).

It is possible to implement a shifting shadow mask to pattern minimum feature sizes of 33 $\mu m$ as needed for a sub pixel in a high resolution display [114]. However, it also adds complexity and cost. In addition, rigid masks are hard to adapt to patterning of curved substrate, as might be needed for roll-to-roll fabrication of structures on flexible substrates.

A simple solution to this problem is to use integrated shadow masks which remain a permanent part of the device structure to pattern the metal electrodes of a display, shown in Figure 4-2. The integrated shadow mask material is usually a photoresist that can be undercut when developed, preventing electrodes from shorting when the metal is blanket deposited. This technique increases the resolution in patterning the OLED material and allows scalability to larger areas. However, it is limited to passive matrix monochrome displays [115].

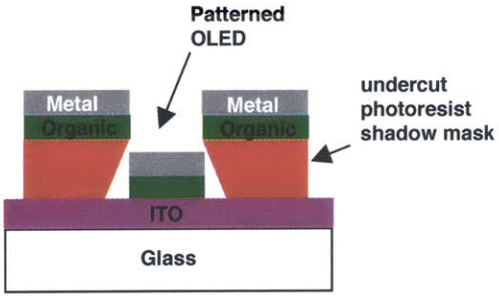


Figure 4-2: Integrated shadow masking technique.

Another shadow mask solution is to use an elastomeric membrane as the shadow mask which makes conformal contact with the substrate. This shadow mask is removed after organic deposition, creating a dry lift-off process of the organic film. By using two masks, it is possible to pattern the red, green, and blue sub-pixels on one substrate, as shown in Figure 4-3. To pattern fine features, the shadowmask thickness is on the order of 10 $\mu m$ and is difficult to handle without breaking. Scaling this method to larger areas remains a difficult challenge due to handling of the thin membrane shadow mask which lacks mechanical strength [19].

## 4.2 Laser techniques

Thermal imaging is a promising technique which is used in OLED production. It allows multiple layers to be transferred at once and is capable of patterning organic materials with micron size resolution. Laser-Induced Thermal-Imaging (LITI) and Laser-Induced Pattern-wise Sublimation (LIPS) are common techniques that use ther-

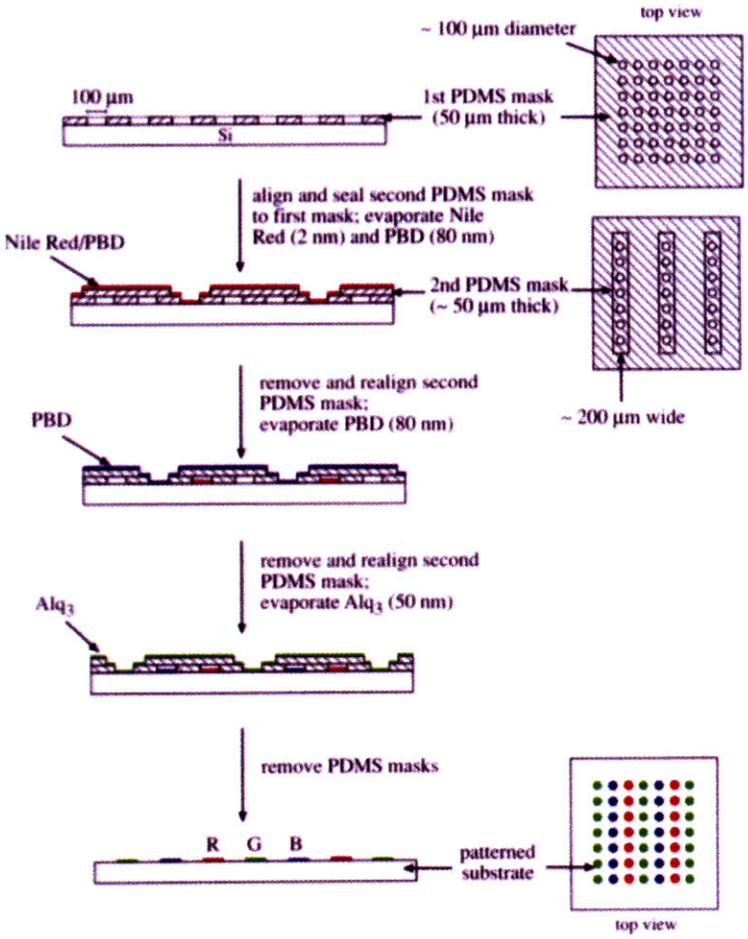


Figure 4-3: Patterning red, green, blue subpixels using two poly(dimethylsiloxane) (PDMS) shadow masks [19].

mal imaging. LITI was first developed, but requires the donor film to make contact with the receiving substrate which causes problems through contamination and transfer quality of the film. This process is shown in Figure 4-4. LIPS improved upon this design by placing a spacing offset from the donor to the receiver and performing the procedure under vacuum. This allows for better film transfer as well as improving the ability to pattern red, green and blue sub-pixels. Although laser patterning is a serial process, it is possible to streamline this technique by using multiple lasers. The largest restriction with using this technique is focusing the laser on the absorption layer to get good resolution. Currently, sub-pixel pitch of 105 $\mu m$ has been demonstrated [21].

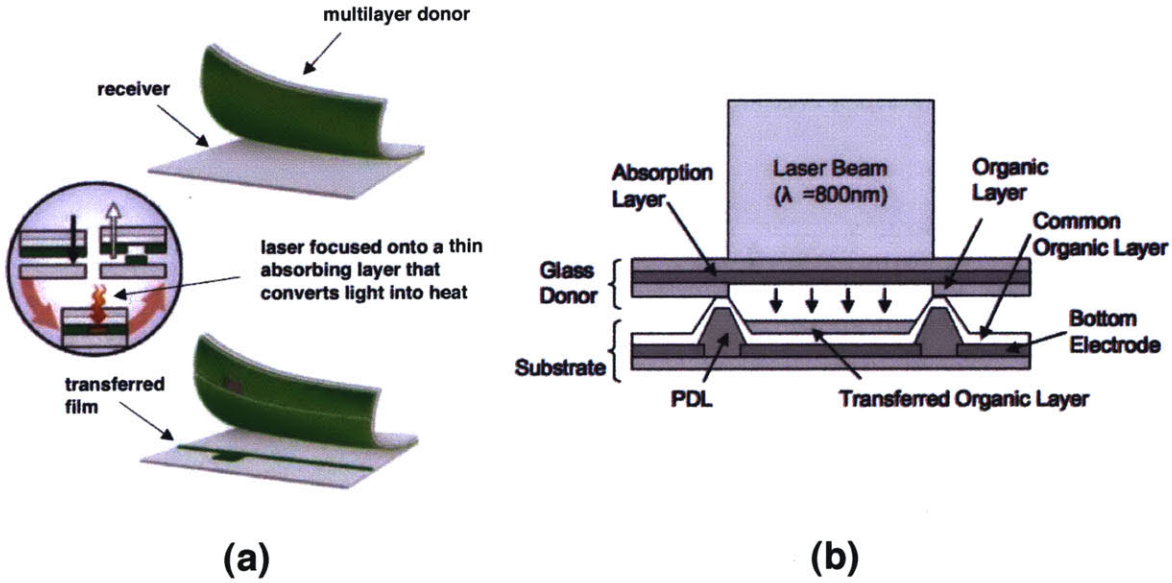


Figure 4-4: (a) Laser induced thermal imaging where multilayer donor is placed in contact with recieving substrate. Laser is focused onto a thin absorbing layer that converts light into heat and transfers donor pattern to receiver. Donor film is removed from reciever, leaving patterned, transferred film [20]. (b) Laser-Induced Pattern-wise Sublimation where donor is spatially separated from receiving substrate [21].

## 4.3 Molecular jet printing

Molecular jet printing enables fabrication of 30 $\mu m$ sized features by using micro-electro-mechanical system (MEMS) printing technology [22]. Organic material is

placed in a thermal effusion cell with a MEMS printhead in line with the sublimation path of the organic material. The substrate is placed on an XY stage and is translated relative to the organic material and printhead, while the opening and closing of the MEMS shutter on the printhead allows for patterning of the material. This procedure is shown in Figure 4-5. It is possible to speed up the technique using a multi-nozzle printhead. However, this technique has not yet been implemented in an industrial setting.

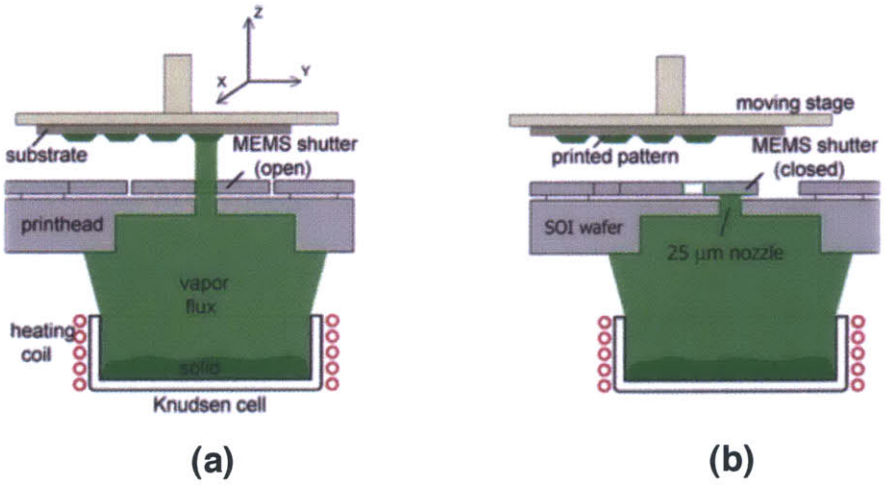


Figure 4-5: MoJet printing process: (a) When MEMS shutter is open, evaporated material passes through nozzle and reaches substrate. (b) Material does not reach the substrate when MEMS shutter is closed. [22]

## 4.4 Contact Stamping

A promising alternative for patterning OLEDs is contact stamping, which has the advantage of being a simple, scalable patterning technique. Contact stamping usually involves a relief stamp to pattern material on the raised features of the stamp. This technique has been applied for patterning both electrodes and organic layers in organic devices. Contact stamping techniques for patterning molecular organic thin films have been demonstrated with both additive and subtractive methods.

### 4.4.1 Additive Techniques

Additive transfer occurs by depositing a blanket film onto a relief stamp and transferring the film on the raised feature of the stamp to a target substrate as shown in Figure 4-6. Additive techniques have been demonstrated from poly(dimethylsiloxane) (PDMS) and rigiflex poly(urethaneacrylate) (PUA) stamps to organic and inorganic substrates with applied pressures and elevated temperatures.

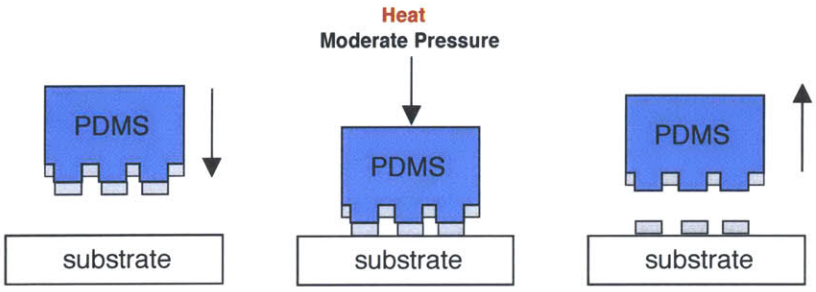


Figure 4-6: Cartoon demonstrating additive transfer of material via contact stamping.

Additive transfer of organic patterned film is made from a relief PDMS stamp to a target substrate using a van der Waals-based organic adhesion mechanism. A relief stamp is coated with an adhesion reduction layer (20-nm-thick layer of Au), coated with an organic transfer layer ($\alpha$-NPD). The substrate is coated with a thin-film organic layer of the same material known as the strike layer. The stamp is then pressed into the substrate, and when the stamp and substrate are separated, the organic layer is transferred to the substrate due to adhesion between the organic strike and transfer layer. The transfer process uses 1.9 MPa of applied pressure at 20 minutes, and can occur at room temperature, although elevated temperatures (60°C) were required to produce nicer edge pattern for the film. For OLED fabrication, a bilayer of Alq3 and $\alpha$-NPD was transferred using this technique. The device performance was not affected by the organic-organic interface introduced into the OLED structure [116].

Additive transfer of electrodes has been demonstrated using a rigid silicon stamp to a flexible PDMS stamp using a cold welding adhesion mechanism in which two metal layers are brought in intimate contact so that electron orbitals of the two metal surfaces interact. Rigid stamps require high pressures around 150 $MPa$ for additive

transfer to occur while flexible stamps require less pressure around 180 $KPa$ [23] [117]. In both cases, a strike layer of metal is first evaporated on top of the organic to facilitate adhesion. After the metal pattern is transferred, a dry etch step is used to remove the strike layer. This process is shown in Figure 4-7.

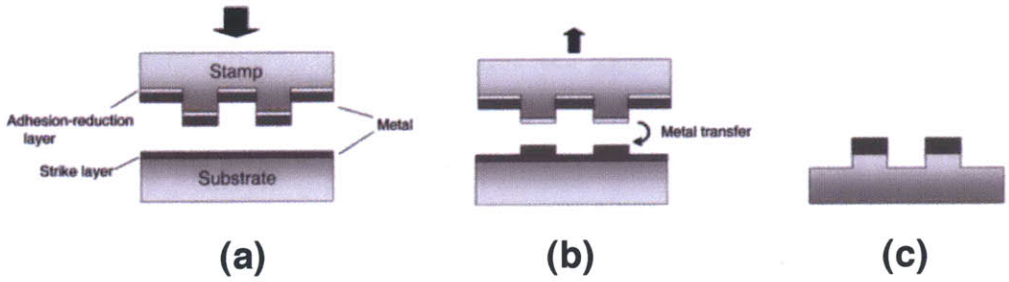


Figure 4-7: Additive transfer of metal electrodes: (a) place stamp on substrate coated with metal strike layer (b) remove stamp, transferring metal that is cold welded to strike layer (c) etch strike layer. [23]

Additive transfer of electrodes can also rely on a physical interlocking mechanism facilitated through adhesion. One technique additively transfers metal electrodes to an organic polymer substrate by heating above the glass transition temperature of the polymer but below the melting point of the polymer. This heating allows the polymer to flow into voids or pores in the surface and interlock the polymer to the metal. The substrate and stamp are then cooled, and the stamp is released. Since the metal adhesion to the organic polymer has been mechanically improved through heating, this adhesion overcomes the weak metal bond to the PDMS when the stamp is lifted off from the substrate, and the metal sticks to the polymer [118]. In this case, there is no residual strike layer, although heating of the material is a step that would be generally avoided if possible to maintain the integrity of the originally evaporated device.

Finally, additive transfer of whole devices has been achieved by using a rigid but flexible PUA stamp. The stamp is supported by a flexible and transparent film of polyurethane elastomer or soft epoxy resin. The stamp is then coated with fluorinated ethylene propylene (FEP) to serve as an adhesion reduction layer. The entire OLED is deposited in reverse order on the stamp and then transferred to an oxygen plasma

cleaned ITO substrate using 1-5 $MPa$ of pressure at 50 $°C$ for five minutes. This process applied to full-color sub-pixel OLED patterning is shown in Figure 4-8.

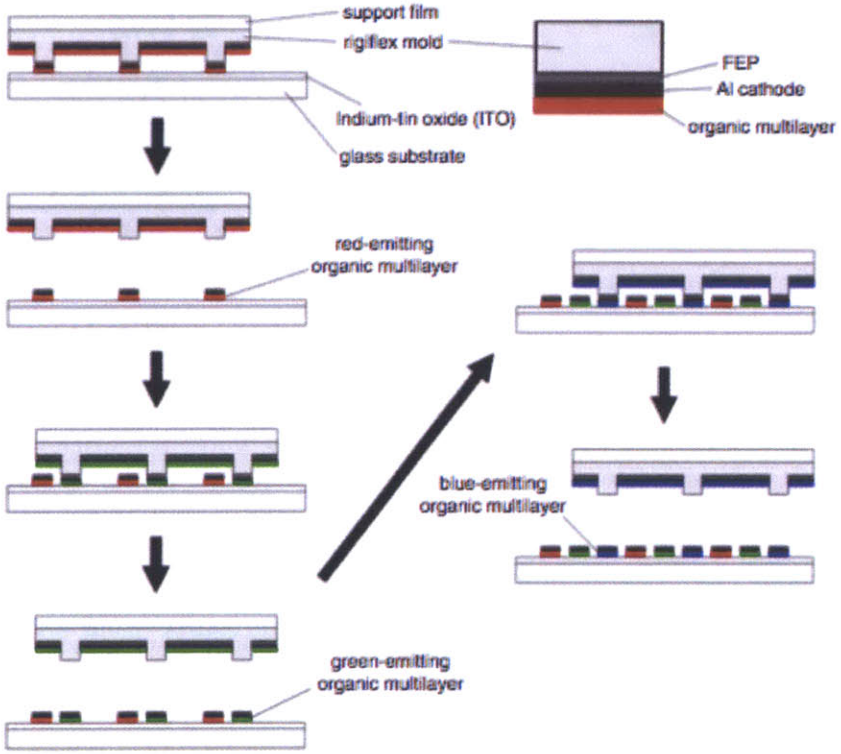


Figure 4-8: Additive contact stamping technique: Whole device transfer of printing for full color displays. [24]

### 4.4.2 Subtractive Techniques

Subtractive patterning occurs by blanket depositing an organic film onto a substrate and subsequently bringing a relief stamp in contact with the film to lift off the organic regions in contact with the raised features of the stamp as shown in Figure 4-9. This stamping technique has been demonstrated with a partially cured epoxy stamp and a PDMS stamp and requires a heating step.

Subtractive stamping techniques for organic materials have been implemented for organic transistor fabrication and include a hot lift-off process [119]. A partially cured epoxy stamp is pressed into an organic film (70 nm thick CuPc) at 10 $kg/cm^2$ for 30 seconds, primarily to fracture the thin film which is a brittle film with weak

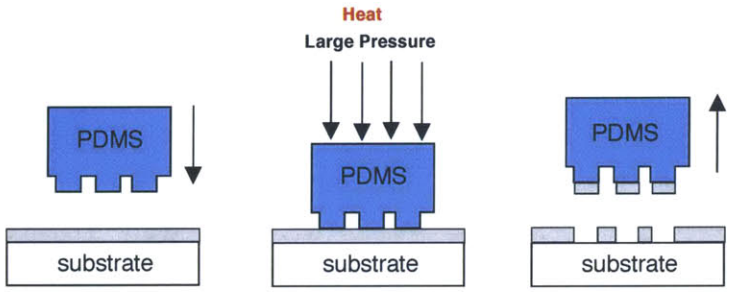


Figure 4-9: Cartoon demonstrating subtractive patterning of material via contact stamping.

cohesive energy between the molecules. Then the pressure is reduced to 2 $kg/cm^2$ with 80-120°C heating for 20 minutes to cure the epoxy and enhance adhesion to the thin film. Failure to do the initial high pressure step results in poor edge definition for patterned films, and failure to do the heating step results in no pattern removal. The sample is then cooled, and the stamp is removed from the substrate, picking up the regions of the thin film in contact with the stamp, leaving a patterned thin film on the substrate.

Other subtractive stamping techniques for organic materials have been demonstrated with a PDMS stamp and no applied pressures on 50 nm thick layer of NPB or Alq3. However, the subtractive technique requires annealing at 90°C for 1 hour before removal of the stamp and organic film after cooling [120]. Higher processing temperatures than the glass transition temperature of the material leads to hole formation or spinoidal dewetting for the thin film. This patterning can be done at atmosphere, but for more consistent results the procedure is done under vacuum, ensuring conformal contact of the PDMS stamp with the organic film.

Subtractive stamping techniques for metal electrodes usually involve a rigid stamp and application of high pressures. High pressures are required to induce fracture of the metal film and create intimate contact of the metal surfaces to facilitate adhesion by cold welding [25]. This process is shown in Figure 4-10.

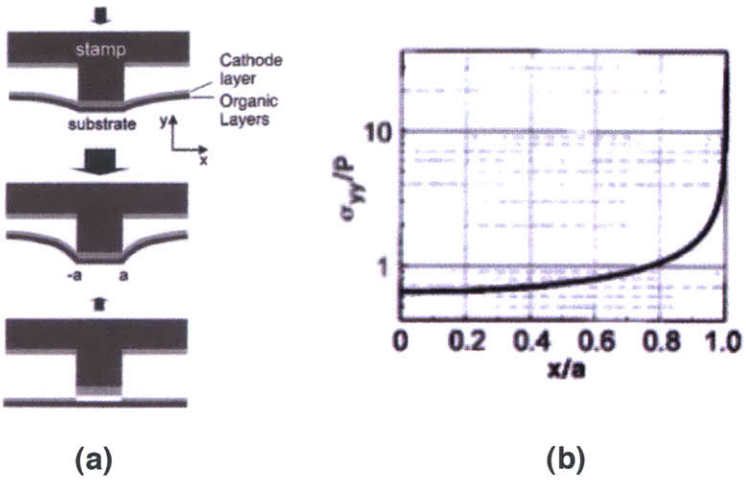


Figure 4-10: Subtractive contact stamping technique for metal electrodes: (a) A depiction of the deformation that occurs with applied pressure and (b) numerical model shows that highest pressure occurs at the edges of the stamp. [25]

## 4.5 Outlook

Commercial fabrication of OLEDs is patterned using shadow masking or laser techniques. Although contact stamping has not been used in commercial production for any type of patterning, Philips Research Laboratories have developed wave printing to enable large area patterning. Wave printing is done by placing a PDMS stamp on a flexible glass backplate to provide rigidity to the stamp. The substrate is brought within 100 $\mu$m of the stamp and low-pressure air around 2 KPa is sent through adjacent valves to grooves in the back of the stamp plate in order to press the stamp in contact with the substrate. This contact point is propagated across the substrate one groove at a time to form a wave [26]. The schematic of a wave printer is shown in Figure 4-11. In addition, contact stamping is compatible with roll-to-roll patterning techniques for OLEDs, which is developed for large production throughput. While contact printing is still in development, use of this patterning technique has the advantage of scalability and high resolution patterning which is not currently achievable in shadow masking and laser techniques.

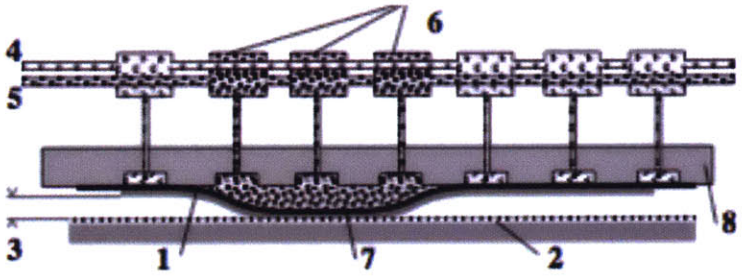


Figure 4-11: Wave printing schematic: (1) Stamp-backplate (2) Substrate (3) working gap (4) Vacuum supply (5) Pressure supply (6) Open valves to create wave (8) Groove plates to allow pressure entry [26]

# Chapter 5

# Patterning Organic Films

## 5.1 Introduction

Contact stamping techniques for patterning molecular organic thin films have been demonstrated with both additive and subtractive methods. Additive techniques for organic films require applied pressures and moderate temperatures around 50°C. Subtractive patterning for organic films requires a heating step around 80-90°C. While these methods work, a technique that does not rely on heating or high pressures that could potentially damage the organic or underlying layers would be preferred. This section introduces such a stamping technique[121].

## 5.2 Procedure

In this chapter, a simple subtractive patterning technique to pattern the organic layer is introduced. Unlike other subtractive patterning techniques, no applied pressure or elevated temperature is required to pattern the organic material. A relief PDMS stamp is placed in contact with an organic film and subsequent removal of the stamp lifts off regions of the organic film in contact with the stamp. This procedure is shown in Figure 5-1. Results of this procedure on a TAZ film are shown in Figure 5-2. Unlike other subtractive contact stamping techniques, this technique does not require any applied pressures or elevated temperatures. This procedure was attempted on a

variety of organic materials and substrates. Organic materials include hole transport materials TPD, Spiro-TPD, NPB, NPAPF, and hole blocking/electron transport materials TAZ, TPBi, and phosphorescent host UGH2. The molecular structure and full names of these materials are shown in Appendix B.

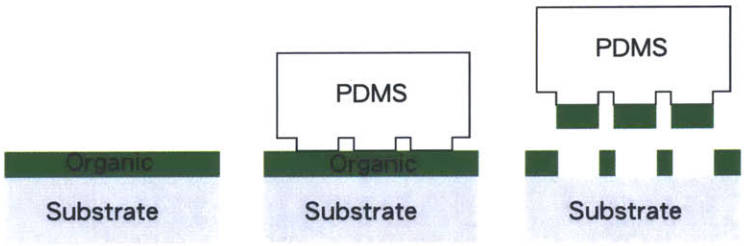


Figure 5-1: Procedure for subtractive patterning of organic thin films.

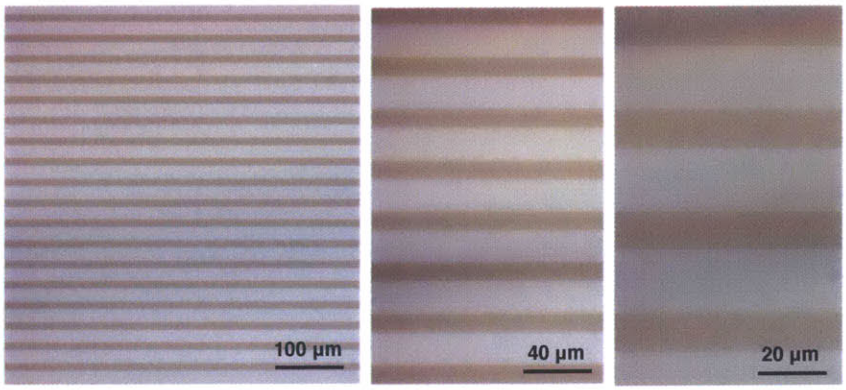


Figure 5-2: Optical microscope image of 100 nm TAZ patterned lift-off. The dark features in this image indicate presence of TAZ layer where lighter regions indicate lift-off of TAZ.

## 5.3 Results

Lift-off film thickness is measured with atomic force microscopy (AFM). Total organic film thickness was normally calibrated using a crystal thickness monitor. For organic films on substrates such as glass, ITO, or PEDOT:PSS, the film thickness is usually a multiple of 10 nm, indicating that a pre-calibrated film thickness was used. For films grown on silicon, it was possible to calibrate the thickness with ellipsometry

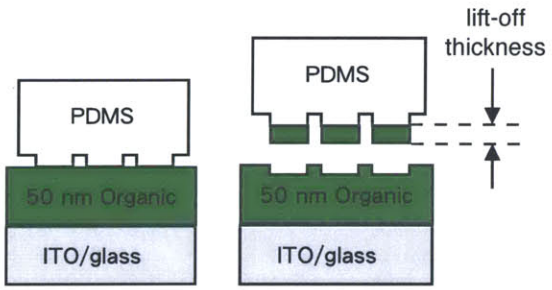


Figure 5-3: Cartoon depiction of partial lift-off with indicated lift-off thickness.

after film growth, and if so, the total film thickness is recorded with 1 nm precision. Error in film thickness measurement can vary up to 2 nm on a substrate surface and up to 4 nm substrate to substrate due to evaporation position for 1 inch substrates, as determined from ellipsometry measurements.

### 5.3.1 Organic material

The organic patterning procedure yields different lift-off thickness when applied to different organic materials. A cartoon depiction of this result which indicates the lift-off thickness is shown Figure 5-3. A 50 nm thick film of each organic material was evaporated on an ITO substrate. The lift-off procedure was applied to the different organic films, and different lift-off thickness resulted depending on the organic film material. Organic material TAZ resulted in nearly complete removal of material. These results are shown in Figure 5-4, and Table 5.1 provides the average and standard deviation for these results. Organic materials TPD, Spiro-TPD, TPBi and NPB had 32, 18, 7, and 5 nm of lift-off thickness, respectively, while no lift-off occurred for NPAPF.

### 5.3.2 Substrate

The substrates surfaces typically used in OLED fabrication are ITO, glass, PEDOT:PSS, and Silicon (Si). A five-minute oxygen ($O_2$) plasma treatment was also used to make the surface more hydrophillic. For 26 nm thick organic TPD film, chang-

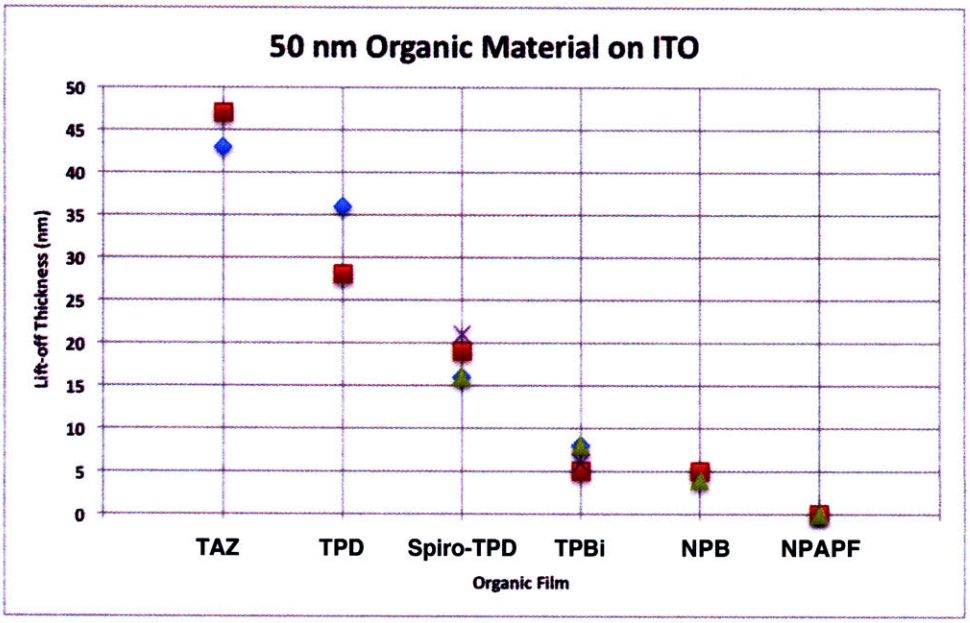


Figure 5-4: Investigation of lift-off thickness dependence on material type.

ing the surface from Si, oxygen plasma Si, to PEDOT:PSS Si resulted in 22, 21, and 22 nm lift-off thickness, respectively. Changing the surface from ITO, oxygen plasma ITO, to PEDOT:PSS ITO changed the lift-off thickness from 22, 20 to 23 nm, respectively. Similar results were obtained for a 50 nm thick organic TAZ film. Changing the substrate surface from Si to ITO did not change the lift-off film thickness of 47 nm. However, changing the substrate to oxygen plasma Si showed a lift-off thickness of 44 nm. There seems to be a consistent decrease in the oxygen-plasma-treated substrate, which could indicate that the oxygen plasma treatment enhances organic adhesion to the substrate, resulting in a reduced lift-off film thickness. However, these variations are also within the measurement error. These results are summarized in Table 5.2.

### 5.3.3 PDMS surface

The PDMS surface can be modified by using a ultra-violet ozone (UVO) treatment. A 5 minute UVO treatment changes the surface properties of PDMS from hydrophobic to more hydrophillic. For 50 nm TPD on Silicon, the lift-off thickness was 33 nm with regular PDMS and 31 nm with UVO PDMS. For 50 nm Spiro-TPD on Silicon, the

Table 5.1: Thickness removal average ($\mu$) and standard deviation ($\sigma$) of at least two data measurements of 50 nm of organic film from ITO substrate.

| | Thickness $\mu$ (nm) | Std Dev $\sigma$ (nm) |
|---|---|---|
| NPAPF | 0 | 0 |
| NPB | 5 | 1 |
| TPBi | 7 | 2 |
| Spiro-TPD | 18 | 3 |
| TPD | 32 | 6 |
| TAZ | 45 | 3 |

lift-off thickness was 12 nm with regular PDMS and 14 nm with UVO PDMS. These results are summarized in Table 5.3. UVO treatment of the PDMS stamp does not have a significant effect on the resulting lift-off thickness of these organic materials.

### 5.3.4 Organic film thickness

The organic film thickness was changed from 10-100 nm on different substrates to see what affect it has on the lift-off thickness. In the following cases, three data measurements were done for each film thickness and averaged. All film thicknesses are in nanometer (nm) units. For an NPB film on PEDOT:PSS/ITO substrate, the average lift-off to total film thickness (lift-off/total) is 4/10, 5/50, and 5/60. For a TPD film on a silicon substrate, the results are 24/26, 32/55, 33/57, and 30/105. For a TAZ film on silicon, the results are 47/50 and 87/92. These results are summarized in Table 5.4.

In the section 5.3.2, it is determined that changing the substrate from ITO, Si, or PEDOT:PSS does not have a large effect on the organic lift-off thickness. Therefore, the general trend for film thickness can be seen even when the lift-off is performed on various substrates. The results for investigated material thicknesses on all different surfaces are shown in Figure 5-5.

For materials such as TAZ, complete layer patterning seems to occur even at increased thicknesses. Increasing the film thicknesses beyond a characteristic thickness

Table 5.2: Thickness removal average ($\mu$) and standard deviation ($\sigma$) of three data measurements of 26 nm TPD from various surfaces. Thickness removal of 50 nm TAZ from various surfaces with three data measurements for Si surface and two data measurements for ITO surface.

| Surface | Thickness $\mu$ (nm) | Std Dev $\sigma$ (nm) |
|---|---|---|
| 26 nm TPD | | |
| Si | 22 | 1 |
| $O_2$ Plasma Si | 21 | 1 |
| PEDOT:PSS/ Si | 22 | 2 |
| ITO | 22 | 3 |
| $O_2$ Plasma ITO | 20 | 1 |
| PEDOT:PSS/ITO | 23 | 1 |
| 50 nm TAZ | | |
| Si | 47 | 3 |
| $O_2$ Plasma Si | 44 | 1 |
| ITO | 47 | 1 |

for other materials usually result in little increase of the lift-off thickness. For NPB and TPD, this characteristic thickness is 5 nm and 30 nm, respectively.

### 5.3.5 Contact angle measurements

Contact angle measurements are useful in approximating the energy of different surfaces. Table 5.5 shows contact angle measurements done on organic, stamp, and substrate surfaces.

## 5.4 Discussion

### 5.4.1 Adhesion analysis

For patterning to occur, the work of adhesion between the PDMS and the organic is greater than the organic cohesion. Appendix C gives a detailed discussion on how to estimate the work of adhesion using contact angle measurements. Table 5.6 shows the work of adhesion between PDMS and organic surfaces, which does not correspond to

Table 5.3: Thickness removal average ($\mu$) and standard deviation ($\sigma$) of three data measurements of 50 nm Spiro-TPD on Si and 50 nm TPD on Si with different stamp surfaces.

| Stamp | Organic Film | Thickness $\mu$ (nm) | Std Dev $\sigma$ (nm) |
|---|---|---|---|
| PDMS | TPD | 33 | 0 |
| UVO PDMS | TPD | 31 | 0 |
| PDMS | Spiro-TPD | 12 | 2 |
| UVO PDMS | Spiro-TPD | 14 | 1 |

Table 5.4: Thickness removal average ($\mu$) and standard deviation ($\sigma$) of three data measurements of various thickness organic from similar surfaces.

| Total (nm) | Lift-off $\mu$ (nm) | Std Dev $\sigma$ (nm) |
|---|---|---|
| NPB on PEDOT:PSS/ITO | | |
| 10 | 4 | 1 |
| 50 | 5 | 0 |
| 60 | 5 | 0 |
| TPD on Silicon | | |
| 26 | 22 | 2 |
| 55 | 32 | 2 |
| 57 | 33 | 2 |
| 105 | 30 | 4 |
| TAZ on Silicon | | |
| 50 | 47 | 3 |
| 92 | 87 | 2 |

a trend with the lift-off thickness obtained from 50 nm thick organic films on ITO. Although organic cohesion is not known explicitly, it is related to the sublimation temperature for an organic material. This trend is confirmed in the patterning results and shown in Figure 5-6. High sublimation temperature materials such as NPAPF are not able to be patterned while low sublimation temperature materials such as TAZ can be patterned completely. Organic materials with intermediate sublimation temperatures can be patterned with varying success.

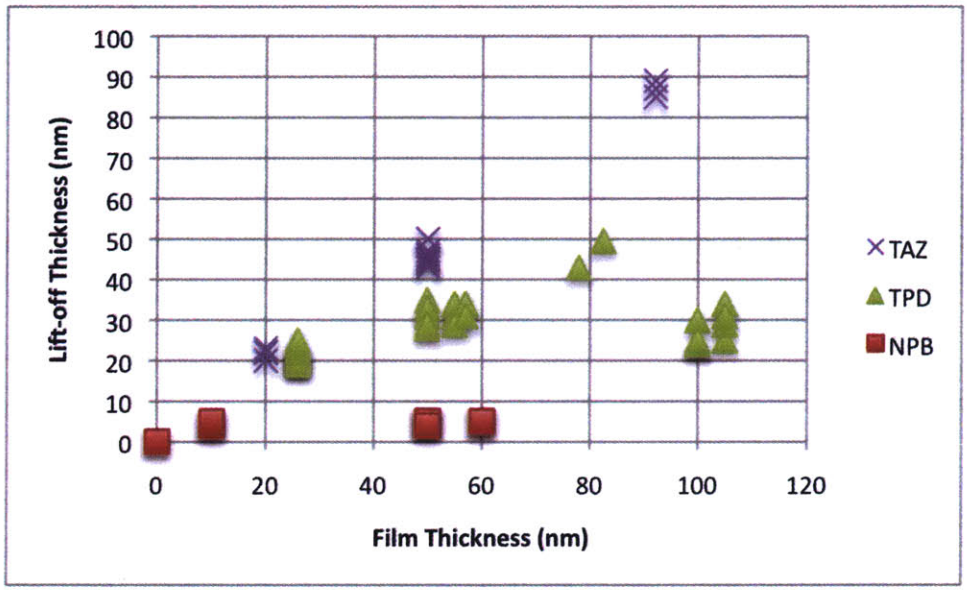


Figure 5-5: Investigation of patterning dependence on film thickness for different organic materials on different substrates.

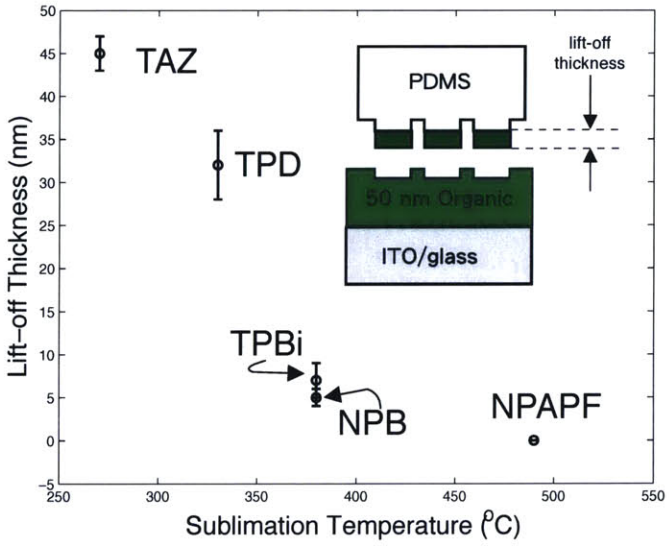


Figure 5-6: Sublimation temperature [27] trend with lift-off thickness of organic materials.

Table 5.5: Contact angle measurement average ($\mu$) and standard deviation ($\sigma$) of at least four data measurements of organic surfaces with de-ionized water (DI $H_2O$) and ethylene glycol (EG).

| | DI $H_20$ | | EG | |
|---|---|---|---|---|
| Surface | $\mu$ (°) | $\sigma$ (°) | $\mu$ (°) | $\sigma$ (°) |
| UGH2 | 104 | 1 | 58 | 5 |
| NPAPF | 91 | 1 | 58 | 4 |
| TPBi | 77 | 2 | 48 | 2 |
| Spiro-TPD | 81 | 0 | 59 | 5 |
| Alq3 | 67 | 4 | 47 | 3 |
| TAZ | 71 | 6 | 56 | 10 |
| TPD | 90 | 3 | 73 | 3 |
| PDMS | 96 | 2 | 76 | 2 |
| ITO | 24 | 3 | 64 | 1 |

Table 5.6: Work of adhesion ($W_{adh}$) between the organic and PDMS.

| Surface | $W_{o,PDMS}$ (mJ/m$^2$) |
|---|---|
| UGH2 | 141 |
| NPAPF | 102 |
| TPBi | 102 |
| Spiro-TPD | 90 |
| Alq3 | 94 |
| TAZ | 85 |
| TPD | 76 |

## 5.5 Complete layer patterning

There are two methods to get complete organic patterning. One method is to pick a low sublimation temperature organic material, such as TAZ. This material can be lifted-off even when increasing the film thickness to 100 nm. The other method is to decrease the thickness of the organic layer to be patterned. For example, TPD has a lift-off thickness of roughly 30 nm for a 50 nm thick film. Decreasing the TPD thickness to 26 nm allows the entire film to be lifted off. Many emissive layers are on the order of 10 nm in thickness, making it possible to pattern the emissive material of an OLED using this stamping technique. Figure 5-7 demonstrates these

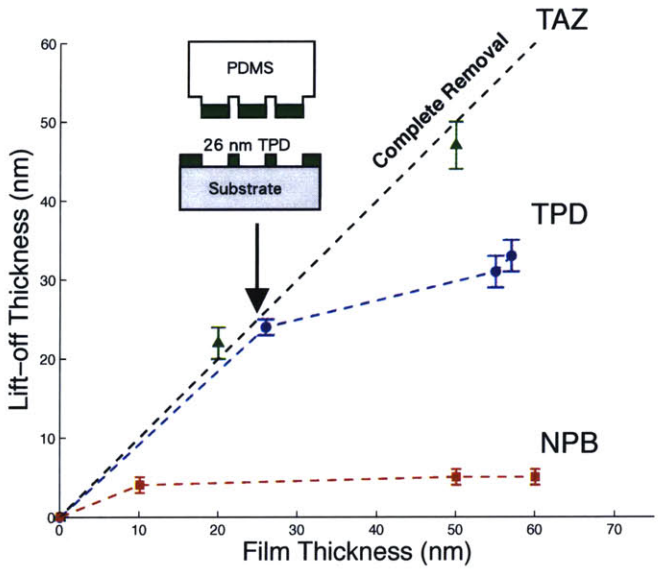


Figure 5-7: Complete patterning with organic materials. Dotted black line indicates complete removal of organic film thickness. Dotted blue and red lines are shown to guide the eye for TPD and NPB removal.

two principles for getting complete removal of a deposited film.

## 5.6 OLED fabrication

### 5.6.1 Two-color OLED

The proposed device structure for a two-color OLED is shown in Figure 5-8a. The TPD/Alq3 interface allows formation of excitons to transfer to Alq3 and emit green light. The existence of the TAZ layer essentially confines excitons to the TPD/TAZ region to emit blue light. Figure 5-8b shows an AFM image of patterned TAZ and the step profile, indicating that some TPD is also patterned. Figure 5-8c is the electroluminescence from such a device. Figure 5-9 shows an example of patterning a red-blue OLED. The stamp is asymmetrical in pitch, and wider pitch indicates lift-off region. The first stamping occurs after TAZ deposition, with the line pattern in the vertical direction, which reveals the underlying TPD layer upon patterning. Then DCM2:Alq3 is evaporated on top,and lifted-off up with the horizontal patterning. The

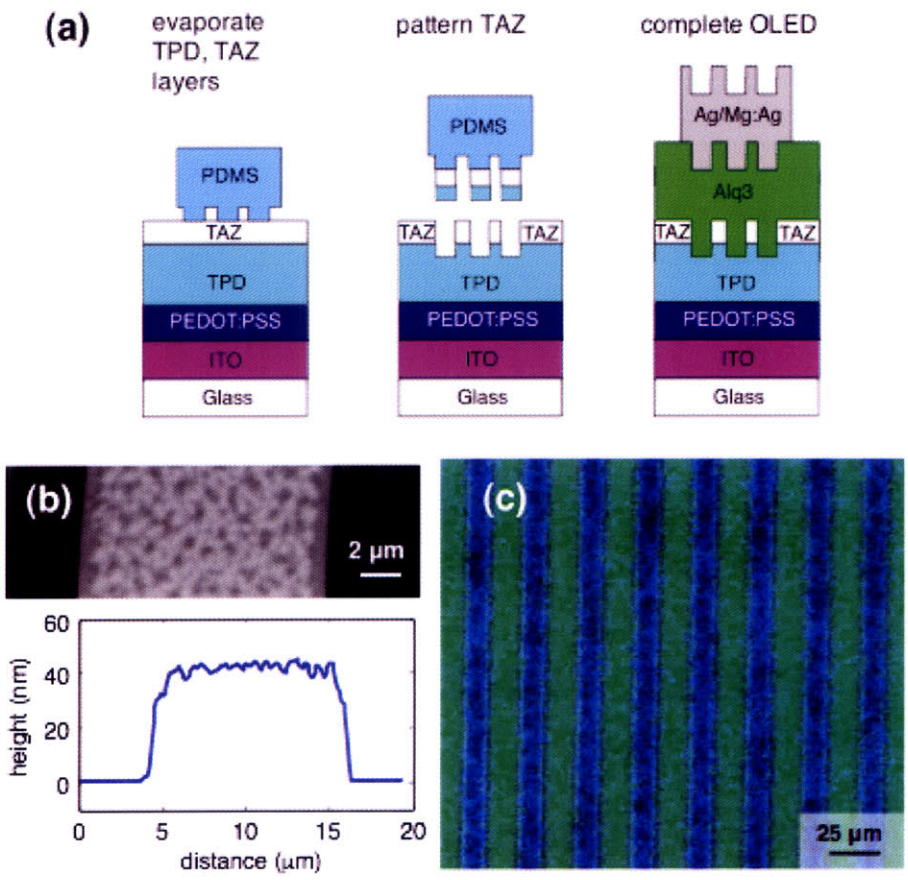


Figure 5-8: (a) Procedure to make two-color OLED, (b) AFM image and step height of patterned TAZ layer, and (c) electroluminescence of completed OLED

non-emissive larger squares shown in the figure indicate 2x pickup of organic material, where device is thin and luminescence is quenched by electrodes. The smaller squares indicate no pickup, where device is too thick to emit at the given voltages.

### 5.6.2 Comparison to shadow masking

To demonstrate compatibility of this subtractive stamping technique in fabrication of OLEDs, we compare this partial patterning technique to a conventional shadow masked OLED and show similar LIV characteristics. It has been shown that the thickness of the TPD layer does not significantly change the LIV characteristics of a typical TPD / Alq3 device. Therefore, an OLED patterned using this subtractive stamping technique as shown which results in a thinner TPD layer should exhibit

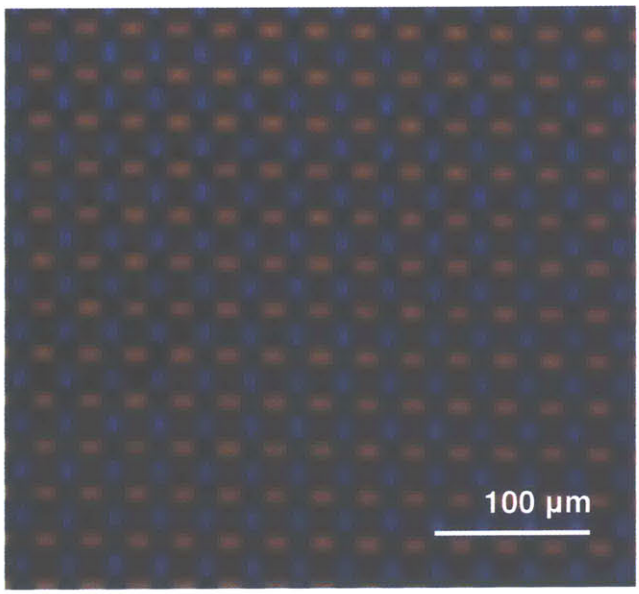


Figure 5-9: Electroluminescence from a red-blue OLED using lift-off technique by patterning the TAZ layer and DCM2:Alq3 layer of a TPD / TAZ / DCM2:Alq3 / Alq3 device.

similar LIV characteristics to the shadow-masked device with thicker TPD layer. Figure 5-10 shows images of the partial patterning of a TPD film on top of Poly(3,4-ethylenedioxythiophene) poly(styrenesulfonate) (PEDOT:PSS) / ITO / glass substrate. The results of the comparison of an OLED with partial lift-off of TPD to the shadow masked OLED are shown in Figure 5-11.

## 5.7 Summary

It is possible to pattern organic material using a contact stamping technique which does not require applied pressure or elevated temperature. The lift-off thickness during patterning is dependent on organic material, with a trend that lower sublimation temperature materials tend toward complete lift-off thickness of original film. To pattern complete layers, a low sublimation temperature materials can be used or a thinner layer than the characteristic lift-off thickness for an organic material can be used. It is possible to pattern geometries such as circles, so this technique is not limited to line patterns. This technique is comparable to shadow masking techniques.

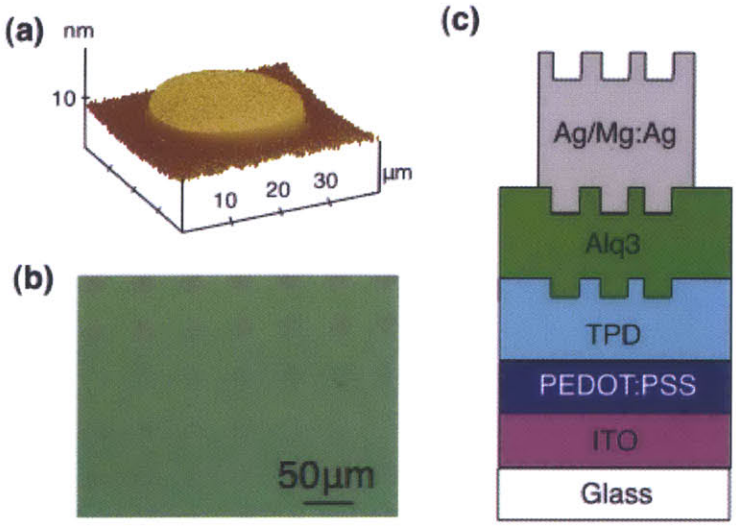


Figure 5-10: (a) AFM image of patterned TPD and (b) electroluminescence of patterned OLED (c) device structure.

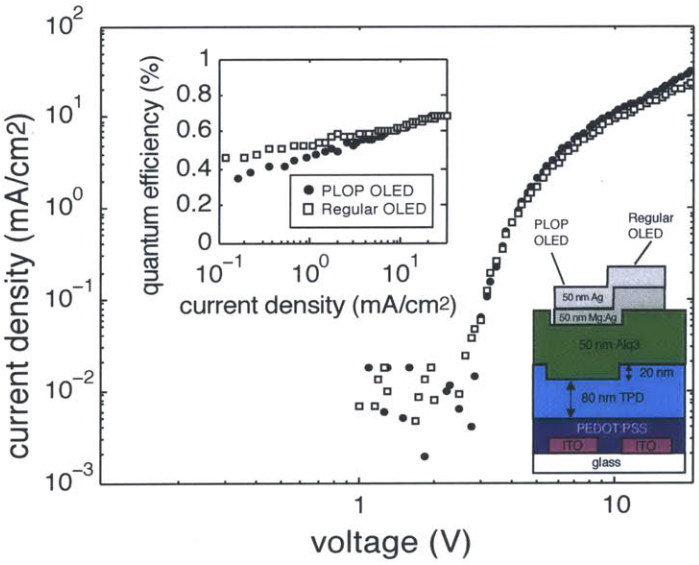


Figure 5-11: Comparison of PDMS lift-off patterned (PLOP) OLED versus regular OLED.

Finally, it is possible to pattern a two-color organic LED structure with 13-micron-sized features using this technique.

# Chapter 6

# Patterning Metal Electrodes

## 6.1 Introduction

Contact stamping for electrodes started as a subtractive stamping technique with a rigid stamp and high pressures, relying on a cold welding mechanism, the idea that placing two metals in close proximity to each other causes good electron orbital overlap and bonding of the two metals to occur [25]. High pressures were required for two reasons: fracturing the metal film for patterning and obtaining intimate contact with the rigid stamp to the substrate. Further development reduced these high pressures by removing the fracturing criteria, switching to an additive technique [23] and then further reduced pressures by using a flexible PDMS stamp [117]. This low-pressure technique employs an adhesion reduction layer on the stamp and a metal strike layer on the substrate that needs to be removed after metal transfer via oxygen reactive ion etching or argon sputtering. To remove the need for applied pressure, a mechanical adhesion mechanism can be applied. This technique additively transfers metal electrodes to an organic polymer substrate by heating [119]. This heating allows the polymer to flow into voids or pores in the surface and interlock the polymer to the metal, overcoming the weak metal adhesion to the stamp. While these methods work, it is still desirable to have a technique that does not rely on heating or high pressures to pattern the metal electrode. This section introduces such a stamping technique.

## 6.2 Procedure

A simple subtractive contact stamping method can be used for patterning OLED electrodes with no requirement of applied pressure, temperature control, or stamp surface modification. Patterning is achieved by placing a relief patterned PDMS stamp in contact with a planar metal electrode film and then rapidly peeling off the stamp. A fast peel rate increases the weak adhesion energy of the stamp to the metal so that no surface treatment, pressure, or temperature control is necessary to lift-off the metal film in contact with the stamp. Here, the adhesion mechanism is a kinetically controllable adhesion of PDMS [122]. The basic concept and examples of patterning metal films on top of organics is shown in Figure 6-1, 6-2, and 6-3.

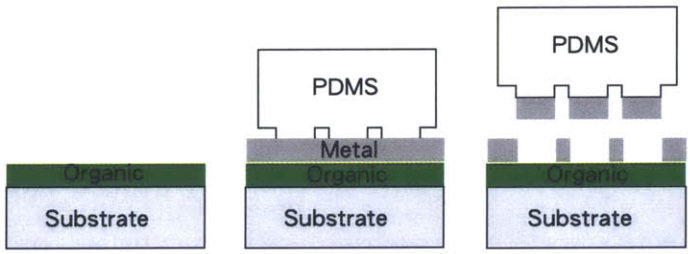


Figure 6-1: Schematic depiction of PDMS lift-off technique for patterning metal electrodes in organic devices. Metal layer deposited on top of organic substrate is detached from the substrate surface when patterned PDMS relief stamp makes conformal contact with the surface and is followed with a rapid peel-off.

## 6.3 Results

### 6.3.1 Metal film thickness

To generate a pattern with this subtractive contact-stamp patterning method, metal film fracture must occur at the edges of the stamp relief features. However, externally applied pressure across the PDMS stamp is ineffective in causing the metal layer to fracture, as it simply leads to distortion of the flexible stamp. This patterning technique relies on the lift-off pressure to fracture the metal film. Consequently, in these demonstrations thin layers of metal are used because they are easier to fracture

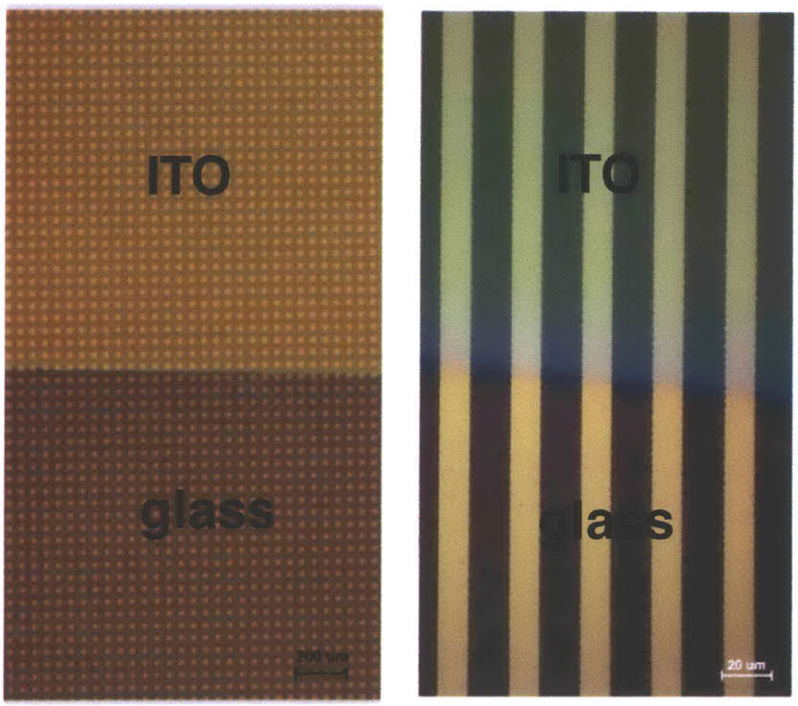


Figure 6-2: (a) 25 $\mu m$ diameter circles and (b) 13 $\mu m$ wide lines of patterned 20 $nm$ thick Mg:Ag on top of 50 nm thick Alq3/50 $nm$ thick TPD/PEDOT/ITO/glass

in in a lift-off process with no applied pressure.

Figure 6-4 demonstrates that an increasing metal layer thickness is difficult to pattern. Good pattern transfer is produced in metal films with layer thickness of 11 $nm$ for patterning 25 $\mu m$ diameter circles. Increasing metal film thickness leads to complete metal electrode removal instead of patterned removal of the film during the PDMS lift-off process. Note, however, that the film thickness and ability to be patterned is dependent on the geometry of the stamp. For circle features of 25 $\mu$m, the film thickness needs to be reduced to 11 nm. With 13 to 25 $\mu$m line patterns, however, good patterning can occur on films that are twice as thick. Decreasing the metal film thickness does not necessarily result in the ability to pattern a film. Metal films become increasingly difficult to lift off as the film thickness is decreased below 10 $nm$, which could be explained by the increasing roughness of the film. Discontinuous metal films are known to form at thicknesses below 10 nm, making it harder for

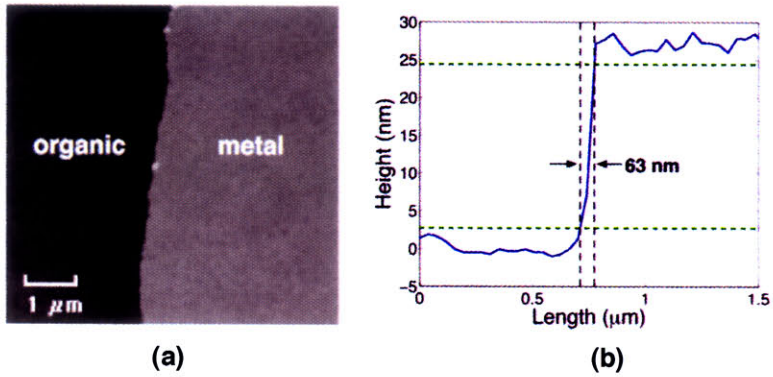


Figure 6-3: (b) Atomic force microscope (AFM) image of patterned 20 *nm* thick Mg:Ag on top of 50 nm thick Alq3/50 *nm* thick TPD/PEDOT/ITO/glass (b) corresponding cross section shown

PDMS to obtain intimate contact with the surface.

### 6.3.2 Peel direction

With transfer of line patterns, better quality image transfer occurs when the peel direction of separating the PDMS stamp away from the substrate is aligned with the relief line pattern. The result of the peel-dependent pattern transfer quality are shown in Figure 6-5. Peeling along the line pattern direction assists propagation of the metal film fracture. In contrast, peeling in the direction perpendicular to the relief stamp line pattern leads to poor pattern definition, since the breakage and release of the metal film must repeatedly occur in a discontinuous fashion. This discontinuous fashion implies that there is actually peeling of the metal film that occurs without a PDMS support when changing from a PDMS to no-PDMS contact region of the stamp. This allows for the formation of triangular patterns in the metal film. The triangular metal films in Figure 6-5d,f is a common shape that occurs with peeling of tape, wallpaper, or other adhesives, and is dependent on elasticity, adhesive energy, and fracture energy. As the film is pulled, energy builds up in the crease that forms where the metal is peeling from the surface. This energy goes towards overcoming the adhesive energy of the metal to the substrate, but some of it can be released by making a narrower film [123].

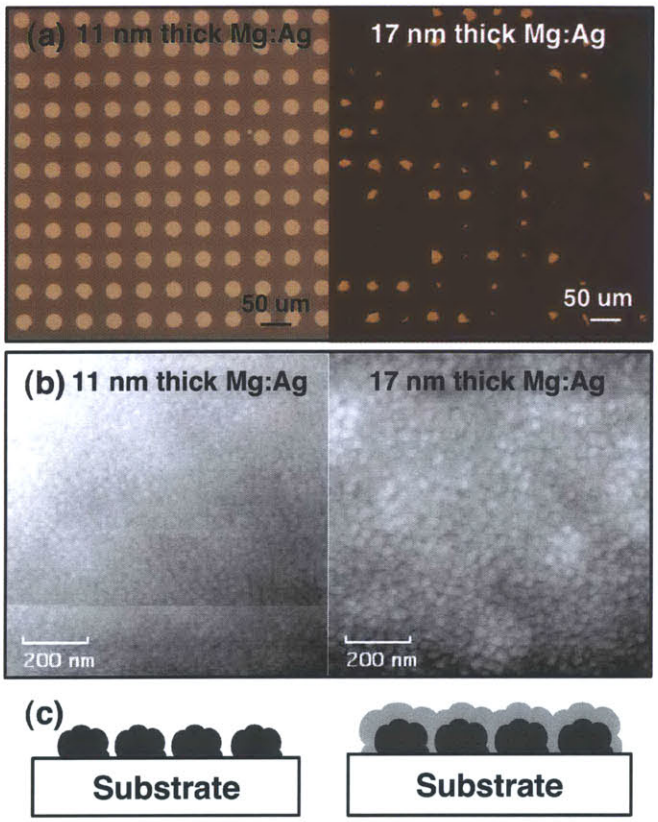


Figure 6-4: (a) Optical micrograph of 25 $\mu m$ diameter circles patterned from Mg:Ag on top of 50 $nm$ thick $Alq_3$/40 $nm$ thick Spiro-TPD/PEDOT/ITO/glass with metal thickness indicated in the figure. For a given pattern, increasing metal film thickness results in lift off but not patterning of the metal film. (b) Corresponding AFM images of metal electrode surface indicating larger grain size for thicker film. (c) Cartoon depiction of metal growth. Initially, metal deposition forms islands, indicated as dark grey blobs on the substrate on the left. With increased deposition of metal, the film becomes more continuous in nature, indicated in the lighter grey film on the right.

### 6.3.3 Contact angle measurements

Contact angle measurements are useful in approximating the energy of different surfaces. Table 6.1 shows contact angle measurements done on OLED interface surfaces.

## 6.4 Discussion

When the typical work of adhesion analysis is applied to this patterning technique, PDMS should not be able to pick up the metal from the underlying substrate. The

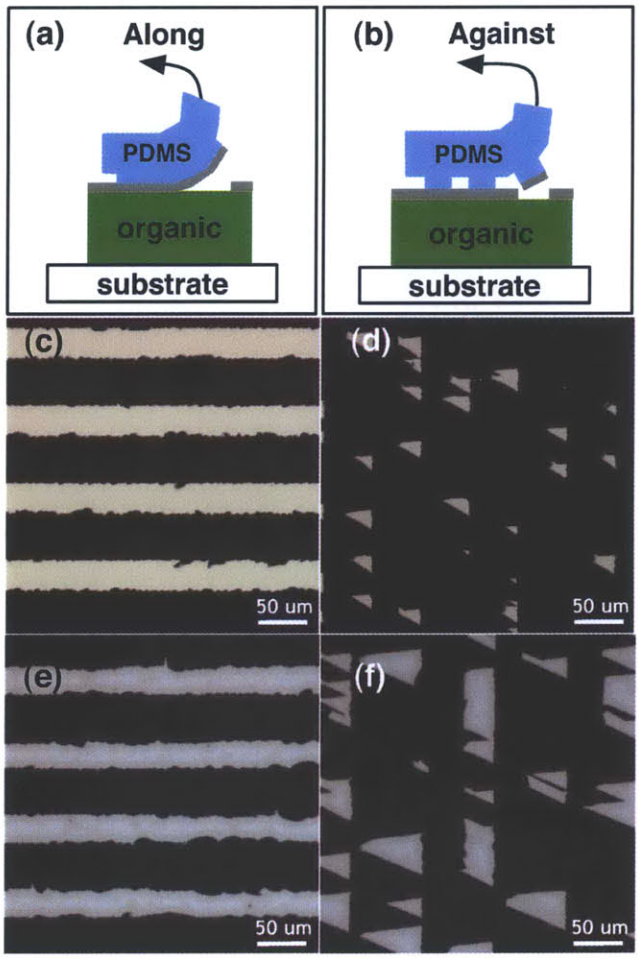


Figure 6-5: Peel direction along (a) or perpendicularly against (b) line pattern of the relief stamp affects patterning liftoff of 20 $nm$ thick Ag (c,d) or 12.5 nm thick Mg:Ag (e,f) film on top of 50 $nm$ thick $Alq_3$/50 $nm$ thick TPD/ITO/glass. Optical micrographs show that peel along (c,e) the line pattern results in patterning of 30 $\mu m$ wide lines with edge roughness of up to $+/-5$ $\mu m$ while peel against (d,f) the line pattern does not result in good pattern transfer.

Table 6.1: Contact angle measurement average ($\mu$) and standard deviation ($\sigma$) of at least two data measurements of OLED interface surfaces with de-ionized water (DI $H_2O$) and ethylene glycol (EG).

| | DI $H_20$ | | EG | |
|---|---|---|---|---|
| Surface | $\mu$ (°) | $\sigma$ (°) | $\mu$ (°) | $\sigma$ (°) |
| PDMS | 96 | 2 | 76 | 1 |
| Mg:Ag | 32 | 0 | 35 | 0 |
| Spiro-TPD | 85 | 0 | 63 | 1 |
| Alq3 | 64 | 3 | 37 | 3 |
| ITO | 23 | 3 | 64 | 1 |

PDMS-metal work of adhesion ($W_{PDMS,Mg:Ag}$ = 16 to 18 $mJ/m^2$) is smaller than metal-organic ($W_{Mg:Ag,Alq3}$ = 65 to 96 $mJ/m^2$), organic-organic ($W_{Alq3,TPD}$ = 43 to 54 $mJ/m^2$), or organic-substrate work of adhesion ($W_{TPD,ITO}$ = 36 to 42 $mJ/m^2$) [124]. However, with a rapid peel rate of the PDMS stamp away from the substrate ($>>$ 10 $mm/s$), the adhesion between the PDMS and metal interface increases due to the kinetically controllable adhesion of PDMS [122], and is able to overcome adhesion between the metal or organic interfaces, allowing liftoff of the metal film from the substrate. With a slow peel rate of the PDMS stamp away from the substrate ($\approx$ 10 $mm/s$), the metal film remains intact and is not lifted off, which is consistent with interfacial adhesion analysis of the PDMS surface in a static state.

## 6.5 Comparison to shadow masking

PDMS lift-off of electrodes has been compared to traditional shadow masking techniques producing similar current voltage and luminance characteristics. The two devices are grown on the same 1 x 1 $in^2$ substrate, using shadow-mask patterning on half of the substrate. After device growth, half of the substrate is patterned using PDMS lift-off technique. Figure 6-6 shows nearly identical current density versus voltage and electroluminescence quantum efficiency characteristics for the two devices, indicating equivalent quality of the PDMS lift-off and shadow masked structures [121].

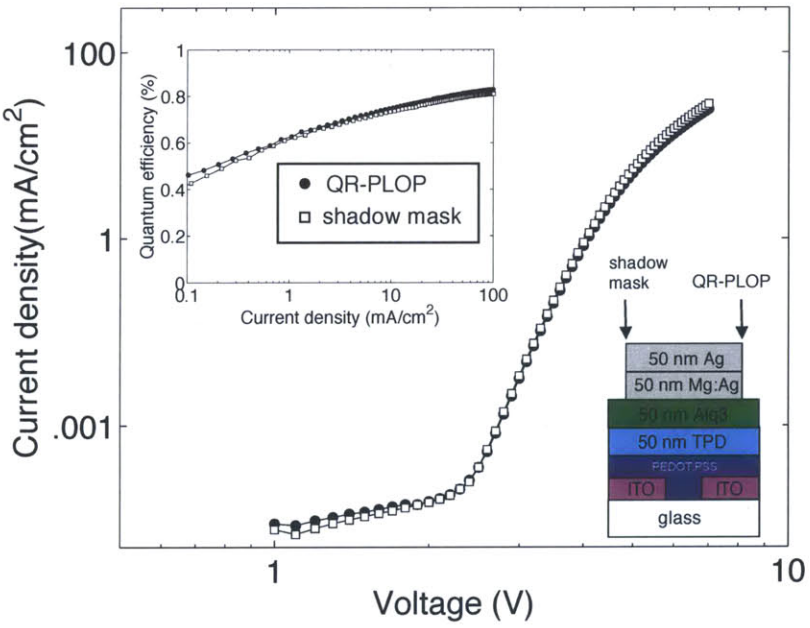


Figure 6-6: Current density versus voltage characteristics of a 2.81 $mm^2$ area OLED with a quick release PDMS lift-off patterned (QR-PLOP) electrode. The completed device consists of 50 nm thick Mg:Ag/50 $nm$ thick Ag on top of 50 $nm$ thick $Alq_3$/50 $nm$ thick TPD/PEDOT/ITO/glass. Also shown are current density vs. voltage characteristics of a 4.34 $mm^2$ area OLED patterned by conventional shadow mask method. (Inset) External electroluminescence quantum efficiency vs. current density for the same devices. Device structure is shown on bottom right.

## 6.6 Summary

In this section, a simple and scalable method for patterning thin Mg:Ag or Ag electrodes has been demonstrated by using a PDMS stamp and no externally applied pressure or chemical surface treatment. Unlike previous demonstrations of subtractive patterning of electrodes, this technique does not rely on cold welding or pressure-induced electrode fracture. However, the technique relies on metal film thickness, geometry of the stamp, peel direction, and separation speed of PDMS stamp to substrate. Finally, this patterning technique is applied to patterning OLED electrodes, demonstrating equivalent performance to the OLEDs patterned by shadow masking.

# Chapter 7

# Quantum dot patterning

## 7.1 Background

Quantum dot light emitting devices (QD-LEDs) are a promising technology for the emissive element in flat panel displays. Colloidal quantum dots (QDs) used as the emitting element in an OLED structure allows tunable emission wavelength, narrow emission band and efficient luminescence. In addition, QD-LEDs have current, voltage and luminance characteristics comparable to commercial OLEDs, as shown in Figure 7-1.

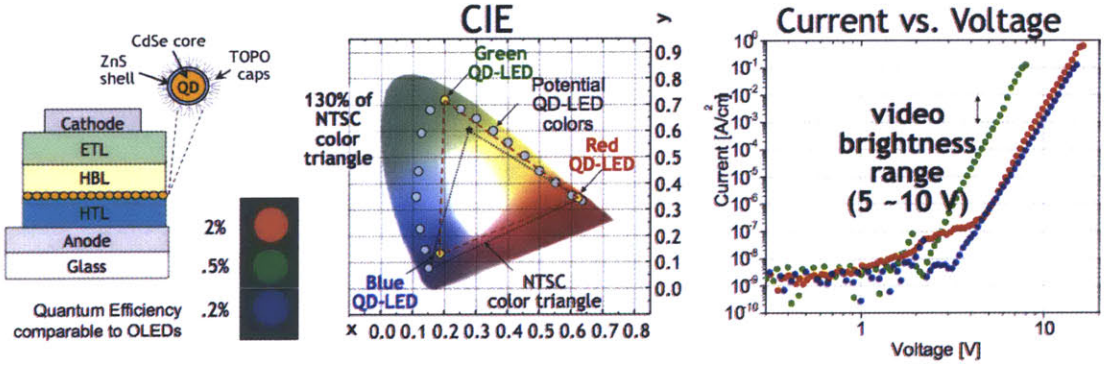


Figure 7-1: QD-LED structure, efficiency, color saturation, and current-voltage characteristics.

## 7.2 Motivation

QD deposition normally involves a spin-coating step: either spin-coat QD/organic solution to phase separate QDs from the organic layer [125] or spin-coat QDs onto a flat or relief stamp and subsequently transfer QDs onto an organic layer [126], as shown in Figure 7-2. Both these techniques do not utilize most of the QD material during the spin-coating process.

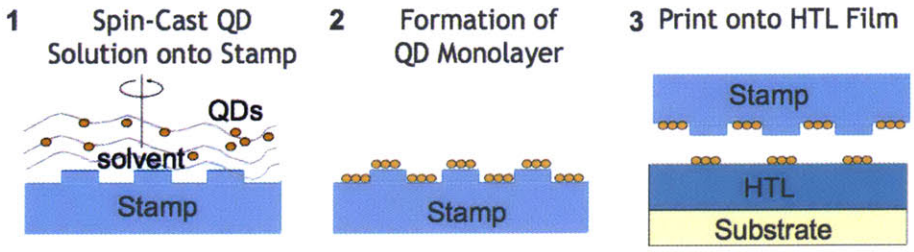


Figure 7-2: Spin-coating and stamping method for fabrication of QD-LEDs.

## 7.3 Proposed solution

An alternative technique is to inkjet print the QDs onto a stamp and then transfer the pattern to organics. In contrast to the low material usage efficiency in the spin-coating process, inkjet printing QDs can utilize almost 100% of the QD solution, drastically improving material usage in fabrication of QD-LEDs and other optoelectronic devices that utilize QD thin films.

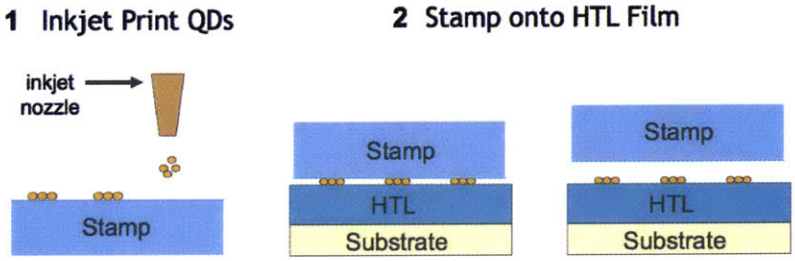


Figure 7-3: QD inkjet patterning and stamping method for fabrication of QD-LEDs.

## 7.4 Results

### 7.4.1 Inking of stamp

The challenge in patterning QDs via inkjet printing lies mainly in producing a uniform QD layer. A phenomena that occurs after printing is a coffee-staining effect when a drying drop deposits a ring of solute at the edge of the drop when the solvent evaporates [127] [28]. This occurs when the solvent contact line is pinned to the substrate and the solvent evaporates faster at the edges than the center of the drop, causing solvent flow from the bulk to the edges of the drop, resulting in edge deposition of solute in a ring formation . Typically, pinning of the contact edges is attributed to irregularities on the surface that are due to roughness or chemical heterogeneity. Sticking and slipping of the contact line also occurs when the pinning of the contact line is also dependent on the solute, leaving rings of particles in a regular drying pattern.

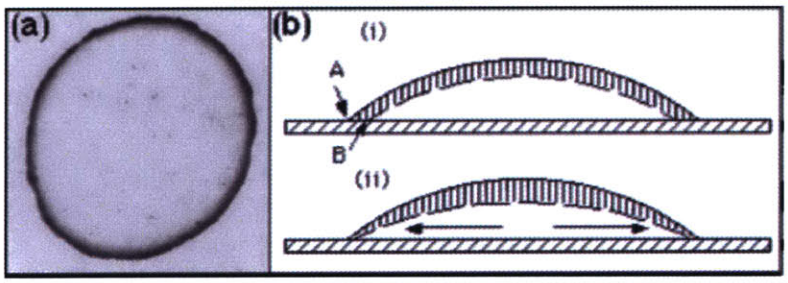


Figure 7-4: Coffee staining effect. [28]

Alcohol and hexane based QD inks have been tested on a PDMS and parylene coated PDMS surface. When using alcohol based QD inks, a parylene coating on the PDMS stamp greatly improves the drying uniformity, as shown in Figure 7-5 and explained by the smaller contact angle measurement of alcohol on the parylene surface shown in Table 7.1. Since the alcohol ink prefers the parylene surface, the ink spreads out on the surface instead of balling up to produce large random clumps of quantum dot islands when the ink dries. Changing the ink to hexane allows for better uniformity of the printed pattern when compared to ethanol inks. Hexane has a lower

contact angle on PDMS and parylene, showing better wetting of the hexane solvent on stamp surface. Hexane has a low surface tension allows the solvent to spread equally on PDMS and parylene surfaces, which is shown in the general uniformity of the printed films. However, the printed drop on the parylene surface allows for greater spreading of the ink than PDMS, as evidenced from the larger diameter of the dried drop. This result could be due to the QDs having a greater affinity for the parylene surface.

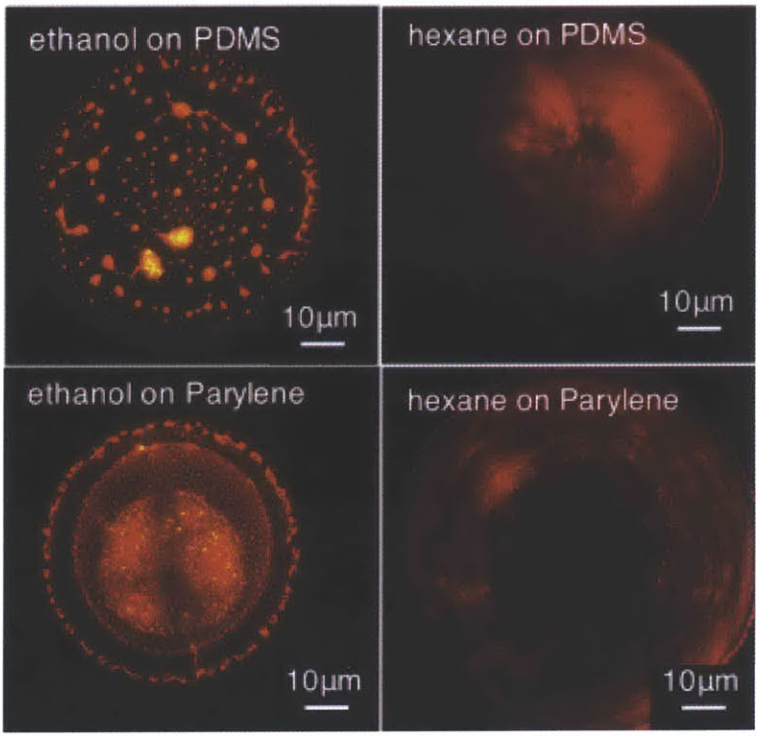


Figure 7-5: Quantum dots printed from ethanol (20 pL drop) or hexane (10 pL drop) onto a PDMS or Parylene surface.

Table 7.1: Contact angle measurement of ethanol, methanol, and hexane on PDMS and Parylene surface.

| | PDMS | Parylene |
|---|---|---|
| Ethanol | 32° | 20° |
| Methanol | 27° | 19° |
| Hexnae | 6° | 6° |

Pattered feature size is dependent on solvent wetting properties. To get 50 $\mu$m feature size with hexane ink which wets the stamp surface better than ethanol or methanol, smaller drop volume must be dispensed as shown in Figure 7-6.

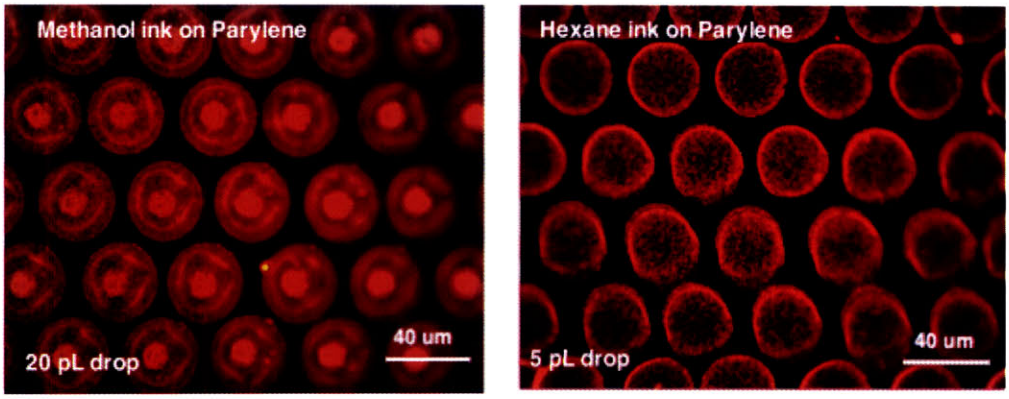


Figure 7-6: Quantum dots printed from methanol or hexane solution onto a Parylene surface.

### 7.4.2 Transfer

Transfer occurs after solvent evaporation of inkjet QDs on the stamp, allowing for integration of a wet patterning technique to a dry organic deposition. Inkjet-patterned QDs from different solvents are readily transfered onto various HTL surfaces: Poly-TPD, Spiro-TPD, and TPD. Figure 7-7 shows an example of this transfer of printed green dots from hexane to a Spiro-TPD surface as well as the result of transferring printed red dots from ethanol onto a TPD surface. After transfer, there is residual QDs left on the stamp as shown in Figure 7-8.

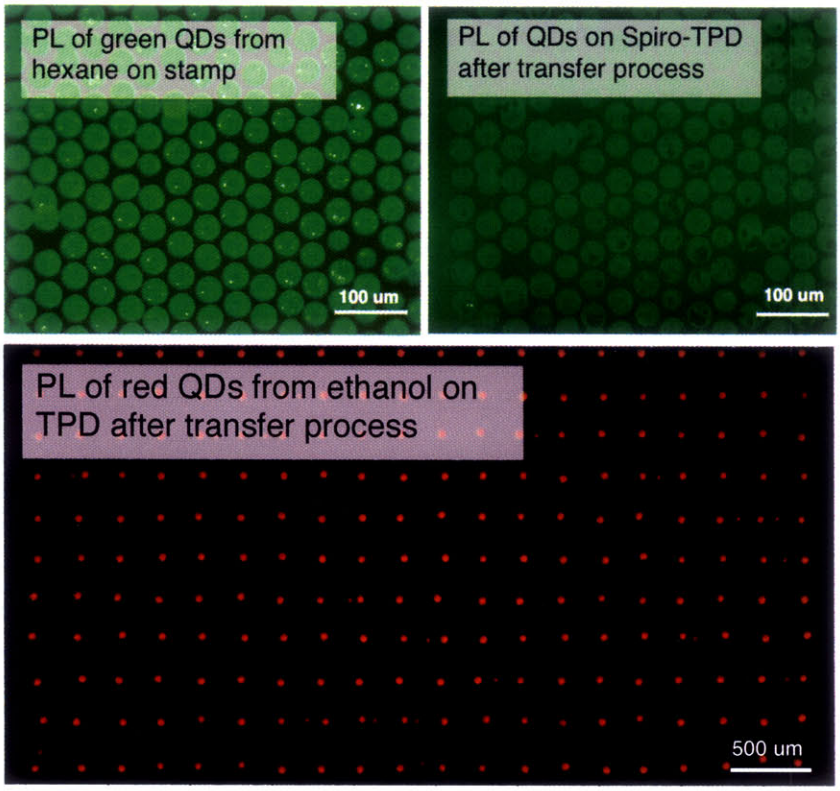


Figure 7-7: Demonstration of pattern transfer from stamp to organic substrate.

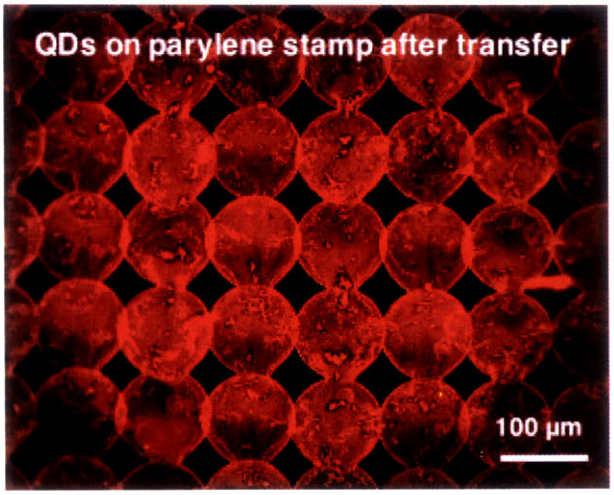


Figure 7-8: PL of residual QDs on parylene stamp after transfer.

### 7.4.3 QD-LED

Finally, after transfer of QDs onto the HTL of the device, the QD-LED is completed by evaporating a possible HTL, ETL, and metal electrodes. Figure 7-9 is an example of EL from a QD-LED with 50-$\mu$m patterned features. The dark spots in the EL emission are the result of extrinsic degradation from the unpackaged device.

Control of the QD layer thickness is important for producing QD EL from the device. Figure 7-10 shows QD PL and EL from inkjet-patterned 60 $\mu$m pitch of 20 pL drop volume. Figure 7-11 shows QD PL and EL from the same ink, but with a 10 pL drop volume, having smaller features, no overlap in patterning, and a more uniform distribution of QDs over the pattern area due to less solvent volume per surface area, diminishing the coffee ring effect during drying. In these two cases, one can see that the results from the patterning are drastically different for EL. In the case for 20 pL volume, the coffee ring effect shows higher concentration of QDs in the PL image at the edge of the circle pattern, which end up emitting bright red in the EL image. In the case of the 10 pL volume, the regions of low concentration of QDs as shown from the PL image end up emitting bright red in the EL image. These images show that it is possible to get EL from inkjet-patterned QDs, but it is highly dependent on the thickness of uniformity of the QD layer.

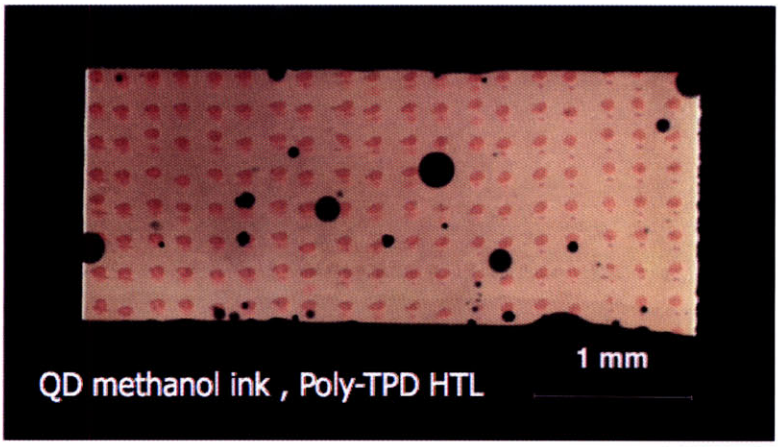


Figure 7-9: Electroluminescence from QD-LED from inkjet printed red QDs in methanol ink from parylene coated PDMS stamp.

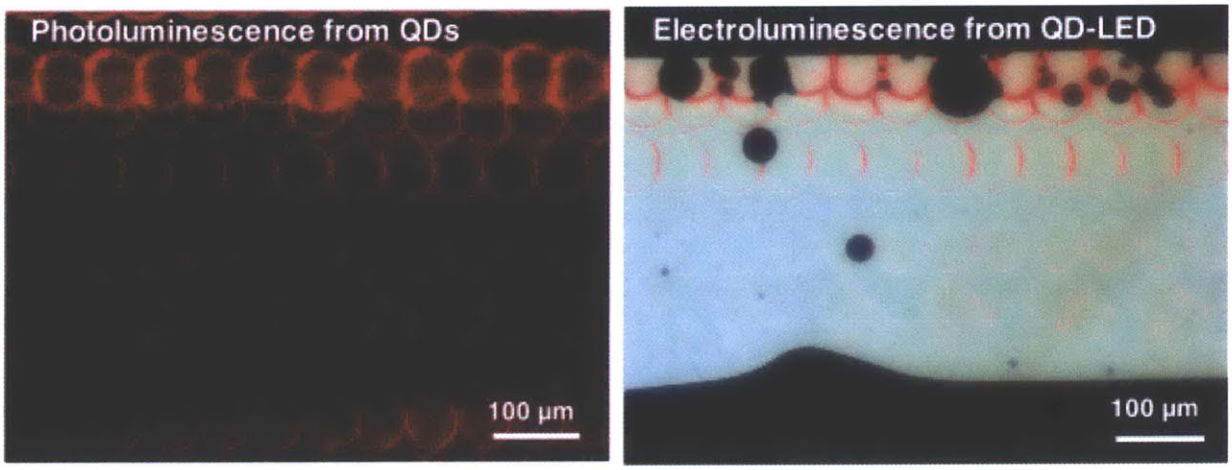


Figure 7-10: EL and PL of a QD-LED with device structure of 50 nm Spiro-TPD, inkjet-patterned QDs, 50 nm TPBi, 50 nm Mg:Ag and 50 nm Ag. Inkjet-patterned red QDs from hexane ink, 60 $\mu m$ spacing with 20 pL drop from PDMS stamp.

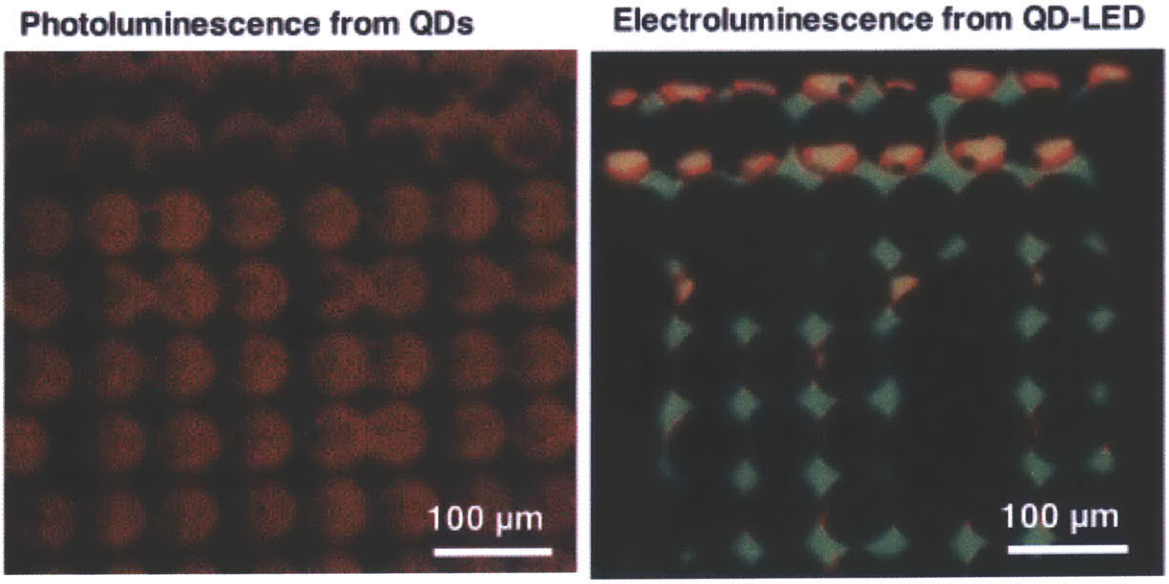


Figure 7-11: EL and PL of a QD-LED with device structure of 50 nm Spiro-TPD, inkjet-patterned QDs, 50 nm TPBi, 50 nm Mg:Ag and 50 nm Ag. Inkjet patterned red QDs in hexane ink, 60 $\mu m$ spacing with 10 pL drop from PDMS stamp.

### 7.4.4 Summary

In this section, a method for patterning QDs has been demonstrated by inkjet-printing the QDs onto a stamp and transferring the QDs onto an organic HTL. While the transfer procedure of the QDs to an organic surface is reproducible and consistent, the main challenge is in patterning uniform films of the QD ink on a stamp surface, which has to be optimized for each ink. Using an alcohol ink with a parylene stamp surface or a low surface tension hexane ink can reduce non-uniform drying on the stamp. Pattern resolution of this technique is dependent on drop volume and ink spreading on a surface. Finally, this patterning technique is applied to patterning QD-LEDs with observable electroluminescence from the QD layer.

# Chapter 8

# Conclusion

This thesis addresses two main challenges for OLED displays, lifetime and fabrication. In terms of OLED stability, degradation comes from chemical reactions that result in non-luminescing products. These reactions are increased through unstable charging of organic materials, heat evolution during device operation, and introduction of reactants through the environment. Degradation is unavoidable, but can be significantly slowed, as shown from very efficient red and green OLEDs with long half-lives. OLED display lifetime is not equal to device half-life, and display lifetime is redefined as 98% lifetime since the average human eye can detect a 2% change in neighboring pixel brightness. It may be possible to produce blue OLEDs one day which have half-lives greater than 300,000 hours (assuming a single exponential decay or 1,000,000 hours for a stretched exponential decay with $\beta = 0.76$) which would give a 50,000 hour display lifetime. However, other sources of instability still affect OLED displays such as ambient temperature, thickness variation, and threshold voltage in TFT pixel drivers. Using a current-correcting optical feedback solution, the display lifetime can be extended to half-life of OLEDs with a three-fold increase in the drive current. Edge-emitted light can be monitored for the feedback solution, allowing normal OLED pixels which avoids the loss of efficiency required with a transparent OLED pixel. An edge-emitted optical feedback solution requires serial pixel calibration with one detector for 10 second calibration time, but multiple detectors can decrease the calibration time. Edge emitted signal from a pixel is related to the inverse distance

to the detector, and in the worst-case scenario for a pixel in a high resolution display, there is twice as much signal to dark current.

In terms of OLED fabrication, contact stamping is able to produce high-resolution patterning with low-cost scalability, in contrast to shadow masking and laser techniques. Multi-colored OLED arrays with minimum feature size of 13 $\mu$m can be produced using a subtractive contact stamping technique. The organic and metal patterning trends are dependent on the material and layer thickness. Both circles and line patterns can be reproduced using this contact stamping technique, demonstrating the ability to pattern a curved a straight line. Although patterning is performed manually in this thesis, care was taken so that the lift-off procedure is done in a similar manner each time. For metal electrodes, the best patterning occurs when the peel direction is straight up and the release rate is faster than 10 mm/sec, producing high yields and good edge definition. For organics, just enough force is applied to slowly release the stamp from the substrate. The evidence of reproducibility for organic film thickness is evidenced by the small standard deviation in film thickness for 2 to 4 different lift-off measurement data points.

In addition, this thesis explores patterning a new OLED structure which uses QDs as the emissive layer in the device. QD-LEDs with 50 $\mu$m features are fabricated via contact stamping of patterned inkjet printed QDs. Inkjet printing QDs allows for increased utilization of the QDs over a spin-cast patterning technique. However, it is difficult to produce uniform patterned QD films. Spin-casting is a non-equilibrium process in which dots form a monolayer. In contrast, inkjet printing dispenses ink onto the surface of a stamp that is allowed to dry by reaching equilibrium conditions which produce non-uniform results. While a low surface energy solvent for the QDs allows for better wetting of the stamp surfaces and therefore improved uniformity of the dried film, the resolution of the QD pattern is reduced. A stamp with relief-features on the order of the sub-pixel pattern causes accumulation of dots on the edges of the pattern. Future work includes investigating a roughened stamp with nanometer-sized feature to help control the drying properties of the ink onto the stamp.

While beautifully patterned OLEDs are demonstrated in this thesis, this work is

by no means complete. The fabrication of these devices are manually stamped on substrates on the order of 1-inch size, a far cry from displays that are two orders of magnitude larger in size. Although the stamping procedures are scalable to larger areas, it is clear that better control of the stamping technique with a mechanized lift-off procedure is necessary. A mechanized lift-off procedure that could control the stamp release speed, peel direction, and lift-off force can also be used to further understand the mechanism for lift-off. Such a procedure could reduce the variation in lift-off thickness of a particular organic film, normalize the lift-off force across organic materials, and be used to compare the pattern-yield for metal films. In addition, although circle and line patterning of organic and metal films confirm the feasibility of patterning unique geometries, additional examination relating geometry and size with patterning yield for metals or lift-off thickness for organics would also be beneficial to further understanding the mechanism for lift-off.

# Chapter 9

# Future Work

The fabrication method described in this thesis for patterning organic and metal films for OLED displays can also be applied towards other applications. Patterning of organic films can be used to make optical gratings or to enhance the efficiency of OLEDs. Patterning thin metal films can be useful for enhancing the light output of OLEDs or as an etch mask for silicon. Thick metal film can be used with the PDMS lift-off technique to make a variable capacitor. In addition, the PDMS lift-off technique can also be applied to patterning oxides.

## 9.1 Optical gratings

The organic patterning technique may be applied to making optical gratings, which could provide a low cost method of producing a spectrometer. Figure 9-1 shows a proposed structure for making an optical grating out of organic and air. The refractive index of most organic material is around 1.7 and the index of air is 1.

## 9.2 Metal enhanced fluorescence

The proximity of a lumophore to a metal surface can cause either an increase or decrease in luminescence. Normally when a metal surface is placed near a fluorophore, the luminescene will be quenched. The metal offers many non-radiative pathways

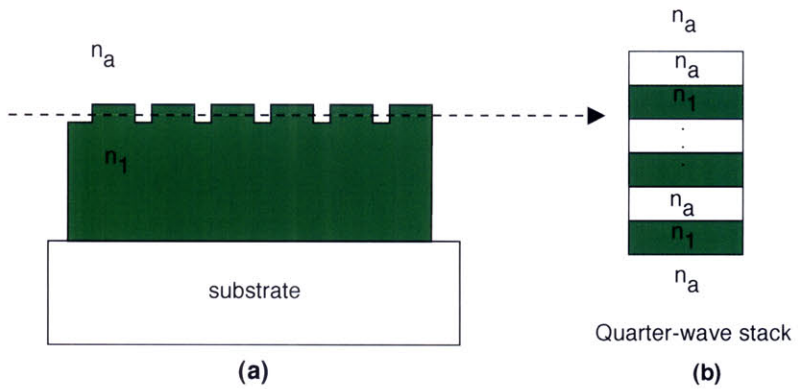


Figure 9-1: (a) Optical grating made out of patterned organic material. (b) Vertical view of lateral structure.

for relaxation and reduces the chance of radiative relaxation. However, it is also possible to have light generation and emission near a metallic surface if the metal surface is rough. The roughened surface allowed excitons to relax on the metal by generating surface plasmon polaritons (SPPs). The SPPs can subsequently scatter from the grating and re-radiate light [128]. Furthermore, enhancement of molecular fluorescence was found in proximity to colloidal metal films [129].

The metal patterning technique used on OLED electrodes may be useful in exploring metal enhanced fluorescence (MEF). The decay rate of excitons in a device can increase when placed in close proximity to a metal film due to direct energy transfer to surface plasmon modes of the metal. If the metal film is structured, these surface plasmons can be transformed into free photons to increase the luminescence efficiency. Figure 9-2 shows a proposed structure to make a MEF OLED by patterning either a metal or organic film near the emissive layer of the structure.

## 9.3 Silicon patterning

The PDMS lift-off technique can be applied on patterning gold on silicon for a low-cost patterning of silicon for use as solar concentrators. Gold can be deposited via electroless deposition onto silicon, and can be patterned using PDMS lift-off. The gold that remains serves as a mask for a wet etch for the exposed silicon. Figure

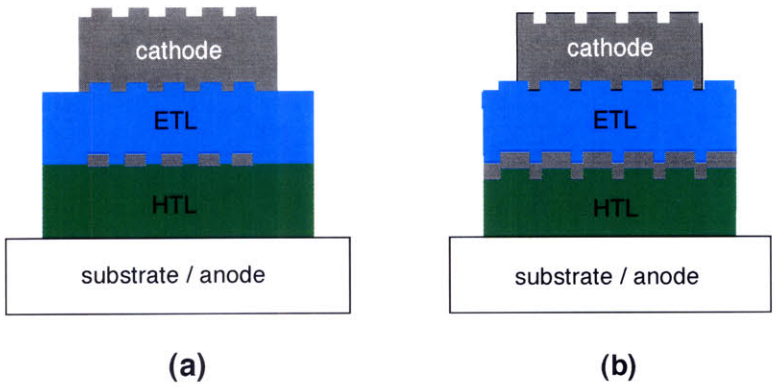


Figure 9-2: Two OLED structures for metal enhanced fluorescence. Structure (a) patterns a thin film of metal in the recombination region of the OLED while structure (b) patterns the organic with subsequent metal deposition.

9-3 shows the process flow for this application. Figure 9-4 shows an example of gold patterning on silicon.

## 9.4 MEMS capacitor

Increasing the film thickness of metal results in complete removal of the metal layer. Using this idea, a complete strip of metal can be lifted off onto the PDMS to form a bridge structure of metal over an air gap as shown in Figure 9-5. Figure 9-8 shows an example of this structure that was made using this technique. By applying a bias on the electrodes, the distance from the two plates of the capacitor can be modified.

## 9.5 Patterning oxides

It is also possible to pattern thin oxide layers using the same stamping technique used on organic and metal patterning. The mechanism is similar to the metal electrodes, and a quick release of the stamp from the substrate is required to enhance the kinetic adhesion property of PDMS. In the example shown in Figure 9-9, a 40 nm thick ITO film on top of organic layers is patterned. The direct application of this patterning technique would be to produce transparent OLEDs.

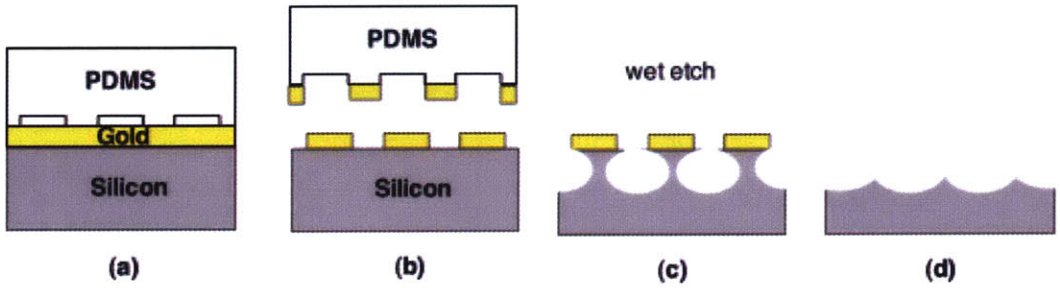


Figure 9-3: (a) Place stamp in contact with gold surface (b) quick release of stamp from surface results in patterning of film (c) use gold as mask and wet-etch silicon to (d) make a rough surface that can serve as a solar-collector.

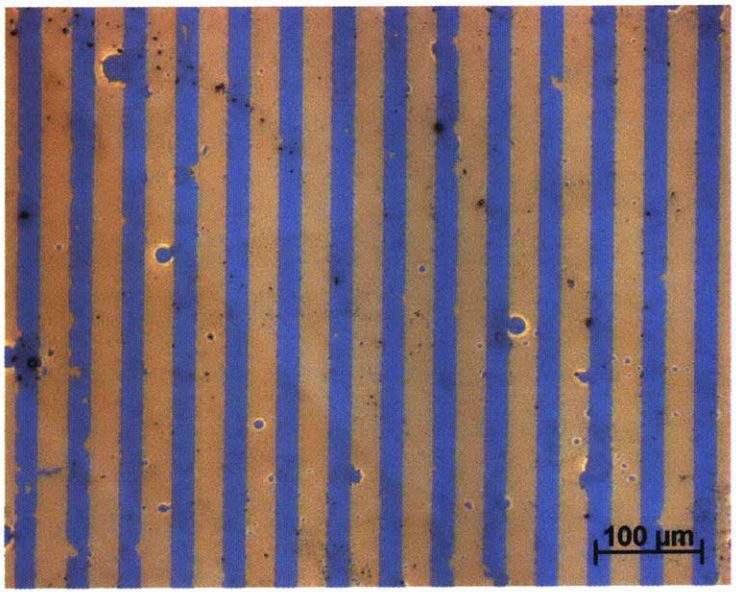


Figure 9-4: Optical microscope image of patterning of gold film on silicon substrate. Defects come from actual substrate, not the patterning.

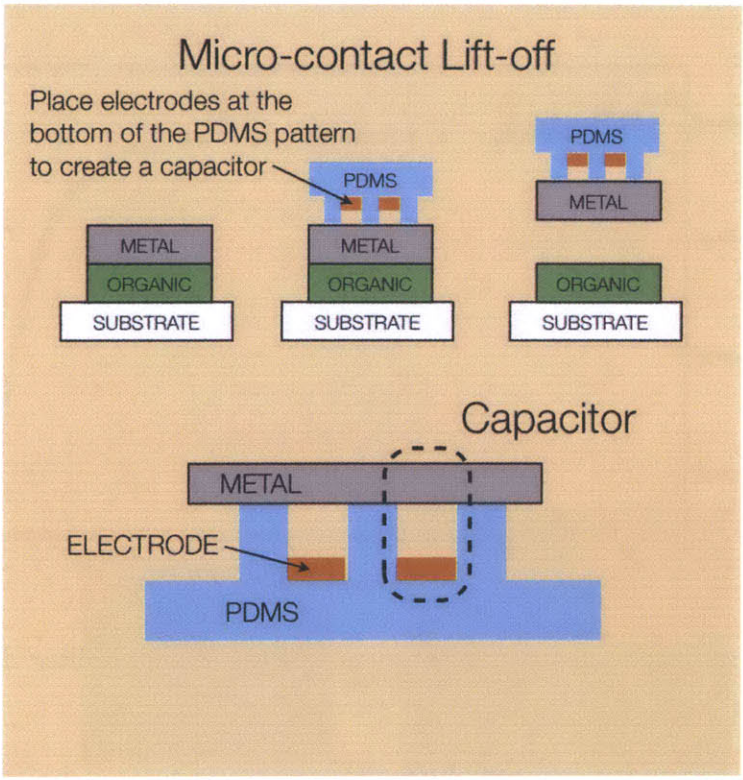


Figure 9-5: Procedure to fabricate a capacitor structure using PDMS lift-off.

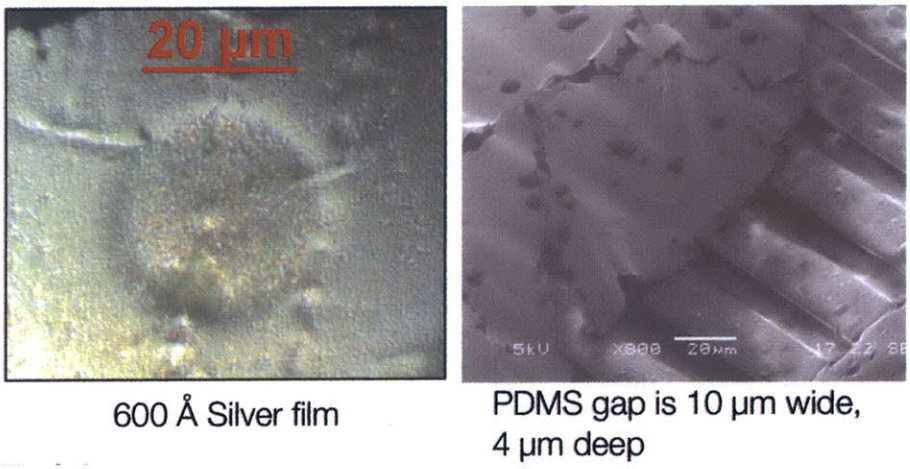


Figure 9-6: Example of metal film on top of an air gap such as a circular dimple in PDMS and spanning parallel lines in PDMS.

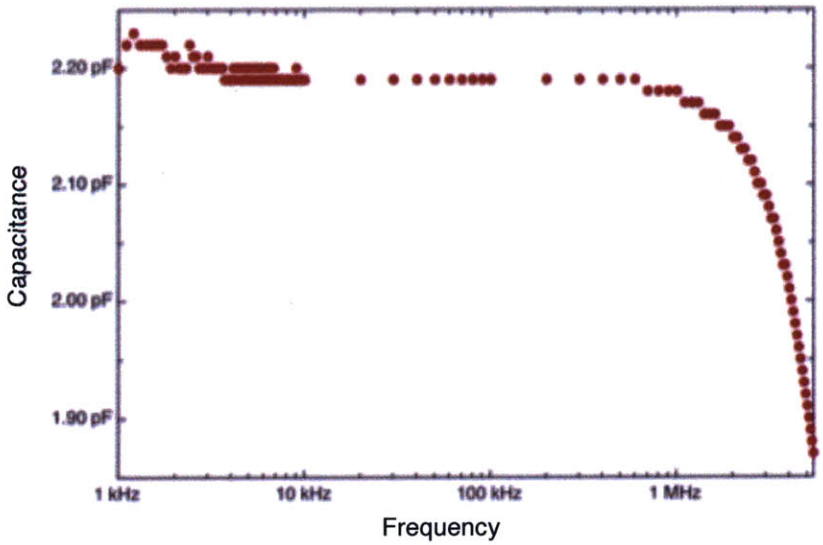


Figure 9-7: Capacitance versus frequency of variable capacitor device. [29]

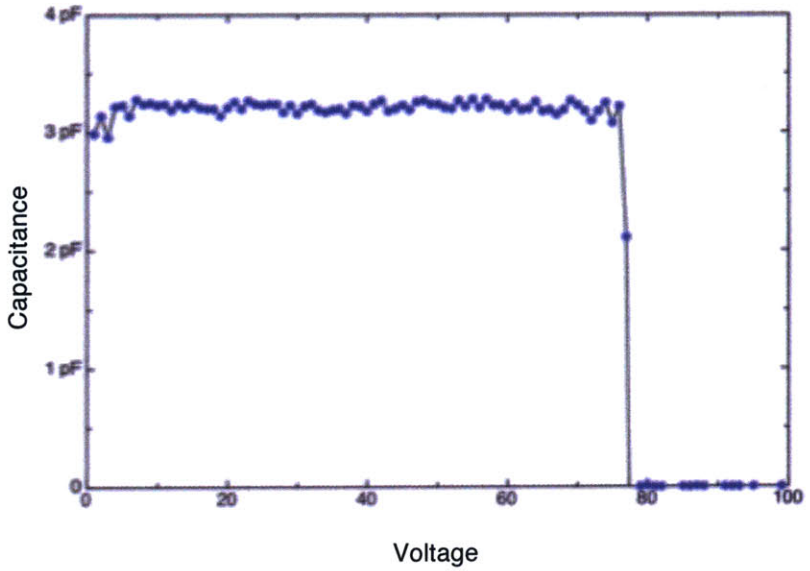


Figure 9-8: Capacitance versus voltage of variable capacitor device. [29]

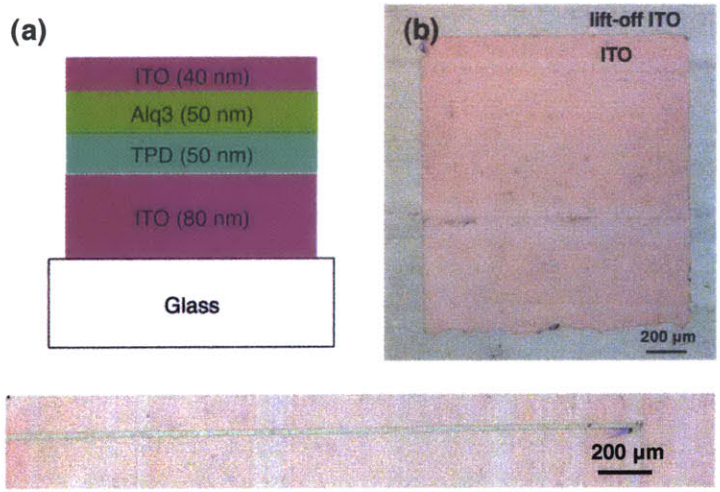


Figure 9-9: Example of a patterned oxide film: (a) Device structure in which top ITO layer is to be patterned (b) resulting patterned ITO square (c) lift-off of an ITO line.

# Appendix A

# Efficiency Calculations

## A.1 Quantum Efficiency

External quantum efficiency is photons out of the device per electrons into the device. The expression for quantum efficiency from measured quantities is expressed in Equation A.1. In this equation, $i_{pc}$ is the photocurrent, $R$ is the responsivity of the photodetector, $E_{ph}$ is the photon energy, $F$ is the form factor, and $i_v$ is the current through the OLED. These parameters will be covered in detail in the following sections.

$$\eta_{ext} = (\frac{i_{pc}R}{E_{ph}F})/i_v \tag{A.1}$$

## A.2 Electrons into device

Electrons going into the device is calculated by

- $i_v$ is the current going into the device in [A] or [Coulomb/s].
- To convert to [electrons/s], divide by $1.6 * 10^{-19}$ [Coulombs/electron]

- The conversion gives units of

$$\frac{[C/s]}{[C/electron]} = [\frac{electron}{sec}] \tag{A.2}$$

## A.3 Photons out of device

Photons coming out of the device can be calculated by

$$\frac{i_{pc}R}{E_{ph}F} \tag{A.3}$$

- $i_{pc}$ is the measured photocurrent [A] from the light coming out of the device
- $R$ is the responstivity of the photodetector to a certain wavelength. For a wavelength of 530 nm, the photodetector has a $R^{-1} = 0.31429[A/W]$.
- $E_{ph}$ is the energy per photon. This can be found using

$$E_{ph} = \frac{1241[eVnm]}{\omega[nm]} * (1.6 * 10^{-19}[J/eV])[photon^{-1}] \tag{A.4}$$

- $F$ is the form factor or the fraction of OLED light that is captured by the photodetector. This factor is unitless. More detail on how to compute this factor is discussed in the next section.
- The final product gives units of

$$\frac{[A][W/A]}{[J/photon]} = \frac{[J/s]}{[J/photon]} = [\frac{photon}{sec}] \tag{A.5}$$

## A.4 Form Factor

- The experimental setup for the data collection of an OLED is shown below. Not all the flux coming out of the OLED is measured by the photodetector. To calculate the form factor, or the amount of light actually captured by the

detector, we need to know two things, how light is emitted from the OLED, and what angle of light is captured by the detector.

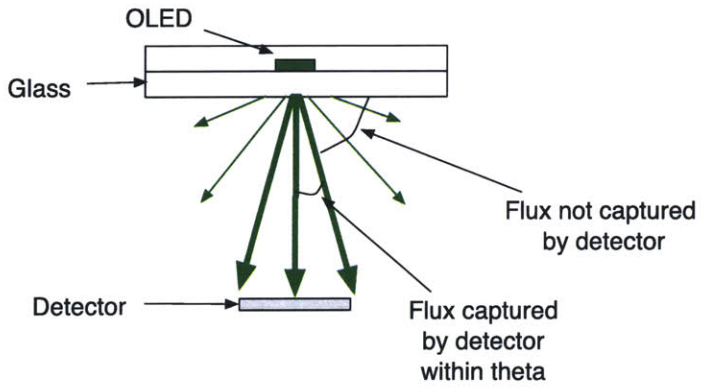


- Emission from an OLED is approximately Lambertian. The flux per solid angle varies as the cosine of the angle from the normal. (Greenham, Advanced Materials 1994, 6, No. 6., p. 491)

- Assuming $L_o$ is the flux per unit solid angle of light leaving the device directly in the forward direction, the total flux from a lambertian source can be calculated.

$$
\begin{aligned}
F_{ext} &= \int_{\theta=o}^{\pi/2} \int_{\phi=0}^{2\pi} L_o \cos\theta \sin\phi d\theta d\phi && \text{(A.6)} \\
&= \int_{o}^{\pi/2} 2\pi L_o \cos\theta \sin\theta d\theta && \text{(A.7)} \\
&= \pi L_o(\sin^2(\pi/2) - \sin^2(0)) && \text{(A.8)} \\
&= \pi L_o && \text{(A.9)}
\end{aligned}
$$

- Define $\theta_o$ as the angle from the normal to the edges of the photodetector. The fraction of flux reaching the detector is

$$
\begin{aligned}
F &= F_{captured}/F_{ext} && \text{(A.10)} \\
&= \pi L_o \cos^2\theta_o/\pi L_o && \text{(A.11)}
\end{aligned}
$$

$$= \cos^2 \theta_o \tag{A.12}$$

- This is the solution for this simple geometry of a point source to a circular photodetector. Other solutions of a Lambertian source to different geometries can be found in the following reference: Thermal Radiation Heat Transfer by Siegel.

# Appendix B

# Materials

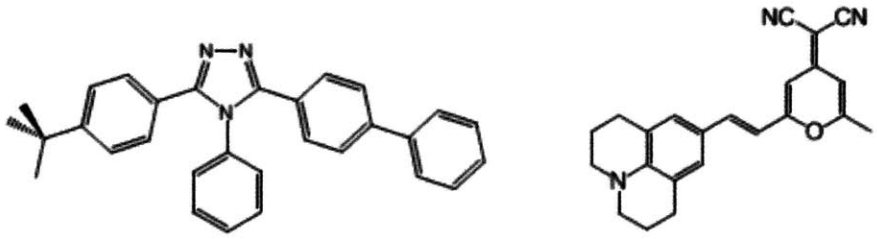


Figure B-1: Chemical structure of hole blocking material TAZ and fluorescent dopant DCM2.

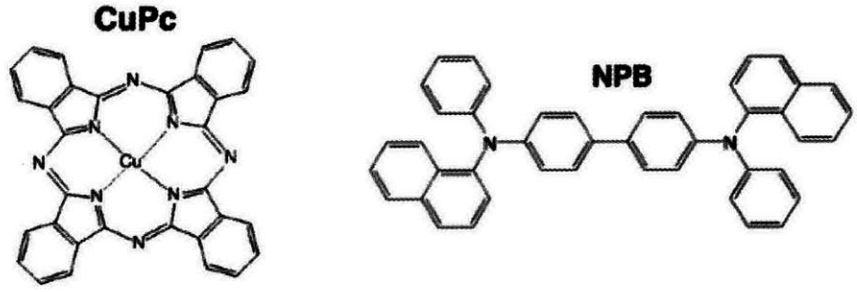


Figure B-2: Chemical structure of hole injection material Phthalocyanine, copper complex, commonly known as CuPc and hole transport material N,N'-Bis(naphthalen-1-yl)-N,N'-bis(phenyl)-benzidine, commonly known as NPB.

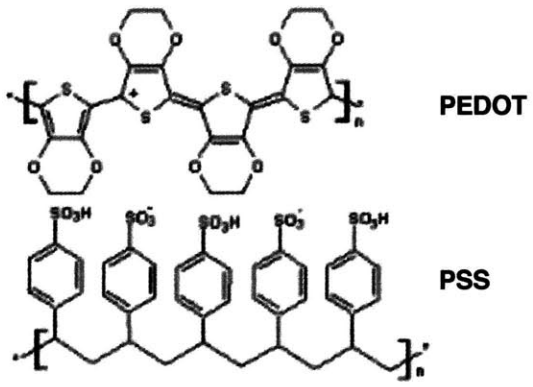


Figure B-3: Hole injection polymer PEDOT-PSS [Poly(3,4-ethylenedioxythiophene)-poly(styrene sulfonate)].

Table B.1: Organic material characteristics: molar mass, glass transition temperature, and thermal gravimetric analysis (0.5% weight loss) of some organic materials. [27]

| organic | MM (g/mol) | Tg (°C) | TGA (°C) |
|---|---|---|---|
| TPD | 516 | 65 | 330 |
| Spiro-TPD | 678 | 102 | 310 |
| NPB | 588 | 99 | 380 |
| NPAPF | 853 | 166 | 490 |
| TAZ | 429 | 70 | 270 |
| TPBi | 654 | 122 | 380 |
| Alq3 | 459 | 170 | 300 |
| UGH2 | 549 | - | 320 |

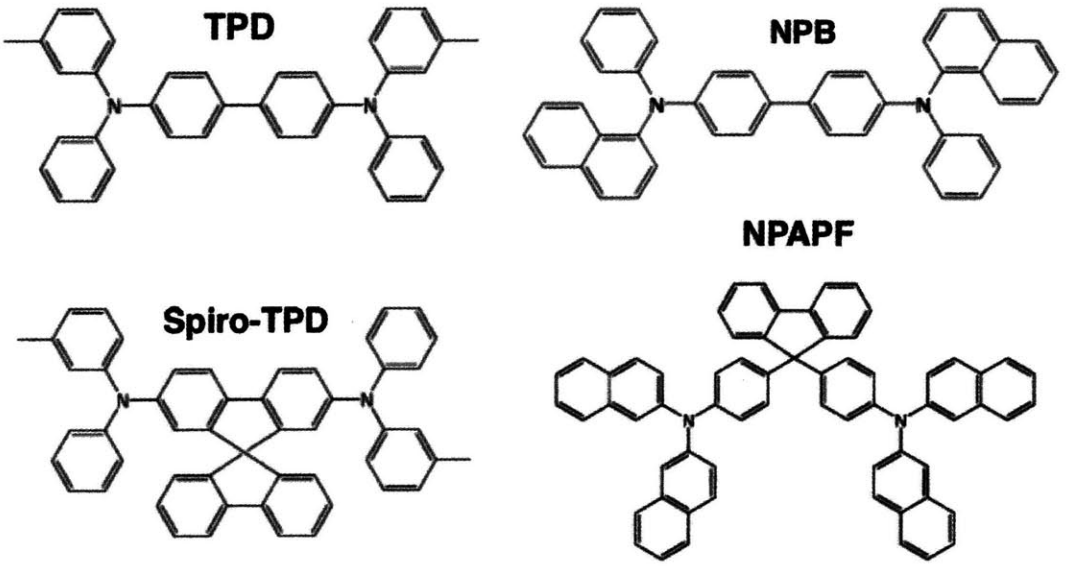


Figure B-4: Structure of hole transporting materials TPD, Spiro-TPD, NPB, and NPAPF.

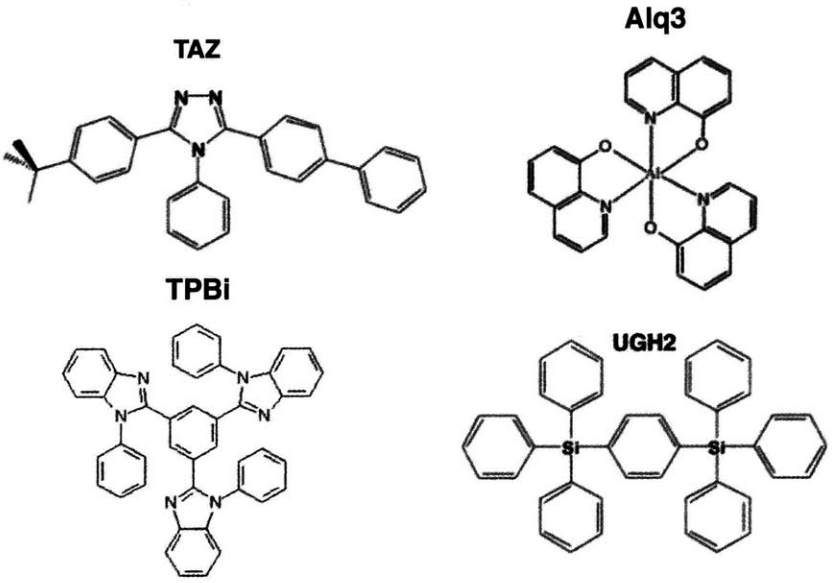


Figure B-5: Structure of hole blocking (TAZ), electron transporting (TPBi, Alq3), and phosphorescent host (UGH2) organic materials.

# Appendix C

# Work of adhesion

Adhesion analysis for contact stamping can be characterized by computing interfacial energy adhesion between layer surfaces. Surface energy of individual layers can be estimated by taking contact angle measurements of well-characterized liquids and estimating the interfacial adhesion between two layers. This basic adhesion analysis allows one to predict feasibility of subtractive lift-off or transfer with contact stamping by comparing interfacial adhesion energy between different layers.

The basic thermodynamic work of adhesion equation can be expressed by the sum of the liquid and solid surface free energy minus the interfacial free energy.

$$W_A = \gamma_s + \gamma_l - \gamma_{sl} \tag{C.1}$$

The thermodynamic work of adhesion is usually applied to liquid and solid surfaces. However, by making a few assumptions, this equation can be applied on solid-adhesive and substrate surfaces. These assumptions are that the surface free energy of a liquid does not change significantly when it solidifies and also that one neglects shrinkage stress of the liquid.

Fowkes proposed that surface free energy of a pure phase could be represented by the sum of contributions arising from

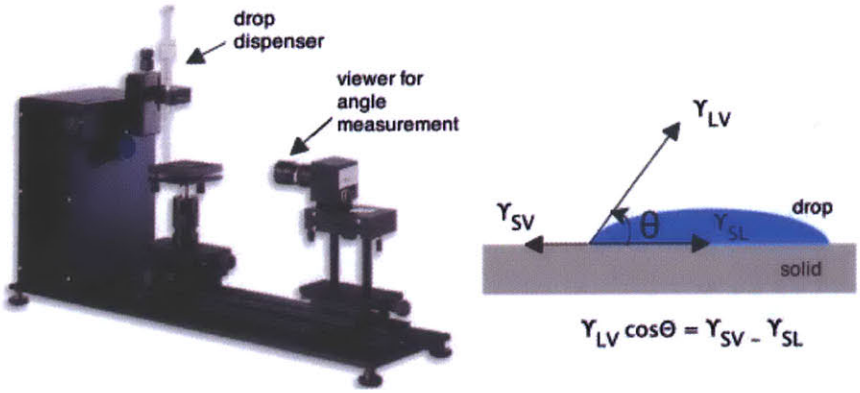


Figure C-1: Contact angle measurement setup to measure contact angle $\theta$ using different solvents and surfaces.

$$W_A = 2(\gamma_a^D \gamma_s^D)^{1/2} + 2(\gamma_a^P \gamma_s^P)^{1/2} \tag{C.2}$$

## C.1 Work of Adhesion Calculation

The following steps are used in the work of adhesion calculation between the adhesive and the substrate.

1. Use table of solvents to obtain surface energy components for liquids used.

   $\gamma_L$ is the total surface energy, and is equal to the sum of the polar and dispersive components.

   $\gamma_L^P$ is polar force component of the surface energy.

   $\gamma_L^D$ is dispersive force component of the surface energy.

2. Measure contact angle for two liquids: $\alpha_1$ and $\alpha_2$ on the solid surface using a goinometer as shown in Figure C-1.

3. Solve the following linear equation for the two unknowns, $\gamma_S^D$ and $\gamma_S^P$, the surface energy components of the solid.

$$\gamma_{L1}(1+\cos\alpha_1) = 2\sqrt{\gamma_S^D\gamma_{L1}^D} + 2\sqrt{\gamma_S^P\gamma_{L1}^P} \quad \text{(C.3)}$$

$$\gamma_{L2}(1+\cos\alpha_2) = 2\sqrt{\gamma_S^D\gamma_{L2}^D} + 2\sqrt{\gamma_S^P\gamma_{L2}^P} \quad \text{(C.4)}$$

Rearrange to make $Mx = b$ form of a linear algebra equation.

$$\begin{bmatrix} 2\sqrt{\gamma_{L1}^D} & 2\sqrt{\gamma_{L1}^P} \\ 2\sqrt{\gamma_{L2}^D} & 2\sqrt{\gamma_{L2}^P} \end{bmatrix} * \begin{bmatrix} \sqrt{\gamma_S^D} \\ \sqrt{\gamma_S^P} \end{bmatrix} = \begin{bmatrix} \gamma_{L1}(1+\cos\alpha_1) \\ \gamma_{L2}(1+\cos\alpha_2) \end{bmatrix} \quad \text{(C.5)}$$

Solve for $x$ by taking $M^{-1}Mx = M^{-1}b$. The inverse of a matrix, $A$ is the following.

$$A = \begin{bmatrix} a & b \\ c & d \end{bmatrix} \longrightarrow A^{-1} = \frac{1}{ad-bc}\begin{bmatrix} d & -b \\ -c & a \end{bmatrix} \quad \text{(C.6)}$$

Therefore

$$M^{-1} = \frac{1}{2\sqrt{\gamma_{L1}^D\gamma_{L2}^P} - 2\sqrt{\gamma_{L2}^D\gamma_{L1}^P}}\begin{bmatrix} \sqrt{\gamma_{L2}^P} & -\sqrt{\gamma_{L1}^P} \\ -\sqrt{\gamma_{L2}^D} & \sqrt{\gamma_{L1}^D} \end{bmatrix} \quad \text{(C.7)}$$

Solve for $\gamma_S^D$ and $\gamma_S^P$ by taking $M^{-1}b$

$$\sqrt{\gamma_S^D} = \frac{\gamma_{L1}(1+\cos\alpha_1)\sqrt{\gamma_{L2}^P} - \gamma_{L2}(1+\cos\alpha_2)\sqrt{\gamma_{L1}^P}}{2\sqrt{\gamma_{L1}^D\gamma_{L2}^P} - 2\sqrt{\gamma_{L2}^D\gamma_{L1}^P}} \quad \text{(C.8)}$$

$$\sqrt{\gamma_S^P} = \frac{-\gamma_{L1}(1+\cos\alpha_1)\sqrt{\gamma_{L2}^D} + \gamma_{L2}(1+\cos\alpha_2)\sqrt{\gamma_{L1}^D}}{2\sqrt{\gamma_{L1}^D\gamma_{L2}^P} - 2\sqrt{\gamma_{L2}^D\gamma_{L1}^P}} \quad \text{(C.9)}$$

4. Solve for the work of adhesion, given that one has already solved the surface

energy components of the adhesive and surface in steps 1-3. The equation is listed below, where the subscripts $a$ and $s$ refer to the adhesive and substrate respectively.

$$W_A = 2(\gamma_a^D \gamma_s^D)^{1/2} + 2(\gamma_a^P \gamma_s^P)^{1/2} \tag{C.10}$$

# Bibliography


[1] Jan Smith. Making colored pictures. *http://www.jegsworks.com/Lessons/lesson5/crt.gif*, 7-13-2008.

[2] HDTVFAQ.org. High-definition lcd screens. *http://www.hdtvfaq.org/hdtv-lcd.html*, 2008.

[3] H. Kawamoto. The history of liquid-crystal displays. *Proceedings of the IEEE*, 90(4):460, 2002.

[4] Wilson Rothman. Sony xel-1 oled tv review (verdict: Small on size, large on beauty). *http://www.gizmodo.com/*, Mar 2008.

[5] J. R. Sheats et al. Organic electroluminescent devices. *Science*, 273:884, 1996.

[6] Y.-F. Liew, H. Aziz, N.-X. Hu, H. S.-O. Chan, G. Xu, and Z. Popovic. Investigation of the sites of dark spots in organic light-emitting devices. *Appl. Phys. Lett.*, 77(17):2650, October 2000.

[7] L. M. Do et al. Observation of degradation processes of al electrodes in organic electroluminescence devices by electroluminescence microscopy, atomic force microscopy, scanning electron microscopy, and auger electron spectroscopy. *J. Appl. Phys.*, 79(9):5118, 1994.

[8] F. Papadimitrakopoulous et al. Chemical and morphological stability of aluminum tris(8-hydroxyquinoline) (alq3): Effects in light-emitting devices. *IEEE Journal on Selected Topics in Quantum Electronics*, 4:49, 1998.

[9] H. Aziz, Z. Popovic, C.P. Tripp, N.-X. Hu, A.-M. Hor, and G. Xu. Degradation processes at the cathode/organic interface in organic light degradation processes at the cathode/organic interface in organic light emitting devices with mg:ag cathodes. *Appl. Phys. Lett.*, 72:2642, 1998.

[10] S. Berleb et al. Interfacial charges and electric field distribution in organic hetero-layer light-emitting devices. *Organic Electronics 1*, 41-47:41, 2000.

[11] Z. D. Popovic, H. Aziz, N.-X. Hu, A. Ioannidis, and P. N. M. dos Anjos. Simultaneous electroluminescence and photoluminescence aging studies of tris(8-hydroxyquinoline) aluminum-based organic light-emitting devices. *J. Appl. Phys.*, 89:4673, 2001.

[12] H. Aziz Z. D. Popovic. Reliability and degradation of small molecule-based organic light-emitting devices (oleds). *IEEE Journal on Selected Topics in Quantum Electronics*, 8(2):362, April 2002.

[13] Z. Shen, P. E. Burrows, V. Bulović, D. M. McCarty, M.E. Thompson, and S. R. Forrest. Temperature dependence of current transport and electroluminescence in vacuum deposited organic light emitting devices. *Jpn. J. Appl. Phys.*, 35:L401, 1996.

[14] I. Tanaka and S. Tokito. Temperature-dependent carrier-transport and light-emission processes in a phosphorescent organic light-emitting device. *Appl. Phys. Lett.*, 87:173509, 2005.

[15] M. A. Baldo, C. Adachi, and S. R. Forrest. Transient analysis of organic electrophosphorescence. ii. transient analysis of triplet-triplet annihilation. *Physical Rev. B*, 62(16):10967–10977, Oct 2000.

[16] Brian J. Thompson, editor. *Organic Light-Emitting Materials and Devices*, volume 1. Taylor and Francis Group, 2007.

[17] P.E. Burrows, V. Bulovic, L. S. Sapochack, D. M. McCarty, and M.E. Thompson. Reliability and degradation of organic light emitting devices. *Appl. Phys. Lett.*, 65:2922, 1994.

[18] R. C. Kwong, M. R. Nugent, L. Michalski, T. Ngo, K. Rajan, Y.-J. Tung, M. S. Weaver, T. X. Zhou, M. Hack, M.E. Thompson, S. R. Forrest, and J. J. Brown. High operational stability of electrophosphorescent devices. *Appl. Phys. Lett.*, 81(1):162, 2002.

[19] D. C. Duffy, R. J. Jackman, K.M. Vaeth, K. F. Jensen, and G.M. Whitesides. Patterning electroluminescent materials with feature sizes as small as 5 um using elastomeric membranes as masks for dry lift-off. *Advanced Materials*, 11(7):546–552, 1999.

[20] G. B. Blanchet, Y.-L. Loo, J.A. Rogers, F. Gao, and C.R. Fincher. Large area, high resolution, dry printing of conducting polymers for organic electronics. *Appl. Phys. Lett.*, 82(3):463–465, 2003.

[21] T. Hirano, K. Matsuo, K. Kohinata, K. Hanawa, T. Matsumi, E. Matsuda, R. Matsuura, T. Ishibashi, A. Yoshida, and T. Sasaoka. Novel laser transfer technology for manufacturing large-sized oled displays. *SID 07 Digest*, 53.2:1592, 2007.

[22] J. Chen, V. Leblanc, S.H. Kang, P.J. Benning, D. Schut, M.A. Baldo, M.A. Schmidt, and V. Bulović. High definition digital fabrication of active organic devices by molecular jet printing. *Advanced Functional Materials*, 17:2722–2727, 2007.

[23] C. Kim, M. Shtein, and S.R. Forrest. Nanolithography based on patterned metal transfer and its application to organic electronic devices. *Appl. Phys. Lett.*, 80(21):4051–4053, 2002.

[24] J. h. Choi, K.-H. Kim, S.-J. Choi, and H. H. Lee. Whole device printing for full colour displays with organic light emitting diodes. *Nanotechnology*, 17:2246–2249, 2006.

[25] C. Kim, P. E. Burrows, and S. R. Forrest. Micropatterning of organic electronic devices by cold-welding. *Science*, 288:831–833, 2000.

[26] D.R. Schneider, D. Burdinski, J. Schellekens, M. Saalmink, and R. Dona. Wave printing (i) : Towards large-area, multilayer microcontact printing. *Mat. Res. Soc. Symp. Proc.*, EXS-2:M4.9.1, 2004.

[27] Luminescence Technolog Corp. Lumtec materials for oled/otft/ofet/osc. *http://www.lumtec.com.tw/*, 2008.

[28] R. D. Deegan. Pattern formation in drying drops. *Physical Review E*, 61(1):475–485, 2000.

[29] L. Kim, J. Yu, and V. Bulović. Microcontact printed mems structures. unpublished, 2008.

[30] M. S. Weaver, R. C. Kwong, V. A. Adamovich, M. Hack, and J. J. Brown. Recent advances in phosphorescent oleds for small- and large-area-display sizes. *J. Soc. Inform. Display*, 14(5):449–452, 2006.

[31] P. E. Burrows, Z. Shen, V. Bulović, D.M. McCarthy, and S.R. Forrest. Relationship between electroluminescence and current transport in organic heterojunction light-emitting devices. *Journal of applied physics*, 79(10):7991, 1996.

[32] M Pope, HP Kallmann, and PJ Magnante. Electroluminescence in organic crystals. *J Chem Phys*, 38:2042–2043, 1963.

[33] P.S. Vincett et al. Electrical conduction and low voltage blue electroluminescence in vacuum-deposited organic thin films. *Thin Solid Films*, 94:171–183, 1982.

[34] C. W. Tang and S. A. VanSlyke. Organic electroluminescent diodes. *Appl. Phys. Lett.*, 12:913, 1987.

[35] S.A. Van Slyke, C.H. Chen, and C.W. Tang. Organic electroluminescent devices with improved stability. *Appl. Phys. Lett.*, 69(15), 2160 1996.

[36] J. Mezyk, J. Kalinowski, F. Meinardi, and R. Tubino. Singlet exciton interactions in solid films of alq3. *Chemical Physics Letters*, 395:321–326, 2004.

[37] M.A. Baldo, D.F. O'Brien, M.E. Thompson, and S.R. Forrest. Excitonic singlet-triplet ratio in a semiconducting organic thin film. *Physical Review B*, 60(20):14422, 1999.

[38] D.Z. Garbuzov, V. Bulovic, P.E. Burrows, and S.R. Forrest. Photoluminescence efficiency and absorption of aluminum-tris-quinolate (alq3) thin films. *Chemical Physics Letters*, 249:433–437, 1996.

[39] C. F. Madigan, M.-H. Lu, and J.C. Sturm. Improvement of output coupling efficiency of organic light-emitting diodes by backside substrate modification. *Appl. Phys. Lett.*, 76(13):1650, 2000.

[40] Madison Gas and Electric. Lighting efficiency comparison. *http://www.mge.com/home/appliances/lighting/comparison.htm*, 2008.

[41] H. Peng et al. High contrast lcd tv using active dynamic led backlight. *SID 07 Digest*, (39.2), 2007.

[42] H. Chen, J. Sung, T. Ha, and Y. Park. Locally pixel-compensated backlight dimming for improving static contrast on led backlit lcds. *SID 07 Digest*, (39.3), 2007.

[43] J. H. Kim, J. H. Lee, J. C. Lim, C.H. Lee, M.H. Song, J.Y. Yoon, H.D. Choi, J.J. Kim, C.H. Oh, and S.D. Yeo. The novel technologies for achieving contrast ratio over 1:600 in ips mode. *SID 04 Digest*, (9.3), 2004.

[44] H. Nakamura and K. Sekiya. Overdrive method for reducing response times of liquid crystal displays. *SID 01 Digest*, (51.1), 2001.

[45] K. Sekiya and H. Nakamura. Overdrive method for tn-mode lcds - recursive system with capacitance prediction. *SID 01 Digest*, (9.5L):114, 2001.

[46] O. Itou, S. Hirot, Y. Sekiguchi, S. Komura, M. Morimoto, J. Tanno, K. Fukuda, T. Ochiai, H. Imayama, T. Nagata, and T. Miyazawa. A wide viewing angle transflective ips lcd applying new optical design. *SID 06 Digest*, (P-231L), 2006.

[47] K. Kalantar. Modulation of viewing angle on an lcd surface through backlight optics. *Journal of the SID*, 11(4):647, 2003.

[48] T. Uesaka, S. Nishimura, T. Toyooka, and E. Yoda. Wide-viewing-angle transflective lcd using hybrid aligned nematic compensators. *SID 05 Digest*, (P-116), 2005.

[49] OLED-Info.com. Oled history. *http://www.oled-info.com/history-page-2*, 2-06-2008.

[50] Plastics Information Europe. Oleds: First sony televisions sold out in japan. *http://www.plasteurope.com*, March 2008.

[51] Jason Chen. Sony's 11-inch xel-1 oled tv finally ships in january for 2500. *http://gizmodo.com/*, Jan 6 2008.

[52] S.R. Forrest. The road to high efficiency organic light emitting devices. *Organic Electronics*, 4:45, 2003.

[53] Samsung News Release. Samsung's super-clear, led-backlit panels now featured in premium lcd tvs. *http://www.samsung.com/us/business/semiconductor/*, Nov 2007.

[54] Sony Press Release. Sony launches world's first oled tv. *http://www.sony.net*, Oct 2007.

[55] P. Muller S. Barth, H. Riel, P. F. Seidler, W. Rieb, H. Vestweber, and H. Bassler. Electron mobility in tris(8-hydroxy-quinoline) aluminum thin films determined via transient electroluminescence from single- and multilayer organic light-emitting diodes. *J. Appl. Phys.*, 89(7):3711–3719, Apr 2001.

[56] Lara Luepke. Response time: the faster, the better? *http://reviews.cnet.com/*, October 2005.

[57] Darren Murph. Sony xel-1 estimated to last customers only half as long as expected. *http://www.engadget.com/2008/05/08/sony-xel-1-estimated-to-last-customers-only-half-as-long-as-expe/*, May 2008.

[58] BChydro. Liquid crystal display (lcd) monitors. *http://www.bchydro.com/business/investigate/investigate30111.html*, Jan 2006.

[59] The Associated Press. Japan backs oled display research. *http://www.cbc.ca/technology/story/2008/07/10/tech-display.html*, 2008.

[60] F. Papadimitrakopoulous, X.-M. Zhang, D. L.Thomsen, and K. A. Higginson. A chemical failure mechanism for aluminum(iii) 8-hydroxyguinoline light emitting devices. *Chem. Mater.*, 8:1363–1365, 1996.

[61] L.S. Liao, J. He, X. Zhou, M. Lu, Z.H. Xiong, Z.B. Deng, X.Y. Hou, and S.T. Lee. bubble formation in organic light-emitting diodes. *J. Appl. Phys.*, 88:2386, 2000.

[62] J. McElvain, H. Antoniadis, M.R. Hueschen, J.N. Miller, D.M. Roitman, J.R. Sheats, and R. L. Moon. Formation and growth of black spots in organic light-emitting diodes. *J. Appl. Phs.*, 80(10):6002, November 1996.

[63] S. J. Chua S. F. Lim, W. Wang. Degradation of organic light-emitting devices due to formation and growth of dark spots. *Mat. Sci. and Eng.*, B85:154–159, 2001.

[64] M. Kawaharada, M. ooishi, T. Saito, and E. Hasegawa. Nuclei of dark spots in organic el devices: detection by dfm and observation of the microstructure by tem. *Synthetic Metals*, 91:113–116, 1997.

[65] D. Koslov, D. S. English, V. Bulović, P. F. Barbara, S.R. Forrest, and M. E. Thompson. Direct observation of structural changes in organic light emitting devices during degradation. *J. Appl. Phys.*, 90:3242, 2001.

[66] H. Aziz, Z. Popovic, S. Xie, A.-M. Hor, N.-X. Hu, C. Tripp, and G. Hu. Humidity-induced crystallization of tris (8-hydroxyquinoline) aluminum layers in organic light-emitting devices. *Appl. Phys. Lett.*, 72:756, 1998.

[67] M. Fujihira, L.-M. Do, A. Koike, and E.-M. Han. Growth of dark spots by interdiffusion across organic layers in organic electroluminescent devices. *Appl. Phys. Lett.*, 68:1787, 1996.

[68] Y. Shen, D. B. Jacobs, G. G. Malliaras, G. Koley, M. G. Spencer, and A. Ioannidis. Modification of indium tin oxide for improved hole injection in organic light emitting diodes. *Adv. Mater.*, 13(16):1234, 2001.

[69] A. Gyoutoku, S. Hara, T. Komatsu, M. Shirinashihama, H. Iwanaga, and K. Sakanoue. An organic electroluminescent dot-matrix display using carbon underlayer. *Synth. Metals*, 91:73–75, 1997.

[70] Y. Shirota et al. Multilayered organic electroluminescent device using a novel starburst molecule, 4,4',4"-tris( -methylphenylphenylamino)tripheny amine, as a hole transport material multilayered organic electroluminescent device using a novel starburst molecule, 4,4',4"-tris( -methylphenylphenylamino)tripheny amine, as a hole transport material. *Appl. Phys. Lett.*, 65(7):807, 1994.

[71] N. Tamoto C. Adachi, K. Nagai. Molecular design of hole transport materials for obtaining high durability in organic electroluminescent diodes. *Appl. Phys. Lett.*, 66(20):2679, 1995.

[72] Shizuo Tokito, Hiromitsu Tanaka, Koji Noda, Akane Okada, and Yasunori Taga. Temperature dependences of electroluminescent characteristics in the devices fabricated with novel triphenylamine derivatives. *IEEE Trans. on Electron Devices*, 44(8):1239, August 1997.

[73] D. F. O'Brien, P.E. Burrows, S.R. Forrest, B. E. Koene, D. E. Loy, and M.E. Thompson. Hole transporting materials with high glass transition temperatures for use in organic light-emitting devices. *Adv. Mater.*, 10(14):1108, 1998.

[74] Vitex Systems. Barix. *http://www.vitexsys.com/new/barix.htm*, 2004.

[75] Z. D. Popovic, S. Xie, N. Hu, A. Hor, D. Fork, G. Anderson, , and C. Tripp. Life extension of organic led's by doping of a hole transport layer. *Thin Solid Films*, 363:6, 2000.

[76] H. Aziz et al. Improving the stability of organic light-emitting devices by using a thin mg anode buffer layer. *Appl. Phys. Lett.*, 89(103515), 2006.

[77] Takeo Wakimoto, Yoshinobu Yonemoto, Jun Funaki, Masami Tsuchida, Ryuji Murayama, Hitoshi Nakada, Hiroyuki Matsumoto, Shigeo Yamamura, and Masaharu Nomura. Stability characteristics of quinacridone and coumarin molecules as guest dopants in the organic leds. *Synth. Metals*, 91:15–19, 1997.

[78] Zoran D. Popovic, Hany Aziz, Carl P. Tripp, N.-X. Hu, Ah-Mee Hor, and Gu Xu. Improving the efficiency and stability of organic light emitting devices by using mixed emitting layers. *SPIE*, 3476:68, July 1998.

[79] Vi-En Choong, Song Shi, Jay Curless, Chan-Long Shieh, H.-C. Lee, Franky So, Jun Shen, and Jie Yang. Organic light-emitting diodes with a bipolar transport layer. *Appl. Phys. Lett.*, 75(2):172, 1999.

[80] Z. D. Popovic, H. Aziz, A. Ioannidis, N.-X. Hu, and P. N.M. dos Anjos. Time-resolved fluoresence studies of degradation in tris(8-hydroxyquinoline) aluminum (alq3)-based organic light emitting devices (oleds). *Synth. Metals*, 123:179–181, 2001.

[81] J.E. Knox, M.D. Halls, H. P. Hratchian, and H. B. Schlegel. Chemical failure modes of alq3-based oleds: Alq3 hydrolysis. *Phys. Chem. Chem. Phys.*, 8:1371–1377, 2006.

[82] T. Ikeda, H. Murata, Y. Kinoshita, J. Shike, Y. Ikeda, and M. Kitano. Enhanced stability of organic light-emitting devices fabricated under ultra-high vacuum condition. *Chem. Phys. Letters*, 426:111–114, 2006.

[83] Masaya Nakai, Hiroyuki Fujii, Tsuyoshi Tsujioka, Yuji Hamada, and Hisakazu Takahashi. Degradation of organic layers of organic light emitting devices by continuous operation. *Jpn. J. Appl. Phys.*, 41:881–884, 2002.

[84] J. Shen, D. Wang, E. Langloi, W.A. Barrow, P.J. Green, and J. Shi C.W. Tang. Degradation mechanisms in organic light emitting diodes. *Synthetic Metals*, 111-112:233–236, 2000.

[85] S. T. Lee, Z. Q. Gao, and L. S. Hung. Metal diffusion from electrodes in organic light-emitting diodes. *Appl. Phys. Lett.*, 75(10):1404, Sept 1999.

[86] L.S. Hung, L.R. Zheng, and M.G. Mason. Anode modification in organic light-emitting diodes by low-frequency plasma polymerization of chf3. *Appl. Phys. Lett.*, 78:673, 2001.

[87] X. et al. Wang. Improved operating lifetime of phosphorescent oled by novel anode coating. *Synth. Metals*, 137:1051–1052, 2003.

[88] D. Zou, M. Yahiro, and T. Tsutsui. Spontaneous and reverse-bias induced recovery behavior in organic electroluminescent diodes. *Appl. Phys. Lett.*, 72:2484, 1998.

[89] D. Zou, M. yahiro, and T. Tsutsui. Improvement of current-voltage characteristics in organic light-emitting diodes by application of reverse-bias voltage. *Jpn. J. Appl. Phys.*, 37:L1306, 1998.

[90] P. Cusumano, F. Buttitta, A. D. Cristofalo, and C. Cali. Effect of driving method on the degradation of organic light emitting diodes. *Jpn. J. Appl. Phys.*, 37:L1406, 1998.

[91] M. Yahiro, D. Zou, and T. Tsutsui. Recoverable degradation phenomena of quantum efficiency in organic el devices. *Synth. Metals*, 111:245, 2000.

[92] P. E. Burrows, S.R. Forrest, T. X. Zhou, and L. Michalski. Operating lifetime of phosphorescent organic light emitting devices. *Appl. Phys. Lett.*, 76:2493, 2000.

[93] S. Moller and S. R. Forrest. Improved light out-coupling in organic light emitting diodes employing ordered microlens arrays. *Journal of Applied Physics*, 91(5):3324, 2002.

[94] Jun Shen and Zhiliang Cao. *Organic Electroluminescence*, chapter Physical Properties of Organic Light-Emitting Diodes in Space Charge-Limited Conduction Regieme. Taylor and Francis Group, 2005.

[95] M. Iodice J. C. Sturm, W. Wilson. Thermal effects and scaling in organic light-emitting flat-panel displays. *IEEE J. Sel. Topics. Quantum Electron*, 4:75–82, 1998.

[96] V. Bulović, P. E. Burrows, and S.R. Forrest. Molecular organic light-emitting devices. *Semiconductors and Semimetals*, 64(5):255–306, 2000.

[97] Jae-Hoon Lee, Ji-Hoon Kim, and Min-Koo Han. A new a-si:h tft pixel circuit compensating the threshold voltage shift of a-si:h tft and oled for active matrix oled. *IEEE Electron Device Letters*, 26(12):897, 2005.

[98] D. Mentley. State of flat-panel display technology and future trends. *Proceedings of the IEEE*, 90:453–459, 2002.

[99] D. H. Hubel. *Eye, Brain, and Vision*, volume 22 of *Scientific American Library Series 22*, chapter The eye. New York: Scientific American Library, 1988.

[100] C. Fery, B. Racine, D. Vaufrey, H. Doyeux, and S. Cina. Physical mechansim responsible for the stretched exponential decay behavoir of aging organic light-emitting diodes. *Appl. Phys. Lett.*, 87(213502), 2005.

[101] R.C. Kwong, M.S. Weaver, M.-H. M. Lu, Y.-J. Tung, A. B. Chwang, T. X. Zhou, M. Hack, and J. J. Brown. Current status of electrophosphorescent device stability. *Org. Electronics*, 4:155, 2003.

[102] M. Childs, G. Nisato, D. Fish, A. Giraldo, A. Jenkins, and M. Johnson. Advanced poly-led displays. *Proc. of SPIE*, 5004:127–139, 2003.

[103] D.A. Fish, M.J. Childs, S.C. Deane, J.M. Shannon, W.A. Steer, N.D. Young, A. Giraldo, H. Lifka, and W. Oepts. Improved optical feedback for oled differential ageing correction. *J. Soc. Inform. Display*, 13(2):131–138, 2005.

[104] B. W. D'Andrade, J. Esler, and J. J. Brown. Organic light-emitting device operational stability at cryogenic temperatures. *Synth. Metals*, 156:405–408, Mar 2006.

[105] E. Lisuwandi, C. Choi, C. G. Sodini, and V. Bulović. Smart active-matrix display drivers for organic light emitting devices. RLE Progress Report 144, MIT, 2001.

[106] E. Lisuwandi. Feedback circuit for organic led active-matrix display drivers. Master's thesis, MIT, Cambridge, MA, 2002.

[107] V. Bulović, G. Gu, P.E. Burrows, S.R. Forrest, and M.E. Thompson. Transparent light-emitting devices. *Nature*, 380:29, 1996.

[108] G. Gu, V. Bulović, P.E. Burrows, M.E. Thompson, and S.R. Forrest. Transparent organic light emitting devices. *Appl. Phys. Lett.*, 68(19):2606–2608, May 1996.

[109] V. Bulović, J.R. Tischler, and J. Yu. Led array with photodetector. U.S. Patent Application 20050088380, filed Oct 23, 2003.

[110] J. Yu. A smart active matrix pixilated oled display. Master's thesis, MIT, Cambridge, MA, Jan 2004.

[111] J. Yu, J. R. Tischler, C. G. Sodini, and V. Bulović. Using integrated optical feedback to counter pixel aging and stabilize light output of organic led display technology. *Journal of Display Technology*, 2008.

[112] V. Bulović, V. B. Khalfin, G. Gu, P.E. Burrows, and S. R. Forrest. Weak microcavity effects in organic light-emitting devices. *Physical Review B*, 58(7):3730–3740, 1998.

[113] Z. Kafafi, editor. *Organic Electroluminescence*, page 11. Taylor and Francis Group, 2005.

[114] K. Utsugi, M. Tamegai, and E. Hasegawa. Fine patterning of lateral three color emitters for organic el devices using a metal mask sliding in vacuum vapor deposition. *SID 00 Digest*, P-30:640, 2000.

[115] Z. H. Huang, G. J. Qi, X. T. Zeng, and W. M. Su. A method for undercut formation of integrated shadow mask used in passive matrix displays. *Thin Solid Films*, 503(246), 2006.

[116] C. Kim, Y. Cao, W. O. Soboyejo, and S.R. Forrest. Patterning of active organic materials by direct transfer for organic electronic devices. *J. Appl. Phys.*, 97(113512), 2005.

[117] C. Kim and S. R. Forrest. Fabrication of organic light-emitting devices by low-pressure cold welding. *Adv. Mater.*, 15(6):541–545, 2003.

[118] Z. Wang, J. Yuan, J. Zhang, R. Xing, D. Yan, and Y. Han. Metal transfer printing and its application in organic field-effect transistor fabrication. *Adv. Mater.*, 15(12):1009–1012, 2003.

[119] Z. Wang, J. Zhang, R. Xing, J. Yuan, D. Yan, and Y. Han. micropatterning of organic semiconductor microcrystalline materials and ofet fabrication by "hot lift off". *J. Am. Chem. Soc.*, 125:15278–15279, 2003.

[120] J. h. Choi, D. Kim, P.J. Yoo, and H.H. Lee. Simple detachment patterning of organic layers and its application to organic light-emitting diodes. *Adv. Mater.*, 17:166, 2005.

[121] J. Yu and V. Bulović. Micropatterning metal electrode of organic light emitting devices using rapid polydimethylsiloxane lift-off. *Appl. Phys. Lett.*, 91(043102), 2007.

[122] M. A. Meitl, Z.-T. Zhu, V. Kumar, K. J. Lee, X. Feng, Y. Y. Huang, I. Adesida, R. G. Nuzzo, and J. A. Rogers. Transfer printing by kinetic control of adhesion to an elastomeric stamp. *Nature materials*, 5:33–38, 2006.

[123] Science Daily. Why wallpaper won't peel off easily and why tape refuses to pull off the roll straight. *http://www.sciencedaily.com/releases*, 2008.

[124] J. Yu and V. Bulović. Micropatterning of metal electrodes for organic light emitting devices. In *2006 MRS Fall Meeting Program and Exhibit Guide*, Nov 2006. Materials Research Society Fall Meeting.

[125] S. Coe, W.-K. Woo, M. Bawendi, and V. Bulovic. Electroluminescence from single monolayers of nanocrystals in molecular organic devices. *Nature Materials*, 420:800, 2002.

[126] L. Kim. Deposition of colloidal quantum dots by microcontact printing for led display technology. Master's thesis, MIT, Cambridge, MA, Feb 2006.

[127] R. D. Deegan, O. Bakajin, T.F. Dupont, G. Huber, S. R. Nagel, and T. A. Witten. Capillary flow as the cause of ring stains from dried liquid drops. *Nature*, 389:827–829, 1997.

[128] S.C. Kitson, W.L. Barnes, and J.R. Sambles. Photoluminescence from dye molecules on silver gratings. *Optics Communications*, 122:147–154, 1996.

[129] Konstantin Sokolov, George Chumanov, and Therese M. Cotton. Enhancement of molecular fluorescence near the surface of colloidal metal films. *Analytical Chemistry*, 70:3898–3905, 1998.